Calorimetric and related studies of disorder in solid electrolyte and similar materials

Peter Gerald Hall

Ph D

The work described in this thesis, carried out during the tenure of a research assistantship at Leicester Polytechnic, is submitted in partial fulfilment of the requirements for the degree of Ph D of the Council for National Academic Awards. Unless otherwise accredited, the work was carried out by the author and has not been submitted in any form for any other degree.

Leicester Polytechnic

April 1984

Collaborating Establishment
Duracell Batteries (U.K) Ltd

Calorimetric and related studies of disorder in solid electrolyte and similar materials

Peter Gerald Hall

Abstract

The design and construction of an adiabatic calorimeter is described. The calorimeter is of traditional design but the control system is new, based around a Commodore PET microcomputer. The first heat capacity measurements made, on a sample of Calorimetry Conference Sapphire between 77 and 315 K, indicated an accuracy within 1%. Since that time substantial improvements to the control system have been made. For most samples studied experimental precision is considerably better than 1%. Even with drift periods as long as 5-6 h, precision is better than 2%.

The first heat capacity studies by adiabatic calorimetry are reported for crystalline $Ag_6I_4WO_4$ and $Ag_{13}I_9W_2O_8$. Both exhibit three transitions, two first order near 198 and 246 K and a continuous transition with a maximum near 275 K. These findings are discussed in relation to previous studies of these electrolytes. The glassy electrolyte $Ag_{13}I_9W_2O_8$ shows no evidence of these transitions, and non-equilibrium behaviour is apparent. The heat capacity differs significantly from the literature data for the glass $Ag_7I_4AsO_4$.

A continuous transition has been found in $[NMe_4]_2Ag_{13}I_{15}$ near 155 K.

To allow a comparison of the electrolyte heat capacities with those of their components, a heat capacity study of Ag_2WO_4 was carried out. Three samples were used: finely divided precipitate; crushed pellets formed from the powder; and a crushed cooled melt. Equilibration times for the first two were long, 1-2 h and 5-6 h respectively. This is in line with published data for another powdered solid. The behaviour of the crushed cooled melt was normal. A small heat capacity anomaly is apparent at 277 K though this may result from slight breakdown of Ag_2WO_4 during melting or from impurity phases present in the original precipitate.

Some results of an extended x-ray absorption fine structure study of a copper(I) electrolyte are presented which suggest that in these systems electrolyte modification occurs during cell discharge.

Introduction

This work would not have been possible without the support and encouragement of my supervisors, Dr R G Linford and Dr D A Armitage, and of the other academic and technical staff of the polytechnic. Their assistance has been so generous that it would be unfair to mention individuals by name. I will, however, allow myself one exception. Most of the x-ray photographs discussed in the following chapters were taken by Mr K Andrews. To him I extend my thanks for his skill and good humour in the face of 'yet another silver tungstate'. Some x-ray photographs are referred to by numbers (A - - -). These correspond to x-ray powder diffraction files maintained at Leicester Polytechnic. Generally it implies that more than one sample of that composition is indexed in those files.

This thesis covers only part of the requirements for the degree of Ph D. I also attended undergraduate and specialist classes in chemical thermodynamics, electrochemistry, lattice dynamics, electronics, microcomputing and glass blowing, as well as a number of external conferences.

In the first year of this project, under the guidance of Dr D A Armitage, I made a study of the details of electronic and microcomputer control as a knowledge of these would be necessary for work on the calorimeter. During this time, the differential thermal analysis instrument, referred to a number of times in the text, was constructed, as also was a microcomputer controlled thermostat.

The major experimental objectives of the project were two-fold:

(i) design and construction of an adiabatic calorimeter of accuracy comparable to that obtained elsewhere

(ii) determination and interpretation of heat capacity curves for a number of solid electrolytes.

This is reflected in the layout of the thesis, the experimental chapters falling approximately into two sections:

(i) chapters 3-7, calorimetry and the calorimeter

(ii) chapters 8-11, novel heat capacity results.

Only in two areas did the results fall below the targets set at the outset of this work. For practical reasons outlined in the text, automatic running of the calorimeter was not taken as far as I would have liked. Secondly, with only one shield, it was not possible to extend the calorimeter operating range significantly above ambient.

The present control system is, however, flexible enough to allow the next operator to introduce both of these features.

Finally, I thank my fellow students for their discussion, help and friendship, and the many people outside the polytechnic whose conversation and correspondence was most valuable. Some of these are acknowledged as 'personal communication' in the references at the end of each chapter. My apologies to those I have not been able to include.

List of Contents

6...

Calorimetric and related studies of disorder in solid electrolyte and similar materials

Peter Gerald Hall

Abstract

The design and construction of an adiabatic calorimeter is described. The calorimeter is of traditional design but the control system is new, based around a Commodore PET microcomputer. The first heat capacity measurements made, on a sample of Calorimetry Conference Sapphire between 77 and 315 K, indicated an accuracy within 1%. Since that time substantial improvements to the control system have been made. For most samples studied experimental precision is considerably better than 1%. Even with drift periods as long as 5-6 h, precision is better than 2%.

The first heat capacity studies by adiabatic calorimetry are reported for crystalline $Ag_6I_4WO_4$ and $Ag_{13}I_9W_2O_8$. Both exhibit three transitions, two first order near 198 and 246 K and a continuous transition with a maximum near 275 K. These findings are discussed in relation to previous studies of these electrolytes. The glassy electrolyte $Ag_{13}I_9W_2O_8$ shows no evidence of these transitions, and non-equilibrium behaviour is apparent. The heat capacity differs significantly from the literature data for the glass $Ag_7I_4AsO_4$.

A continuous transition has been found in $[NMe_4]_2Ag_{13}I_{15}$ near 155 K.

To allow a comparison of the electrolyte heat capacities with those of their components, a heat capacity study of Ag_2WO_4 was carried out. Three samples were used: finely divided precipitate; crushed pellets formed from the powder; and a crushed cooled melt. Equilibration times for the first two were long, 1-2 h and 5-6 h respectively. This is in line with published data for another powdered solid. The behaviour of the crushed cooled melt was normal. A small heat capacity anomaly is apparent at 277 K though this may result from slight breakdown of Ag_2WO_4 during melting or from impurity phases present in the original precipitate.

Some results of an extended x-ray absorption fine structure study of a copper(I) electrolyte are presented which suggest that in these systems electrolyte modification occurs during cell discharge.

1

The Heat Capacity of Solids

To raise the temperature of a material it is necessary to provide it with heat or energy. How much energy depends on the material and the temperature at which the experiment is carried out.

If the temperature of the material is raised by an amount ΔT then the average heat capacity over the temperature interval $T \rightarrow T+\Delta T$ is

$$C_{av} = q/\Delta T$$

where q is the energy input.

Since heat capacity varies, sometimes quite sharply, with temperature, it is often useful to write this definition as[2]

$$C = dq/dT.$$

For practical purposes the heat capacity is usually defined as

molar heat capacity at constant volume C_v

or

molar heat capacity at constant pressure C_p.

This allows the heat capacity to be written in terms of the thermodynamic functions internal energy, U, and enthalpy, H.

$$C_p = (\partial H/\partial T)_P \tag{1.1}$$

$$C_v = (\partial U/\partial T)_V. \tag{1.2}$$

C_v is the form most readily obtained from theoretical work. It is difficult to measure for solids and, if required, must be obtained from C_p. C_p and C_v are related.[1]

$$C_p - C_v = \alpha^2 TV/\kappa \qquad (1.3)$$

where

$$\text{isobaric expansivity } \alpha = (1/V)(\partial V/\partial T)_P \qquad (1.4)$$

$$\text{isothermal compressibility } \kappa = -(1/V)(\partial V/\partial P)_T \qquad (1.5)$$

Equation (1.3) is always positive so C_p is always larger than C_v. Though expansivity and compressibility can be measured experimentally, this is often difficult.

The thermodynamic functions...

A knowledge of the thermodynamic functions, Gibbs energy, enthalpy and entropy for example, is valuable in describing the properties of materials. Of particular importance is a knowledge of the relative values of these functions as these determine chemical stability and reactivity.

... enthalpy...

It is clear from the definition of C_p (equation 1.1) that this property can be used directly to give values for changes in enthalpy with temperature.

$$H(T2) - H(T1) = \int_{T1}^{T2} C_p . dT \qquad (1.6)$$

Only relative enthalpies can be obtained in this way. If an absolute scale is required, it is necessary to choose some convenient, though arbitrary, standard state and define its enthalpy. For this reason, in tabulations of thermodynamic data, enthalpies are listed as, for example, $H - H$(at 0 K) or $H - H$(at 298.15 K).

A similar problem arises with formation enthalpies. In this case, the formation enthalpies of the elements are defined as zero at 1 atm (101 325 N m^{-2}). Formation enthalpy values

for compounds are provided by heat of reaction measurements. The use of combustion or bomb calorimetry together with Hess's law calculations has produced data for a wide range of compounds.[3]

In some cases, such as combustion in oxygen or halogens,[4] reaction of the elements gives formation enthalpies directly. Sometimes more circuitous methods are necessary.[5,6]

How the various experimental techniques are used together to give extensive enthalpy plots can be seen in reference 7 where adiabatic, drop and solution calorimetry are used to provide thermodynamic data for the lithium silicates Li_2SiO_3 and $Li_2Si_2O_5$.

Reaction calorimetry allows one to determine energy changes occurring during a reaction. Related calorimetric techniques can be used to measure energy changes occurring during changes of phase. The most commonly used of these methods is differential scanning calorimetry (d.s.c.). Using this technique both enthalpy and entropy changes occurring during the transition can be measured since, at equilibrium,

$$\Delta_{tr}H = T\Delta_{tr}S.$$

The phase change enthalpy (or entropy) can also be obtained by observing the effect of pressure on the transition temperature

$$[S(\text{phase 2}) - S(\text{phase 1})](dP/dT) = V(\text{phase 2}) - V(\text{phase 1}).$$

A study of this type has recently appeared describing several of the phase transitions in silver iodide.[8] In that work, values obtained by both direct and indirect d.s.c. methods are compared.

The state function entropy may be defined[2]

$$S(T2) - S(T1) = \int_{T1}^{T2} đq(\text{reversible})/T. \qquad (1.7)$$

In a system at constant pressure

$$C_p = (đq/đT)_P.$$

Combining the two equations

$$S(T2) - S(T1) = \int_{T1}^{T2} (C_p/T).dT. \qquad (1.8)$$

Thus, if we have a heat capacity function between $T1$ and $T2$, the entropy change involved in the change in temperature can be evaluated. Further, the third law of thermodynamics postulates that the entropy of a perfectly crystalline solid is zero at 0 K. If $T1$ in equation (1.8) is 0 K, then the total entropy of the material at any temperature can be obtained from heat capacity measurements alone.

Heat capacity measurements near 0 K are difficult. The function must therefore be extrapolated to zero from the lowest temperature of measurement. It is assumed that there are no heat capacity anomalies in that temperature region, though such anomalies are not uncommon.

Experimental temperatures very close to 0 K can now be obtained. For example a calorimeter has been described with a resolution of 10^{-11} J K^{-1} at temperatures below 0.1 mK.[9] It should be noted that as the temperature approaches zero, very small heat capacity anomalies can have a significant effect on the calculated entropy.

Some materials do not form perfect crystals at 0 K. These compounds are said to possess residual entropy. Carbon monoxide is a simple example. For these compounds it is possible to determine

the residual entropy by comparison of the calorimetric value with that obtained by some other method. Since the comparisons are generally made at room temperature, extremely good experimental data are required as differences of only one or two per cent may be involved. A review of these comparisons for hydrates is given in reference 10 (p 486-495 and 502-503).

It has been suggested that some solid electrolytes possess residual entropy.[11] This would be possible if positional disorder of the conducting ion were 'frozen in' at 0 K. The work described in this thesis does not extend to low enough temperature for an estimate of total calorimetric entropy to be made. In any case, sufficient complementary data are not available. There is considerable uncertainty in the value given for the residual entropy in $RbAg_4I_5$ so the conclusions of that work[11] must be treated with caution.

Pitzer,[12] using his own and Kelly's data,[13] concluded that silver iodide retains no disorder at 0 K.

...and Gibbs energy

Changes in Gibbs energy occurring during a reaction can be obtained by combining enthalpy and entropy data.

In many cases, particularly for reactions in solution or in the gas phase, the most usual way of determining Gibbs energy changes is by means of equilibrium constant (K) measurements

$$\Delta_r G^{\ominus} = -RT \ln K^{\ominus}. \qquad (1.9)$$

For a general discussion see chapters 5-7 of reference 2.

A further method for determining Gibbs energy changes, which is particularly suitable for solid electrolyte systems, is based on the measurement of cell e.m.f. (E)

$$\Delta_r G = -zFE \qquad (1.10)$$

where F is the Faraday constant and z is the number of electrons transferred in the reaction equation. Differentiation of equation (1.10) allows the method to be extended to the determination of reaction entropy

$$\Delta_r S = (\partial E/\partial T)_P zF. \qquad (1.11)$$

Some examples of these determinations, their scope and experimental details are given in references 14-16 for solid state systems.

Extensive studies of this type have been made for silver iodide[17] and silver sulphide.[18] The results are probably not as reliable as those obtained by other methods. On the other hand, the method can be applied in situations where it is difficult to obtain data by other means. Topol and Owens, for example,[19] have determined the relative stabilities of compounds and mixtures in the systems AgI-MI where M = Rb, K, NH_4. These contain the electrolytes MAg_4I_5.

An extension of their method to compounds in the system AgI-$N(CH_3)_4I$ is clearly possible. The heat capacity of one of these compounds is considered in chapter 11.

Atomic motion

The energy introduced into the sample is stored in the form of vibrations of the atoms. Each atom may be taken to be a point vibrating as a harmonic oscillator about its lattice position - or rather as three oscillators since the vibration may be resolved into three components.

The energy, ϵ, of a harmonic oscillator can be written

$$\epsilon = \tfrac{1}{2}\hbar\omega + n\hbar\omega \qquad (1.12)$$

where $\hbar$ is Plank's constant divided by 2π, ω is the angular frequency of oscillation and n is an integer. The term $\hbar\omega/2$ is the zero point energy of the oscillator and makes no contribution to the heat capacity.

The average energy of an oscillator in a system containing a very large number of particles, each with a vibrational frequency ω, is[20]

$$\epsilon_{av} = \hbar\omega/[\exp(\hbar\omega/kT) - 1]. \tag{1.13}$$

Einstein

If the solid is allowed just one vibrational frequency, the total thermodynamic energy for N atoms can be written

$$U = 3N\epsilon_{av} \tag{1.14}$$

and the heat capacity (C_v as the solid is not allowed to expand)

$$C_v = d(3N\epsilon_{av})/dT. \tag{1.15}$$

Evaluation of equation (1.15) shows that it has the same form as experimental heat capacity curves (figure 1.1). That is, it approaches zero at low temperature and a maximum, $3NR$, at higher temperature. Figure 1.1 illustrates why different solids, with different characteristic frequencies, reach the maximum at different temperatures.

Einstein's curves are not expected to agree exactly with experimental results since the assumption of a single vibrational frequency is too great. Even so, such functions can be used to estimate the contribution of individual vibrating species to the heat capacity of a solid. This has been done, for example, in a study of the effect of the mobile cations on the low temperature heat capacity of β-alumina solid electrolytes.[21]

The allowed ω values

To obtain calculated heat capacity functions that agree more closely with experimental data, a more realistic estimate of the allowed vibrational frequencies is necessary. The system is allocated a range of frequencies, for each of which there is an associated average energy $\epsilon_{i\mathrm{av}}$. The total vibrational energy, E, is

$$E = \Sigma_i g_i \epsilon_{i\mathrm{av}} \qquad (1.16)$$

where g_i is the number of harmonic oscillators of frequency ω_i. If g_i can be defined by a continuous function

$$E = \int \epsilon_{i\mathrm{av}} g_i \, \mathrm{d}\omega \, . \qquad (1.17)$$

It is then necessary to obtain the function g_i and the limits of integration.

Debye

The vibrations of a Debye solid are those of acoustic waves in a solid continuum. Again, as in the Einstein case, we are only interested in the vibrational or 'lattice' heat capacity so the thermodynamic energy, U, is equated with E in equation (1.17). A Debye heat capacity curve is shown in figure 1.1. In figure 1.2, the shapes of the g_i functions for Einstein and Debye models are given.

At very low temperatures the Debye model predicts that[23-25]

$$C_{\mathrm{v}} \propto T^3 \, . \qquad (1.18)$$

Considerable effort has been devoted to experimental verification of this dependence, though there has been debate about how low the temperature would have to be before such dependence could be expected.[26]

For many materials, deviation from Debye behaviour is significant. Much of this deviation can be put down to deficiencies in the frequency distribution g_i.

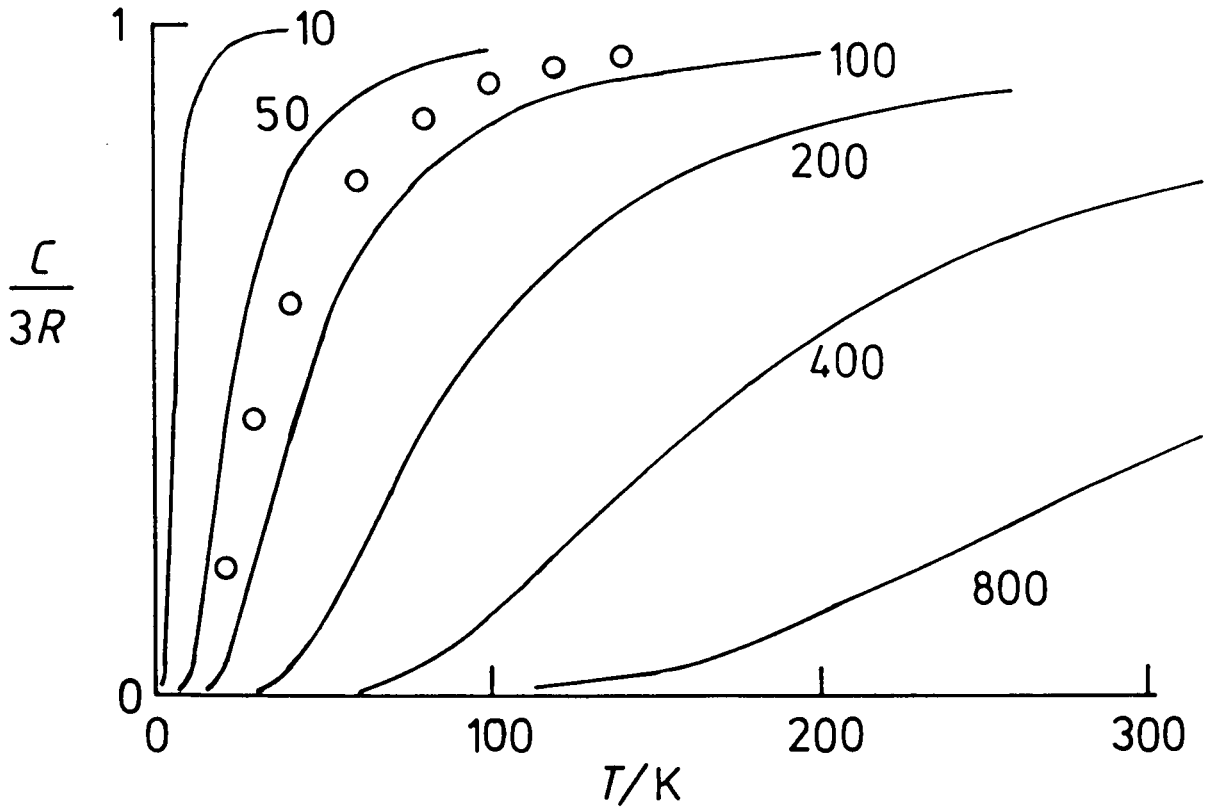

Figure 1.1 Heat capacity functions for harmonic oscillators: solid lines Einstein $\bar{\nu}_E/cm^{-1}$ values marked against the curves; o Debye ($\bar{\nu}_D/cm^{-1}$ = 100).

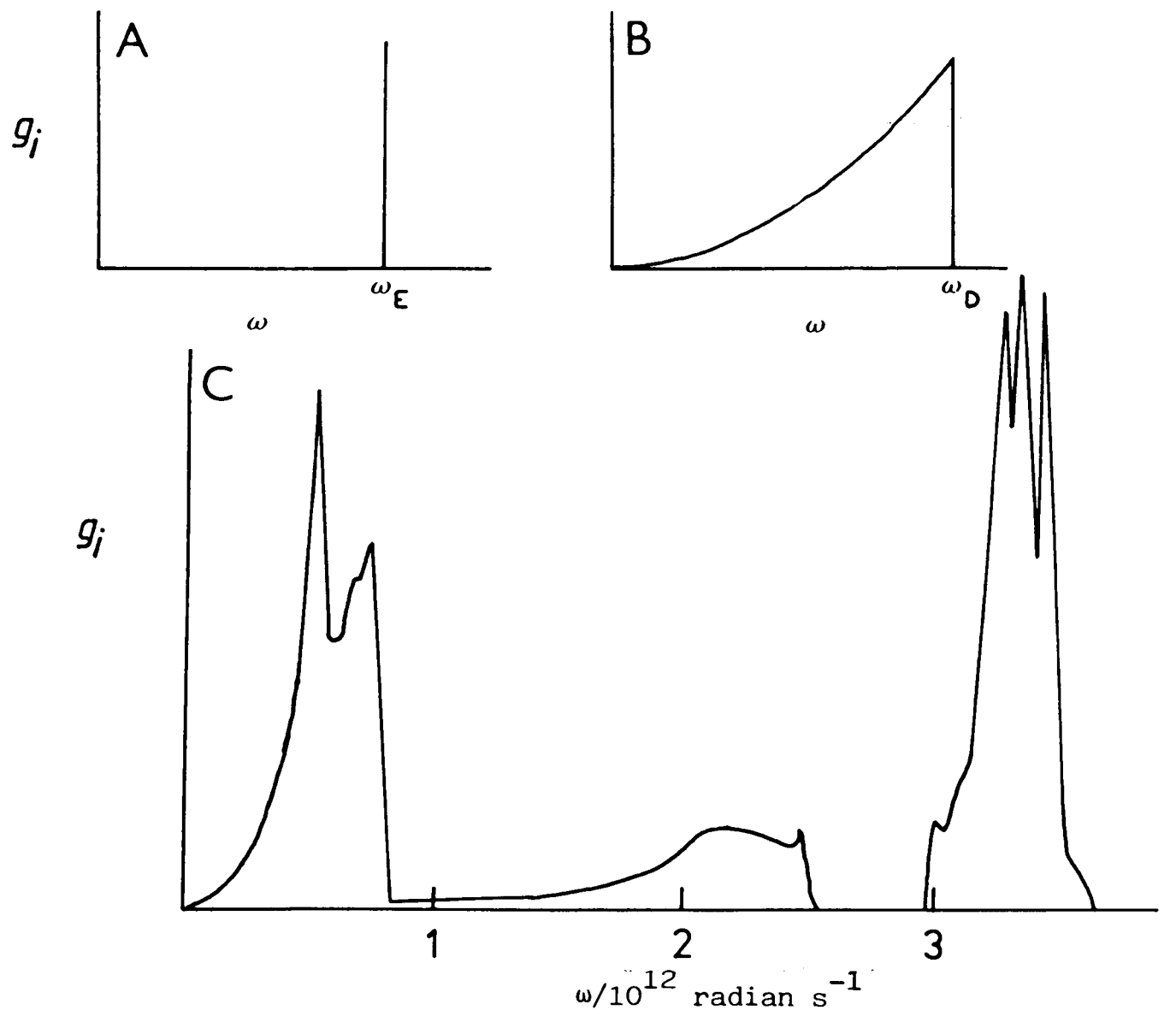

Figure 1.2 The shapes of the frequency distribution functions, g_i: A Einstein; B Debye; C a real solid, silver iodide.[28]

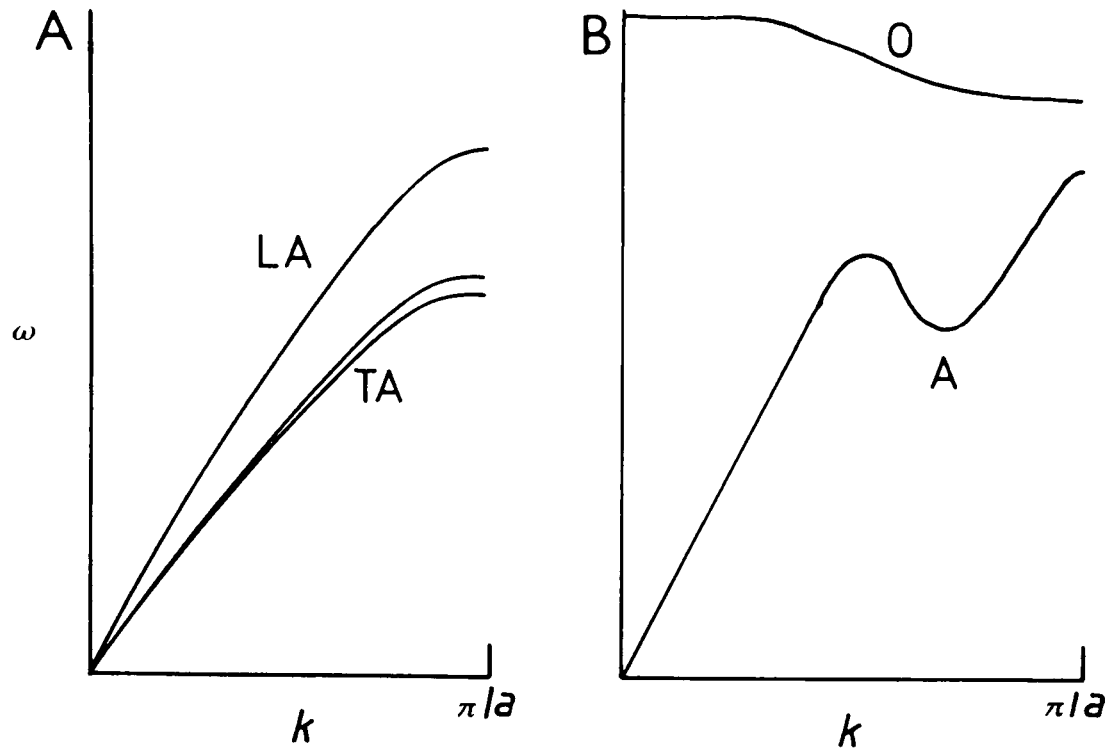

Figure 1.3 Frequency against wavenumber plots: A a linear one atom-type chain showing one longitudinal (LA) and two transverse (TA) acoustic modes; B an optic mode (O) arising from inclusion of a second atom type, and the effect on an acoustic mode (A) of second neighbour interactions.[25] a is the atom-atom spacing.

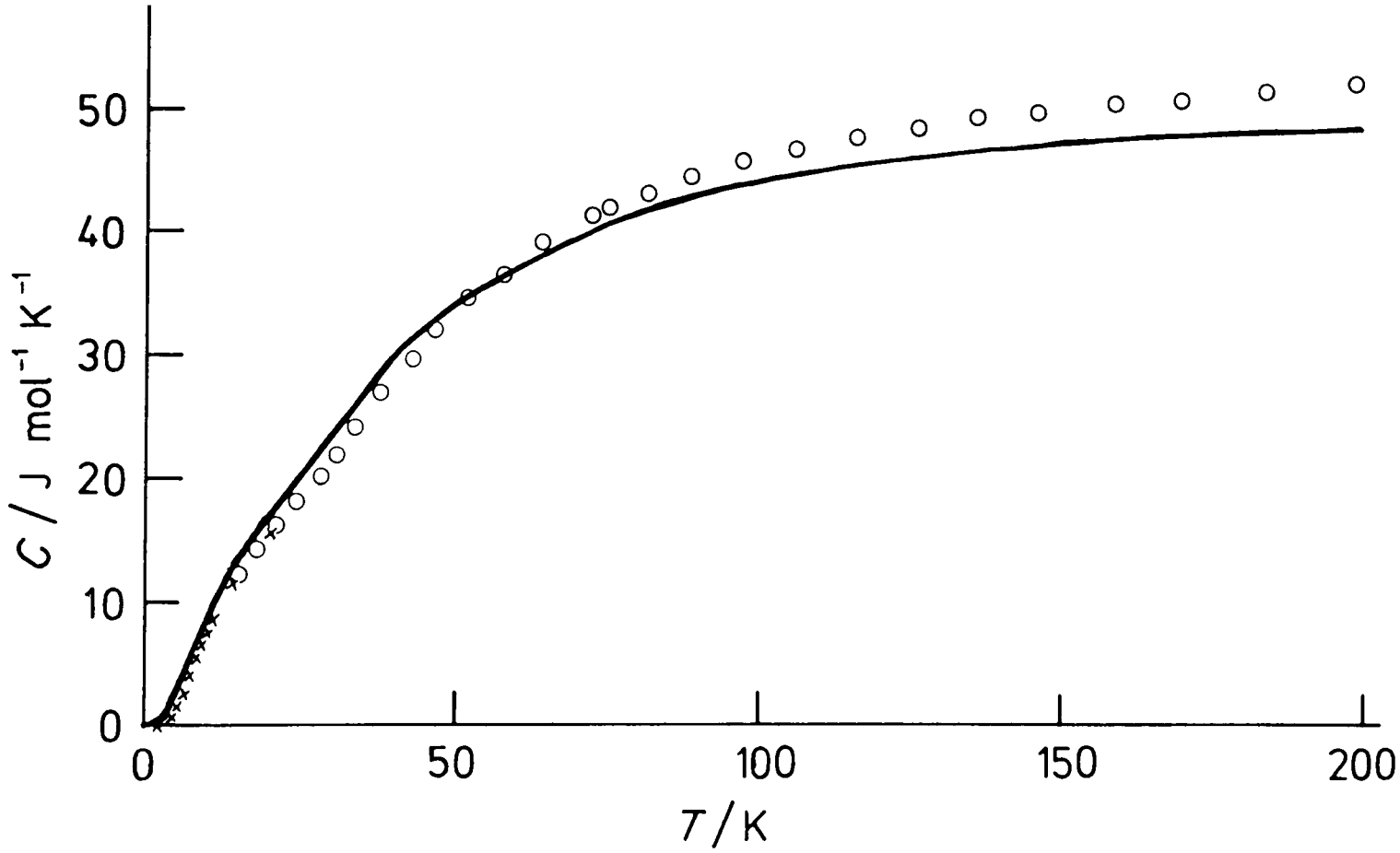

Figure 1.4 The calculated heat capacity of silver iodide [28] (solid line): experimental points from references 12 (o) and 29 (x). An error in the units of reference 29 has been corrected and all [illegible] calories to joules.

Beyond Debye

Calculations of the frequencies available to chains of atoms vibrating as harmonic oscillators indicate that the frequencies are not the same as those allowed in a continuum.[23-25] A simple linear relationship no longer exists between frequency and wavevector, k ($|k| = 2\pi/\lambda$). The new equations relating ω and k are known as 'dispersion relationships'. For a one atom-type chain with only nearest neighbour interactions, the dispersion relationship is illustrated in figure 1.3A. Complications arise if second neighbour interactions are included (figure 1.3B) or if the chain contains a second atom type (figure 1.3B).[25]

From these relationships it is, in principle, possible to calculate the corresponding g_i functions, and hence the vibrational heat capacity of the system. The calculation of dispersion equations for real cases is, however, extremely difficult.

In a few cases sufficiently detailed data have been obtained using neutron inelastic spectroscopy; for example,[27,28] the low temperature heat capacities of the solid electrolytes lithium nitride and silver iodide have been calculated (see figures 1.2C and 1.4).

The crystalline Ag^+ electrolytes studied in this work are thought to behave as normal ionic solids at low temperatures,[29] though no studies below 77 K were made during this work.

Some solid electrolytes are unusual in that they exhibit anomalously high low temperature heat capacities; for example, β-alumina,[21,30] lithium nitride,[31] the ceramic material nasicon and some minerals.[32] The low temperature behaviour of these materials has much in common with that observed in glasses (for a brief review of glass properties see reference 33).

Anharmonicity

A number of factors contribute to the differences between calculated lattice heat capacities and experimental heat capacities, among which are magnetic and electronic effects. These, however, are not considered in this thesis.

As the temperature of a solid is raised, the constituent atoms deviate further and further from harmonic behaviour.

The harmonic oscillator model predicts that

(i) there is no thermal expansion

(ii) atom-atom force constants are independent of temperature and pressure

(iii) isothermal and adiabatic properties are the same

(iv) the heat capacity approaches a maximum as the temperature rises

(v) the atoms are tied to fixed lattice points

(vi) the various lattice vibrations are independent of one another

(vii) there are no crystal boundary effects.

Though these predictions are not strictly correct, the harmonic oscillator remains the best model available, and improvements to account for anharmonicity are difficult.[25]

References to chapter 1

1 See for example M L McGlashan, Chemical Thermodynamics, Academic Press, 1979.

2 E B Smith, Chemical Thermodynamics, Clarendon, 2nd edn, 1978.

3 Chemical Thermodynamics Volume 1, Specialist Periodical Report, The Chemical Society, 1973: M L McGlashan p 1; E F G Herrington p 31; A J Head p 95.

4 M N Jones and H A Skinner in Annual Reports C, The Royal Society of Chemistry, 1979, 76, 253.

5 D R Torgeson and Th G Sahama, *J Amer Chem Soc*, 1948, 70, 2156.

6 US Bureau of Mines Circular 8853, 1981: E J Prosen p 152; J M Stuve p 161; K O Bennington p 173.

7 F O Bennington, M J Ferante and J M Stuve, US Bureau of Mines Report of Investigations RI 8187, 1976.

8 B-E Mellander, B Baranowski and A Lunden, *Phys Rev B*, 1981, 23, 3770.

9 A Cruz-Uribe and J V Trefny, *J Phys E*, 1982, 15, 1054.

10 N G Parsonage and L A K Staveley, Disorder in Crystals, Clarendon, 1978.

11 W V Johnston, H Wiedersich and G W Lindberg, *J Chem Phys*, 1969, 51, 3739.

12 K S Pitzer, *J Amer Chem Soc*, 1941, 63, 516.

13 K K Kelly, US Bureau of Mines Bulletin no. 350, 1932; no. 374, 1936.

14 Y K Rao, reference 6, p 179.

15 S C Schaefer, reference 6, p 203; S C Schaefer, US Bureau of Mines Report of Investigations RI 8301, 1978; RI 8405, 1980.

16 K Kiukkola and C Wagner, *J Electrochem Soc*, 1957, 104, 308; D O Raleigh, *Progr in Solid State Chem*, 1967, 3, 83.

17 N E Quaranta and J C Bazan, *Solid State Ionics*, 1983, 11, 75.

18 H Schmalzried, *Progr in Solid State Chem*, 1981, 13, 119.

19 L E Topol and B B Owens, *J Phys Chem*, 1968, 72, 2106.

20 R P H Gasser and W G Richards, Entropy and Energy Levels, Clarendon, 1974.

21 D B McWhan, C M Varma, F L S Hsu and J P Remeika, *Phys Rev B*, 1977, 15, 553.

22 E S R Gopal, Specific Heats at Low Temperatures, Heywood, 1966.

23 C Kittel, Introduction to Solid State Physics, Wiley, 5th edn, 1976.

24 H M Rosenberg, The Solid State, Clarendon, 2nd edn, 1978.

25 W Cochran, The Dynamics of Atoms in Crystals, Arnold, 1973.

26 M Blackman, *Rep Progr in Physics*, 1941, 8, 11.

27 W Kress, H Grimm, W Press and J Lefebvre, *Phys Rev B*, 1980, 22, 4620.

28 W Bührer, R M Nicklow and P Brüesch, *Phys Rev B*, 1978, 17, 3362.

29 H G Leduc and L B Coleman, *Solid State Ionics*, 1981, 5, 469.

30 P J Anthony and A C Anderson, *Phys Rev B*, 1977, 16, 3827.

31 E Gmelin and K Guckelsberger, *J Phys C*, 1981, 14, L21.

32 E Gmelin and R Villar, *Physica B*, 1981, 108, 1003.

33 S Hunklinger, *J Physique, Colloque C6 suppl 8*, 1978, C6-1444.

2

Phase Transitions

Under different conditions of temperature and pressure, many materials exist in different structural forms. The most obvious examples of this behaviour are solid-liquid and liquid-gas transitions. There are, however, many examples of solid-solid transitions. Each solid form is characterized by its own symmetry properties and thermodynamic functions. Transitions between solid phases are visible as kinks or discontinuities in the experimental heat capacity curves.

The transitions of interest in this work involve the movement of atoms relative to one another. Others involve more subtle effects, changes in electronic or magnetic properties, but these will not be discussed here.

Classification of phase transitions

A number of authors have attempted to classify phase transitions in terms of the shape of the thermodynamic functions close to the phase change. One of the first classifications was that of Ehrenfest, though his scheme has been much modified and extended since.[1]

Consider a solid with two forms A and B that transform at a temperature T_{AB}. At T_{AB} the phases are in equilibrium so the chemical potential of the compound in phase A will equal that in B:

$$\mu_A = \mu_B \ .$$

G will thus be a continuous function of temperature. This may not be true, however, of other thermodynamic properties. The Ehrenfest classification is based on finding discontinuities in derivatives of the free energy.

For example, at constant temperature, the first order derivative of Gibbs energy with respect to pressure is

$$(\partial G/\partial P)_T = V$$

while at constant pressure

$$(\partial G/\partial T)_P = -S$$

Discontinuities in these first derivative functions give rise to first order transitions. The behaviour of G,H and S for a first order transition is shown schematically in figure 2.1. Some real examples, taken from this work are shown in figure 2.2.

First order changes are characterized by latent heats, volume changes, thermal hysteresis and (often) large structural changes. The occurrence of latent heats makes d.t.a. and d.s.c. particularly useful for studying these transitions. Thermal hysteresis is evidenced by the different transition temperatures obtained during heating and cooling cycles (see later chapters).

Second order transitions occur if there is a discontinuity in a second order derivative

$$(\partial^2 G/\partial T^2)_P = -C_p/T$$

$$(\partial^2 G/\partial P^2)_T = (\partial V/\partial P)_T \; [= -V\kappa]$$

$$(\partial^2 G/\partial P \partial T) = (\partial V/\partial T)_P \; [= V\alpha]$$

where α and κ are defined in chapter 1. The behaviour of G,H and C_p/T for a second order transition is illustrated in figure 2.3.

Higher order behaviour can be described but such a description is of doubtful physical significance. Many authors prefer to

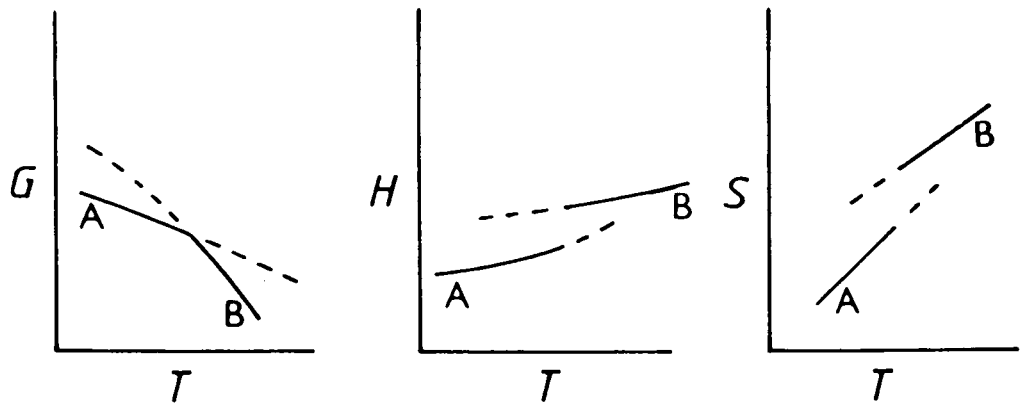

Figure 2.1 The behaviour of the thermodynamic quantities Gibbs energy, enthalpy and entropy as a function of temperature close to a first order phase transition. A and B refer to the functions for the low and high temperature forms, respectively.

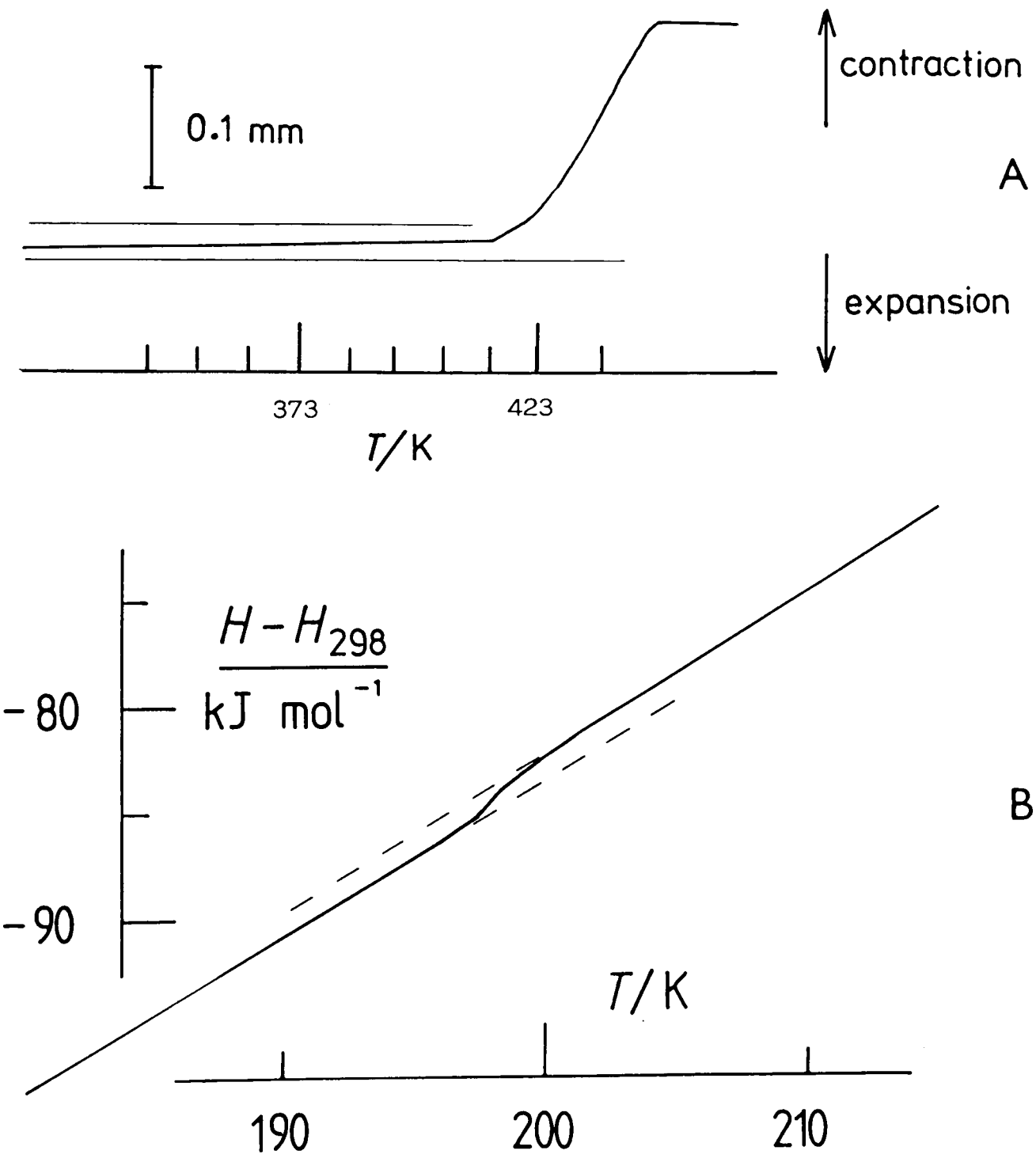

Figure 2.2 For caption see following page.

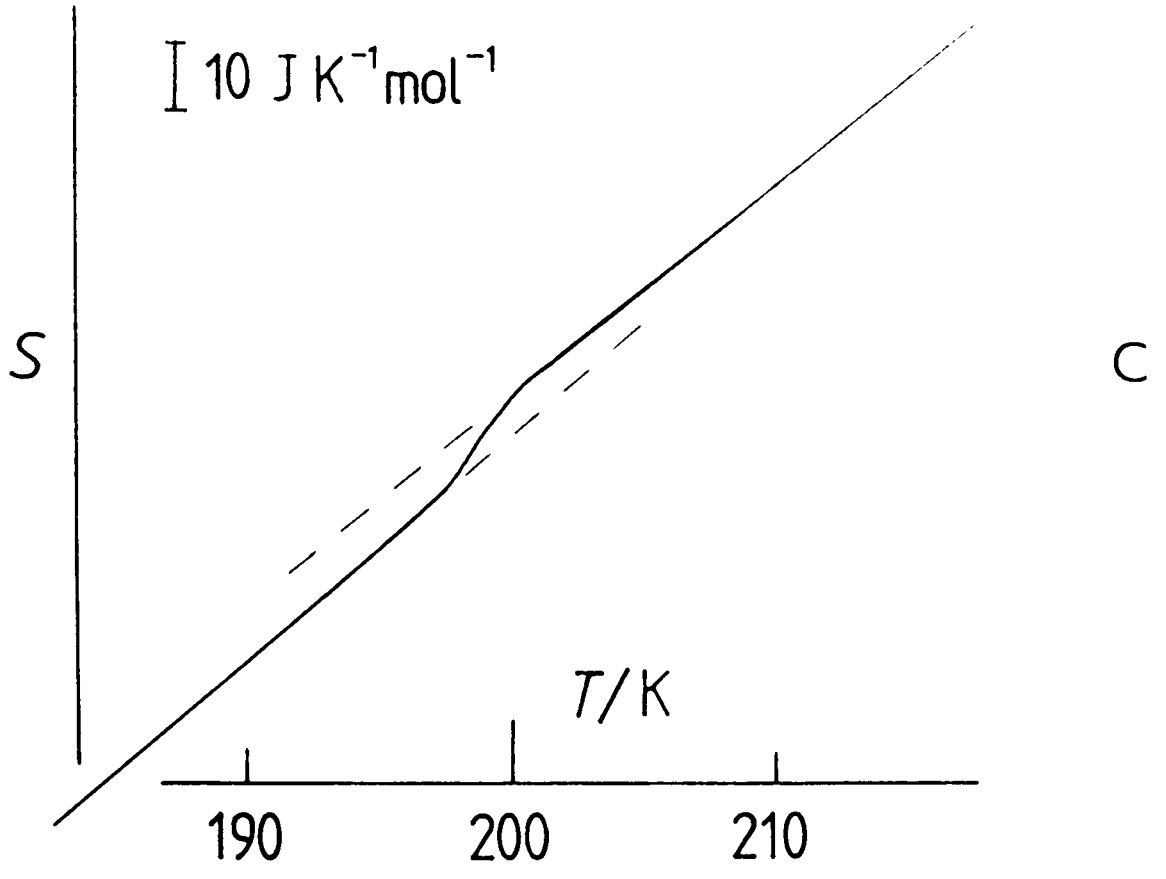

Figure 2.2 Some of the characteristics of first order transitions observed during this work. A, Contraction of a silver iodide pellet (thickness about 5 mm) at the 419 K transition as seen by thermomechanical analysis. B and C, discontinuities in enthalpy and entropy, respectively, at the lower first order transition in $Ag_{13}I_9W_2O_8$.

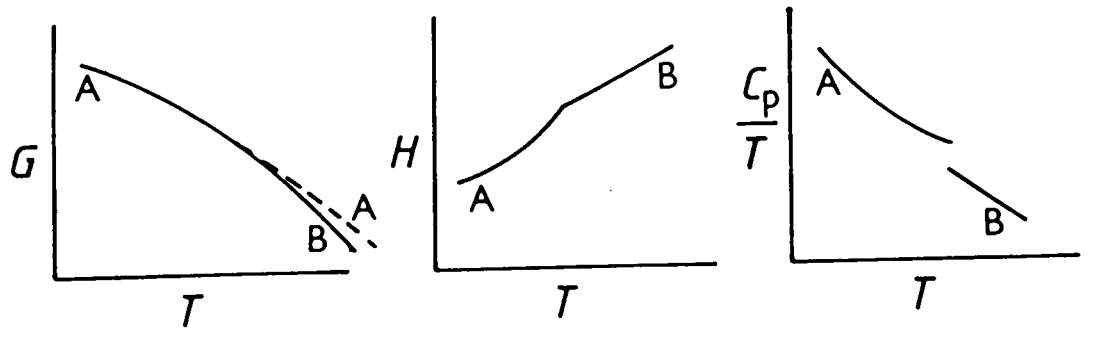

Figure 2.3 The behaviour of the thermodynamic quantities Gibbs energy, enthalpy and C_p/T for a second order transition. C_p/T is a second derivative of Gibbs energy.

divide transitions into just two classes[2]

(i) first order or discontinuous

(ii) continuous, which covers all higher order Ehrenfest transitions.

This classification fits in well with the requirements of the most common theoretical treatment of phase transitions, that of Landau.[3,4]

It should be borne in mind that the two classes represent the limits of a range of behaviour rather than two distinct types.

Many theories have been produced to describe the behaviour of solids close to phase transitions.[5] Only two examples will be outlined here.

Order parameters

It is useful to be able to express thermodynamic functions in terms of some property which changes at the transition. A variable widely used for this purpose is known as the 'order parameter', so named because it was first used to describe order disorder transitions of the type shown by β-brass($Zn_{48}Cu_{52}$).

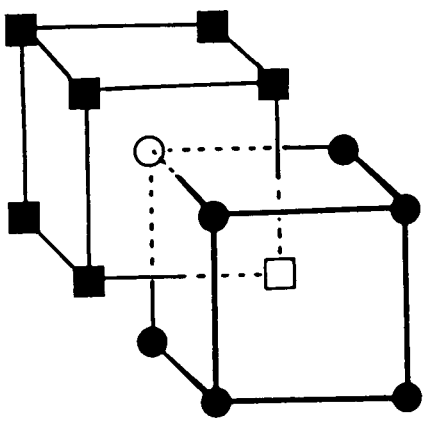

The body centred structure can be described as two interlocking simple cubic systems, represented in the drawing by circles and squares. At low temperature one system is occupied by copper and the other by zinc. As the temperature is raised, disordering occurs and atoms begin to appear on 'wrong' sites until, above 740 K, the atoms are totally disordered over all sites. This provides one of the simplest definitions of order parameter

$$\xi = \frac{\text{number of atoms on right sites - number of atoms on wrong sites}}{\text{number of atoms on right sites + number of atoms on wrong sites}}$$

where $0<\xi<1$.

The order parameter thus defined is usually known as the 'long range' order parameter. In a real system some local ordering of near neighbours will occur, so short range order, defined in terms of near neighbours, will generally be greater than long range order.

The term order parameter is not restricted to order-disorder transitions. Any changing property may be used as a basis for ξ. Two examples of the definition of order parameter are given in figure 2.4. One case is clearly similar to that described here, while in the other neither $\xi=0$ nor $\xi=1$ can be said to represent loss of order.

Landau theory

The Gibbs energy is considered to be a function of temperature and order parameter[4]

$$G \equiv G(T,\xi).$$

(Note that where I use Gibbs energy, it is often more usual to use Helmholtz energy, A, where

$$G = H - TS$$

$$A = U - TS.)$$

Landau assumed that G can be represented as a power series in ξ. Since ξ is less than unity, the series will converge and higher powers of ξ will become less and less significant. In addition, since $\xi=1 \equiv \xi=-1$, only even powers of ξ are significant. In the β-brass case, $\xi=-1$ corresponds to the Cu and Zn atoms having swopped lattice positions. For all practical purposes this is identical with the $\xi=1$ situation.

Even at quite a simple level Landau theory is able to predict many of the changes in thermodynamic properties close to phase transitions. In addition some differences between first order and continuous transitions can be explained.[3]

A Landau-type theory, known as the 'quasi-chemical' model, has been widely applied in theoretical studies of phase transitions in solid electrolytes.[6,7] In this model, the system free energy, usually Helmholtz energy, is considered to be a combination of two terms. One is an energy term as used by Landau and the other is a configurational term resulting from the large configurational entropy of the mobile ions.[6,7]

There are limitations to the application of Landau theory. To some extent, all Landau transitions are continuous. At least they begin as continuous, though some may be interrupted at a critical temperature where they become discontinuous. The continuous nature of the transition imposes restrictions on the allowed symmetry relationships between adjacent phases. The symmetry of the low temperature form is lower than that of the high temperature form; its symmetry belongs to a sub-group of the high temperature form.[4,8]

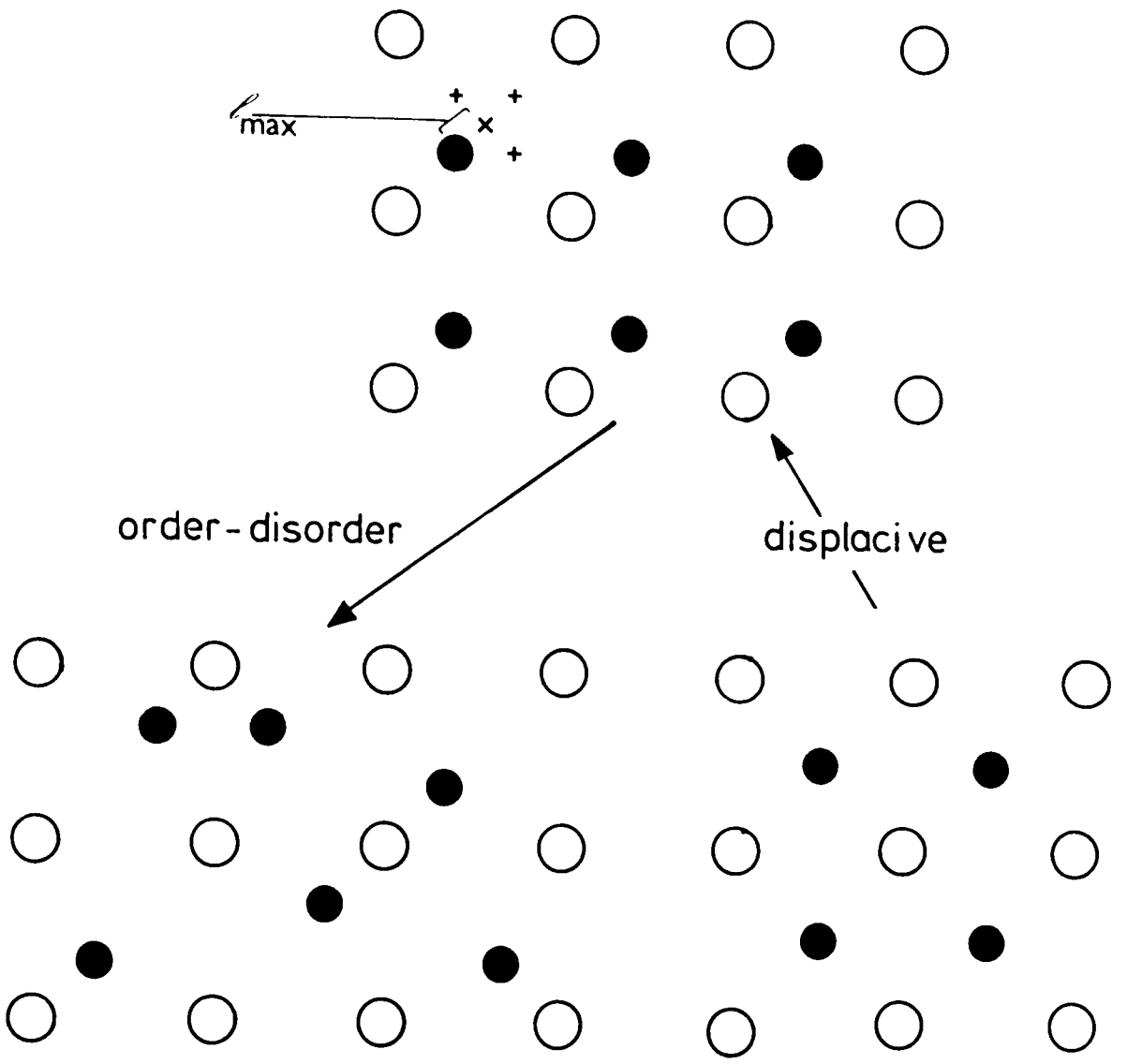

Figure 2.4 A two dimensional representation of two types of continuous transition for which an order parameter can be defined simply.

Order-disorder: the black atoms are disordered among their own sites and those marked +

$$\xi = \frac{\text{number of black atoms on their correct sites } (\bullet) \text{ minus } \tfrac{1}{3} \text{ number of black atoms on wrong sites } (+)}{\tfrac{1}{4} \text{ total number of sites}}$$

For complete order (top) $\xi = 1$; for disorder $\xi = 0$ since there will be three times as many atoms on wrong sites as on right sites making the numerator zero.

Displacive: if the value of the displacement ℓ in the lower phase is zero, increasing to ℓ_{max} in the upper phase then

$$\xi = (\ell_{max} - \ell)/\ell_{max}$$

In the 'ordered' phase $\xi = 1$; in the upper 'disordered'

Soft mode theory

In the harmonic oscillator model of a solid, the force tending to restore an atom to its equilibrium position is temperature independent. In a real solid, however, force constants do vary with temperature; the forces are made up of attractive and repulsive components. In some cases, a situation may arise where the variation in these force constants with temperature causes the restoring forces on a vibrating atom to disappear. When this happens, the square of the atom vibrational frequency, ω^2, also approaches zero. This vibrational mode is said to go 'soft'.[9] This behaviour has been observed experimentally by Raman, infra-red and neutron studies.

Examples of such transitions on a two dimensional lattice are given in figure 2.5.

Some of the most detailed studies of this behaviour have been made on solids with the perovskite ($CaTiO_3$) structure, ABX_3. A review of these studies is given in reference 10.

By no means all transitions are characterized by mode softening.

Phase transitions in solid electrolytes

In many solid electrolytes, conductivity becomes significant only at temperatures above a phase transition. The occurrence of these transitions is not essential, however, for the existence of a conducting state. This is obviously true for electrolytes like ß-alumina, but it is also the case for solids like silver bromide and copper(I) iodide. In copper(I) iodide, the conducting state is often associated with the phase transitions

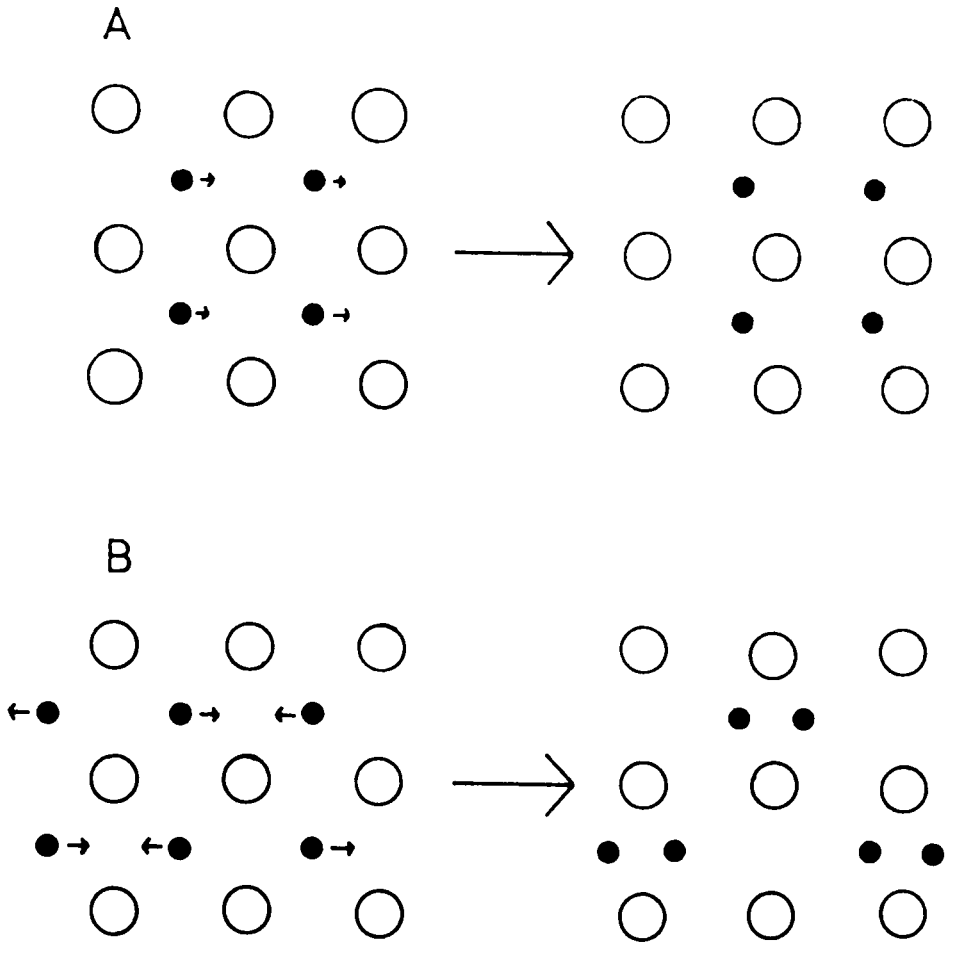

Figure 2.5 Displacive 'soft mode' transitions. The small arrows represent the vibrational mode going 'soft'. A is known as a zone centre phonon, $|k| = 0$, $\lambda = \infty$. B is known as a zone boundary phonon, $|k| = \pi/a$, $\lambda = 2a$ (a is the lattice constant of the left hand phase). Note that in A the unit cell size is unchanged; in B the lattice constant is doubled.

even though conductivity is also significant in γ-CuI at 500 K (see chapter 12).[11]

Solid electrolytes provide examples of a very wide range of structural phase transitions. Some, like that in silver iodide (see chapter 10), are clearly first order and are associated with a large increase in ionic conductivity. Others are continuous transitions of an order-disorder type similar to that in β-brass. This is the case for the fluorite and anti-fluorite structures where a gradual transition, often called a Faraday transition, extends over a large temperature region. In the fluorite structures, CaF_2, $SrCl_2$, PbF_2, anion conductivity results from substantial disordering of one set of ions over their own low temperature sites and a number of interstitial (Frenkel) sites. Description of an order parameter on the basis of anion disorder is possible but difficult because agreement has not been reached on which interstitial sites are occupied. In fact the situation may be complicated by different interstitial sites becoming available over different temperature ranges. Qualitatively the heat capacity behaviour of these compounds is similar to that observed in β-brass.[12,13]

The plots for $[NMe_4]_2Ag_{13}I_{15}$ and (pyridinium)Ag_5I_6 (chapter 11) demonstrate the variety of heat capacity behaviour associated with continuous transitions.

In other cases, more than one transition may be involved; $Ag_{13}I_9W_2O_8$ (chapter 8), the compounds MAg_4I_5 (M = K, Rb, NH_4)[14,15] or possibly $HgAg_2I_4$.[16]

The compound $RbAg_4I_5$ illustrates the problems involved in classifying phase transitions. Theoretical studies based on

heat capacity results[15] indicated that the transition should be considered as continuous. More recent results, however, indicate that the transition has a significant first order character.[17,18]

A number of classification systems peculiar to solid electrolyte studies have been proposed[19] but these are of limited scope and are not considered in this thesis.

Glass transitions

One other transition type is mentioned later in the experimental chapters. This, the glass transition, does not fit well into any classification system. It is a transition between two non-equilibrium states, the supercooled liquid and the glass. It often exhibits a number of physical characteristics normally shown by first order transitions, volume change, hysteresis and apparent latent heat effects in d.t.a. and d.s.c. studies. It is on the other hand often described as a second order transition since no symmetry change is involved in the transition. A continuous transition is certainly what one would expect on the basis of plots of thermodynamic functions for'ideal' glass forming behaviour.[20,21] In fact, theoretical models may be chosen to predict either first or second order behaviour.[22]

Glass heat capacity, transition temperature and the thermal behaviour observed at the transition are markedly dependent not only on sample history but also on the rate at which the measurements are carried out. For these reasons, and since it may never be possible to observe an ideal glass transition,[22]

it is perhaps best if this transition type remains outside the classification system for transitions between equilibrium states.

Pressure and other variables

In all cases considered in this work phase changes are induced by changing the system temperature. Phase changes can equally well be brought about by changes in pressure.[23] Other variables may also affect the relative stabilities of solid phases. Order-disorder transitions have been induced by grinding,[24] and zinc blende-wurtzite equilibria are sensitive to grinding and surface area.[25]

Calorimetric studies of the effects of applied stress on phase transitions have been made.[26]

Sample impurities and inhomogeneities are also known to affect transition behaviour, and these have been proposed as an explanation for the differences in experimental results for the 208 K transition of $RbAg_4I_5$.[15,18]

References to chapter 2

1 N G Parsonage and L A K Staveley, Disorder in Crystals, Clarendon, 1978, chapter 1.

2 A R Ubbelohde, *Quart Rev*, 1957, 11, 246.

3 C Kittel and H Kroemer, Thermal Physics, W H Freeman, 1980.

4 L D Landau and E M Lifshitz, Course of Theoretical Physics Volume 5, Statistical Physics, Pergamon, 2nd edn, 1968.

5 Many of these are discussed briefly in chapter 3 of reference 1.

6 S Strässler and C Kittel, *Phys Rev A*, 1965, 139, 758; M J Rice, S Strässler and G A Toombs, *Phys Rev Letters*, 1974, 32, 596.

7 M B Salamon in Physics of Superionic Conductors (Topics in Current Physics 15), ed M B Salamon, Springer-Verlag, 1975, p 175.

8 W Cochran in Structural Phase Transitions and Soft Modes, ed E J Sammuelsen, E Andersen and J Feder, Universitetsforlaget, Oslo, 1971, p 1.

9 W Cochran, The Dynamics of Atoms in Crystals, Arnold, 1973; *Ferroelectrics*, 1981, 35, 3.

10 M E Lines and A M Glass, Principles and Applications of Ferroelectrics and Related Materials, Clarendon, 1979, chapter 8.

11 B K Verma, V Pratup and H B Lal, *Japan J Appl Phys*, 1981, 20, 1665.

12 A S Dworkin and M A Bredig, *J Phys Chem*, 1968, 72, 1277.

13 C E Derrington, A Navrotsky and M O'Keeffe, *Solid State Comm*, 1976, 18, 47.

14 W V Johnston, H Wiedersich and G W Lindberg, *J Chem Phys*, 1969, 51, 3739.

15 R A Vargas, M B Salamon and C P Flynn, *Phys Rev B*, 1977, 17, 269.

16 B Baranowski, M Friesel and A Lunden, *Solid State Ionics*, 1983, 9/10, 1179.

17 J Genossar, A Gordon, M O Steinitz and R Weil, *Solid State Comm*, 1981, 40, 253; M Midorikawa and Y Ishibashi, *J Phys Soc Japan*, 1981, 50, 3837.

18 V N Andreev, V G Goffman, A A Gur'yanov, B P Zakharchenya and F A Chudnovskii, *JETP Letters*, 1982, 36, 73.

19 These are discussed in S Hackwood and R G Linford, *Chem Rev*, 1981, 81, 327.

20 C N R Rao and K J Rao, Phase Transitions in Solids, McGraw-Hill, 1968, p 146-147.

21 J H Gibbs in Modern Aspects of the Vitreous State Volume 1, ed J D Mackenzie, Butterworths, 1960, p 152.

22 R Parthasarathy, K J Rao and C N R Rao, *Chem Soc Rev*, 1983, 12, 361.

23 C W F T Pistorius, *Progr Solid State Chem*, 1976, 11, 1.

24 A E Ermakov, E E Yurchikov, E P Elsukov, V A Barinov and Yu G Chukalkin, *Sov Phys Solid State*, 1982, 24, 1112.

25 K Imamura and M Senna, *J Chem Soc Faraday I*, 1982, 78, 1131; G J Russell, A T Fellows, S Oktik, E Ture and J Woods, *J Mater Sci Letters*, 1982, 1, 176.

26 S Stokka and K Fossheim, *J Phys C*, 1982, 15, 1161.

3

Determination of Heat Capacity by Adiabatic Calorimetry

It was suggested earlier that if we knew the complete dispersion relationships for a solid, we would be able to calculate its heat capacity. Unfortunately these relationships are so complex and incompletely known that this is rarely possible.

The heat capacity must therefore be determined experimentally. Since this work is concerned with solids, only those methods suitable for solids will be considered. The experimental work described in this thesis is based on the adiabatic method [1,2] so this is reviewed in some detail. Some other methods will be described briefly with the emphasis being placed on how they differ from adiabatic calorimetry and how the results obtained complement those derived from adiabatic calorimetry.

Heat capacity

Heat capacity is a measure of the variation of sample energy - enthalpy in the case of constant pressure experiments - with temperature.

From chapter 1

$$C_p = (\partial H/\partial T)_p \qquad (3.1)$$

To make such measurements, it is clear that we require some means of introducing energy into the sample and some means of measuring the sample temperature.

Adiabatic - without gain or loss of heat

Ideally the sample should be kept in an adiabatic environment; that is, it does not exchange heat with its surroundings. Under such conditions it can be maintained indefinitely at a constant temperature, T. One further condition is necessary; the sample must be in an equilibrium state or, if in a metastable state, its rate of conversion to the equilibrium state must be negligibly small. If this condition is not met, spontaneous changes within the sample will cause the sample temperature to change.

Once the sample is at a stable equilibrium temperature, we perform work on the sample (converted to heat q) and measure the rise, ΔT, to the new equilibrium temperature. In the limit of infinitely small q and ΔT, we obtain the heat capacity (3.1). In practice the heat capacity is obtained as

$$C_p = q/\Delta T \qquad (3.2)$$

at a temperature $T + \Delta T/2$. This is a good approximation to (3.1) if the variation of heat capacity with temperature is close to linear over the temperature interval of the measurement. If the heat capacity function is curving sharply, corrections can be made[3] but these are not entirely satisfactory.

It is impossible to maintain a sample under truly adiabatic conditions so we must make as close an approximation as we can. Instead of no energy exchange, we attempt to provide an environment in which energy gain and loss are small and equal. Thus the energy exchange makes no contribution to the controlled heat input, q.

A number of precautions are taken in setting up such conditions.

(i) The sample is surrounded completely by a shield. If the shield is at all times at the same temperature as the sample then no net flow of heat should occur between the two. This assumes that both sample and shield surfaces are at a uniform temperature - there are no temperature gradients on the surfaces. During a heating period the shield must follow the sample.

(ii) The sample must be supported within the shield and electrical connections will be required so that measurements can be made. These supports and connections should have low thermal conductivity. In addition, before they approach the sample they should be brought to the temperature of the sample.

(iii) To avoid problems of convection and air conduction, the sample and its shield should be within a vacuum chambe

(iv) Heat exchange by radiation can be minimized by ensuring that all surfaces are of low thermal emissivity. Highly reflecting polished surfaces are often employed; for example, gold or chromium plating.

Heat input

There are a number of methods by which heat can be introduced intc the sample. The simplest and the most common is by means of an electrical resistance heater. Usually this is a wire but other electrical elements can be used.[4,5] Non-electrical methods include radiation absorption by the sample. This method is more commonly applied to a.c. calorimetry (see later) but can be used in adiabatic systems (laser flash calorimetry[6]).

With an electric heater, the measurement of energy input is straightforward. It is a function of voltage drop across the heater, current flowing and heating period. During heating from time t_0 to t_t the energy dissipated can be written as

$$E = \int_{t_0}^{t_t} VI.\mathrm{d}t \qquad (3.3)$$

where V is the voltage drop and I the current flowing. In equation (3.3) V and I may be functions of t. If V and I are constant then

$$E = VI.\Delta t \text{ or } E = (V^2/R)\Delta t \qquad (3.4)$$

where Δt is the heating period and R is the resistance of the heater.

To measure the heat input we require three pieces of information:

(i) heating period

(ii) voltage drop (as a function of time if necessary)

(iii) either current flowing or heater resistance (again as a function of time if necessary).

Temperature

Some form of thermometer is required to measure sample temperature. Since the temperature intervals are small, a few kelvin or less, it is necessary to measure temperature with a high degree of precision. Above about 50 K platinum resistance thermometers have proved to be the most suitable. These are commercially available, are very stable and reliable, and a considerable amount of research has been devoted to cataloguing their characterist

Other wire resistors are also suitable provided that they are stable to thermal cycling. They have the advantage of cheapness and often have a greater resistance variation with temperature than does platinum. For example, Franke and Hegenbarth[8] used a lead resistance thermometer in their heat capacity study of strontium

titanate. Over the limited temperature range studied, they assumed that resistance varied linearly with temperature. More often it is necessary to calibrate the resistor against a standard thermometer and then fit the resulting resistance-temperature relationship to mathematical function.

If the sample heater is a metal resistor, this can also act as a thermometer provided that certain precautions are taken - isolation of the separate items of circuitry, timing of the two functions, etc.

It can be seen from table 3.1 that nickel is a particularly useful thermometer material because of its high sensitivity; twice that of platinum. This property is made use of in some commercial thermometers. Nickel is combined with other metals, mostly manganin, to provide a sensor with a linear temperature against resistance relationship.[9]

At temperatures below about 50 K metals are less suitable because of their low resistivity and small temperature coefficients. In this region carbon or semiconductor (doped silicon, germanium or gallium arsenide, for example) sensors are used. The temperature range of study dictates which type of sensor is chosen. Some examples are shown in table 3.2.

The use of semiconductor thermometers is becoming very much more common over all temperature ranges, and the US National Bureau of Standards has produced a lengthy report on the stability of thermistors.[10]

A single thermistor is suitable only for a limited range of temperature (about 220 - 420 K for the example in table 3.3). This limit arises from the exponential dependence of resistance on temperature. However, over most of its working range a thermistor has an enormous resistance variation, giving it very high sensitivity.

Table 3.1

Resistivities and temperature coefficients of metals at 20 °C *

metal	resistivity / ohm cm	temperature coefficient / ohm cm K^{-1}
copper	10	0.003
lead	22	0.003 9
nickel	7.8	0.006
platinum	10	0.003
constantan	49	0.000 01
manganin	44	0.000 01

* Handbook of Chemistry and Physics, 53rd edn 1972-73, CRC Press, Cleveland Ohio, 1972.

Table 3.2

Approximate resistance values of some low temperature thermometers †

sensor	*R*/ohm	*R*/ohm	*R*/ohm	useful range
(i) carbon	at 100 K	at 3 K	at 0.03 K	
Allen Bradley	100	5000		1-100 K
Speer		200	8000	up to 10 K
(ii) germanium	at 77 K	at 4 K		
CR 2500	15	2500		4-100 K
CR 250		250	several thousand	below 0.3 K

† Carbon Resistance Thermometers, Data Sheet S47; Germanium Resistance Thermometers, Data Sheet S59, Oxford Instruments.

Table 3.3

Resistance changes between 0 °C and 100 °C for two thermometers

sensor	approximate resistance/ohm at 0 °C	at 100 °C
platinum resistance	25	35
thermistor (RS Components 151-221)	16 500	340

This high sensitivity was demonstrated for the d.t.a. instrument built during this work. The temperature difference thermocouples were replaced by two thermistors. These, in a simple bridge circuit with a 1.5 V battery, produced temperature difference signals that could be fed directly to a chart recorder. The thermocouple signals had to be amplified several hundredfold to produce an equivalent signal. The tiny signals were sometimes swamped by other effects such as inductive pick-up from the heater windings.

In table 3.3 the resistance changes between 273 and 373 K are compared for a 25 ohm platinum thermometer and a 5 kohm thermistor

Thermistors are also very small. The example in table 3.3 is an elipsoid bead 2.4 x 1.4 mm with a mass of 0.04 g.

The great sensitivity of thermistors has allowed some very detailed heat capacity measurements to be made by the adiabatic method. For example, Reese and May[11] examined the shape of the heat capacity peak at about 122.5 K in KH_2PO_4. Close to the peak maximum, temperature increments of 0.014 K were used. Similarly, Matsuo et al.,[12] in studying the transition in $SnCl_2.2H_2O$, employed temperature increments of 0.01 - 0.03 K. Their calorimeter contained both a platinum resistance thermometer for normal, about 1 K increment measurements and a thermistor for peak shape studies.

It should be noted that all resistance thermometers act as heaters. It is essential that the heat generated is either negligible relative to other heating effects or that it is accounted for in the heat capacity calculations. It is also important that the heat generated be dissipated otherwise the thermometer will become warmer than the sample.

For platinum resistance thermometers with a room temperature value of about 25 ohm, currents of about 1 mA are usually recommended; lower currents are used for higher resistance values. Semiconductor thermometers have a very high resistance at (usually) the low temperature end of their range so very low currents are required, of the order of micro amps. See for example the references given in table 3.2.

As the temperature range of study rises above room temperature, resistance thermometers give way to thermocouples. A thermocouple for measuring temperature will have a cold junction at some reference temperature and the other junction on the sample. The couple produces a small voltage that is a function of temperature. A wide variety of couples can be used but for accurate work those based on precious metals are most reliable; for example, platinum/platinum-13 % rhodium and gold/gold 0.03 % iron. The signals are small, a few microvolts per kelvin. Some couples, for example copper/constantan or iron/constantan, are more sensitive but they are more susceptible to corrosion, damage due to thermal cycling and impurity effects.[13]

Sensitivity can be improved by use of thermopiles which consist of a number of thermocouples in series.

Despite their poor sensitivity thermocouples are sometimes used in low temperature calorimeters (see for example reference 14 where chromel/0.07 atom % iron in gold is used for the temperature range 4 to 300 K). More often, however, thermocouples are reserved for higher temperature work where signals are larger.[15]

The sensors described so far form the bulk of calorimetric thermometers. However, in principle any property which varies with temperature can be used as the basis for a thermometer.

In quartz crystal thermometers,[16] the crystal resonant frequency varies with temperature. At very low temperatures, the variation of magnetic or nuclear magnetic properties of certain materials can be used.[17]

Thermometry and temperature measurement are the subject of numerous books and reviews.[13,16-19]

Supporting the sample

The sample, thermometer and heater are usually housed within a sample vessel. Ideally this vessel should be chemically inert, have a high thermal conductivity and have a heat capacity that varies smoothly over the temperature range of interest. In addition, to obtain the best possible numerical data, the heat capacity of the vessel (and thermometer and heater) should be small relative to that of the sample.

To minimize the surface area of the container relative to its volume - hence reducing both radiative surface and mass - the ideal vessel shape would be spherical.[20] However, more often a cylinder is used.

The heater and thermometer should be placed symmetrically within the sample. This provides the best situation for dissipation of heat from the heater and most rapid equilibration of sample and thermometer. In addition, this situation allows the vessel surface to be as uniform and smooth as possible. In many calorimeters the heater and thermometer are housed in a

cylindrical well along the vessel axis.[3] For simplicity, often just the thermometer is within the well and the heater is wound over the vessel surface.[21-23] This procedure does, however, introduce problems which will be discussed in chapter 6.

The most common vessel material is probably copper because of its cheapness, workability, good thermal conductivity and chemical inertness. Slight improvements in the last factor can be made by plating the copper with silver or silver and gold. Where copper is unsuitable platinum alloys have been used. Silver has also been used successfully at temperatures up to about 1000 K.[26]

For very high temperature work materials like tantalum are necessary,[24] though these are very difficult to work.

The sample need not always be housed within a vessel. For non-volatile single crystal or bulk samples, it is possible to dispense with the container. The heater and thermometer may be attached to a tray onto which the sample is fixed.[25] Alternatively the heater and thermometer may be bonded to separate plates which form a sandwich around the sample.[27,28]

For large bulk samples it is possible to use the sample itself as the support for heater and thermometer. Holes may be drilled in the sample to take the heater and thermometer. This method is particularly suitable for metals[25] but has also been used for ceramics[29] and glasses.[30]

Controlling the shield

As well as the temperature of the sample, it is also necessary to measure the temperature difference between the sample and the shield. For this, high resolution and reproducibility are necessary though absolute accuracy is not always important.

This measurement is most easily made by means of a thermocouple with one junction on the sample and the other on the shield. The voltage signal produced when the system moves out of adiabatic balance is used to drive the shield heater. In many cases, different parts of the shield may have their own thermocouple-heater systems.[24,31] A separate heater may also be provided to bring the electrical leads to the sample temperature.[23]

Separate shield and vessel thermometers can be used instead of thermocouples to measure the temperature difference.[28]

If one has sufficient confidence in the adiabatic control, the temperature measuring thermometer may be placed on the shield rather than in the sample.[32,33] The sample temperature is then shield temperature less shield-sample temperature difference. The main advantages in this are fourfold.

(i) Reduced mass of the sample vessel; hence the sample contributes a bigger proportion of the total heat capacity

(ii) Four fewer wires to the vessel; this reduces heat leak problems and makes removal of the vessel simpler. The possibility of damage to the thermometer during sample removal is reduced.

(iii) Various thermometers may be attached to the shield since its mass is not critical; the most suitable can be chosen for a particular study.

(iv) Sample containers are more easily exchanged enabling different sizes, configurations and materials to be employed.

The major disadvantage is the difficulty of determining the shield-sample difference accurately.

Heating the sample

The response of an ideal system to a heat pulse can be represented as in figure 3.1A. Adiabatic conditions are maintained at all times. The constant temperature regions before and after the heat input are known as the drift periods. In practice, temperatures during drift periods are not constant and a slight, linear, temperature rise or fall occurs with time (figure 3.1B). It is desirable that the slopes be small and as similar as possible before and after heating. If the slopes in the before and after drift periods are not identical, it is necessary to make an extrapolation to determine the temperature rise.

The ideal cases in figure 3.1A and B suggest that the thermal conductivity of the system is very high and that the new equilibrium is established immediately. While the thermal conductivity of the container can be made high by a suitable choice of construction material, the same is not true for the sample - unless the range of samples is to be severely restricted. Different sample materials will exhibit different behaviour and individual samples may not respond in the same way at all temperatures. Sample preparation method will also affect the sample's thermal properties. More realistic behaviour is shown in figure 3.1C and D.

Extrapolation to determine the temperature rise is usually to the mid-point of the heating period (figure 3.1 C and D). However, since shield control during the heating period is based on conditions in the before-drift period, it may in some cases be better to extrapolate to the end of the heating period (see figure 3.1E). This point will be returned to later.

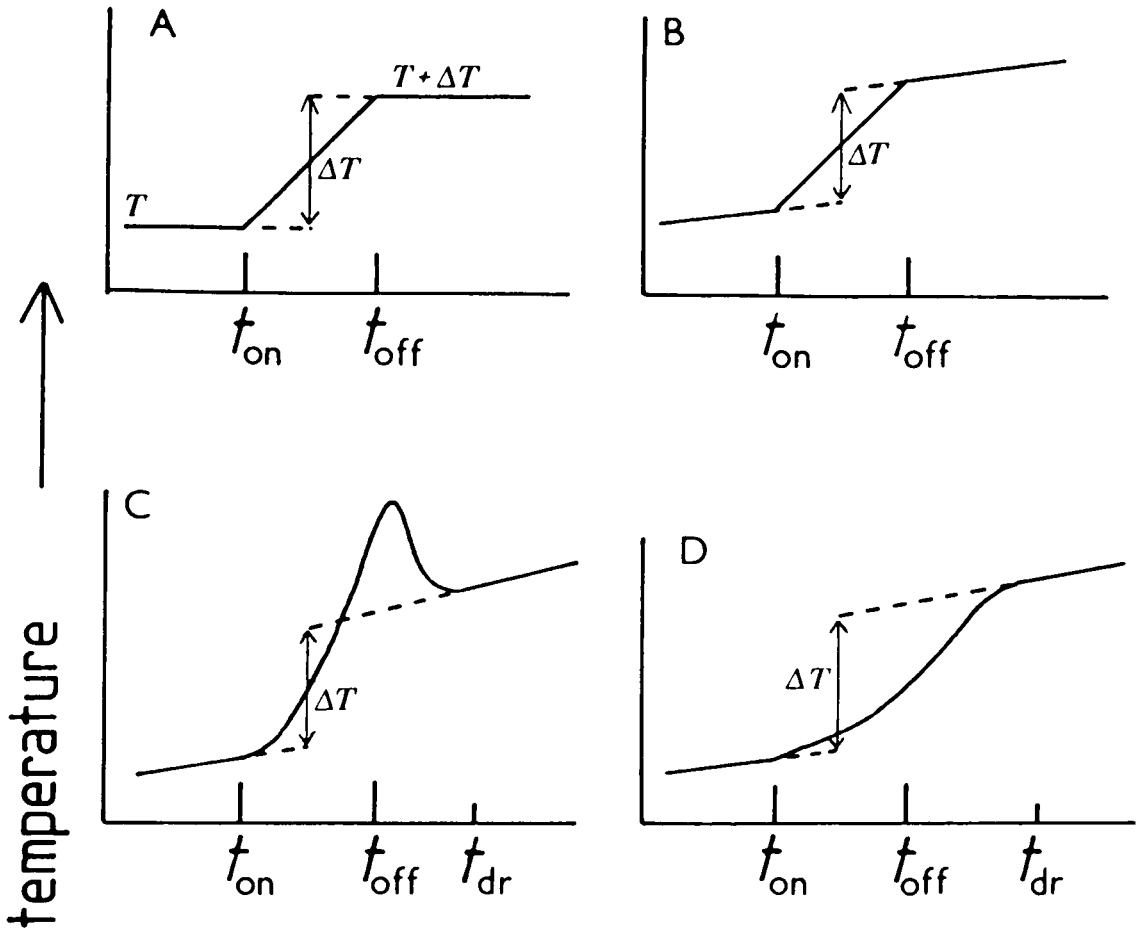

Figure 3.1 Response of a sample to a heat pulse: A and B, ideal systems; C and D, more realistic curves exemplified in this work by (C) the poorly conducting powders (silver tungstate, $[NMe_4]_2Ag_{13}I_{15}$) and (D) the large-particle materials with a higher thermal conductivity (alumina, $Ag_{13}I_9W_2O_8$); E, a system with different before and after drift curves, used in this work for some studies below 100 K.

Sample equilibration

For samples with high thermal conductivity, the time required to reach equilibrium may be relatively short, a few minutes in this work. However, with powdered insulators very long equilibration times are possible. A number of techniques are used to increase the rate at which thermal equilibrium is reached:

(i) using bulk or compressed samples[15,26-30]

(ii) using metal vanes or wires within the sample space[34] (see reference 38 for a related method)

(iii) mixing metal particles with the sample

(iv) using a low pressure of an exchange gas within the sample vessel.[3,21,22]

All these methods have their drawbacks: (i) is clearly not always suitable, (ii) and (iii) involve an increase in mass relative to that of the sample and (iii) introduces an added uncertainty - mass of metal. Method (iv) requires a complicated filling process, adsorption effects may be a problem and small leaks in the sample vessel become important.

Shield errors

It has been assumed so far that the shield can follow the sample exactly. This is not necessarily true. Any deviation from the set conditions will have an effect on sample temperature. This may be negligible, but will not always be so. To make corrections, it is necessary to have drift plots of temperature against time for various shield error conditions. For a particular heat capacity measurement, the sample temperature change resulting from a shield error will be given by

$$\text{temperature change} \propto \int \text{shield error}.dt$$

or proportional to the area under the shield error against time curve. To evaluate this in terms of a correction to ΔT, the proportionality constant must be determined. To do this, the shield is deliberately off-set from its adiabatic position and the drift produced is measured. The area under these curves - deliberate error against t - can be related to the observed temperature change of the sample. Unfortunately these correlations must be obtained at a large number of temperatures since the effect of shield error varies with temperature.

Good shield control requires a sophisticated control system, though modern electronics and microprocessing techniques have simplified matters greatly. Most workers use commercially available controllers (Leeds & Northrup, for example[21,24,31,34]) but these are not now essential thanks to the flexibility of microcomputers. Reference 14, for example, describes a particularly simple form of microcomputer shield control.

The system can be simplified by not insisting that the shield follow the sample temperature during a heating period. This alters the mode of operation from adiabatic to isothermal.

Isothermal calorimetry

The adjective isothermal refers to the sample's surroundings - the shield. The shield temperature remains constant during a heating period, either at the initial sample temperature or at some chosen temperature up to the expected final sample temperature. Before the advent of electronic controllers, these calorimeters were simpler to operate than adiabatic

ones. They still are simpler but the simplicity is more than balanced by the greater difficulty and uncertainty in determining ΔT. The use of isothermal calorimeters is now limited to very low temperature studies. In fact, at very low temperatures a distinction between the adiabatic and isothermal techniques is often not made (see later).

An exhaustive account of the method and the heat loss corrections involved is given in reference 35.

Pulsed versus continuous heating

It has been suggested so far that heat is introduced in discrete steps and that the average heat capacity is calculated for each temperature interval. This is the commonest method but not the only one. If heating and temperature measurement are continuous, it is possible to obtain the heat capacity at any temperature as the gradient of the energy input against temperature curve. This method has its advocates[15] but is by no means generally applicable. The heating rate must be slow enough to allow equilibrium to be maintained at all times. For many samples this would involve extremely slow heating. At these very slow rates extraneous heat gain or loss becomes significant relative to the controlled input.

However, for metals or thin bulk samples this method can produce very detailed results. The method forms the basis of adiabatic scanning calorimetry.[36]

With computer control systems it is possible to perform continuous and pulse measurements with the same instrument.[27]

Temperature ranges

Traditional methods of calorimetry cover a very wide range of temperature from very low[37] to very high.[15,25]

At temperatures below room temperature the vacuum chamber is usually surrounded by a coolant, liquid nitrogen or helium for example, and one shield between the sample and the outer vacuum can is often sufficient. At higher temperatures it becomes more difficult to maintain adiabatic conditions. For a given shield-sample temperature difference, heat losses become larger, mainly as a result of the rapid increase in radiative energy transfer.[3] To counter this problem it is usual to have more than one shield. The true adiabatic shield surrounds the sample and around this is a further shield (or several shields) at a temperature slightly below that of the inner shield. An oven replaces the coolant bath.

In addition to the heated and controlled shields, radiative losses may be further reduced by the use of 'floating' shields interspaced between the controlled shields or between the sample and first shield.[15,31]

As the temperature is raised above ambient the demands on the materials employed become greater; common solders, varnish and adhesives become unsuitable. Some examples of how these problems have been tackled are given in references 15, 16, 24, 31, 32, 38 and 39.

Because of the difficulties of high temperature adiabatic calorimetry, an alternative method of heat capacity determination has been used.

Drop calorimetry

Strictly speaking it is not heat capacity that is measured by this method, but rather relative sample enthalpy. The name derives from the fact that the sample is literally dropped from a known high temperature state in to a container at some lower temperature reference state. The total energy released to the container is determined, hence the enthalpy change for the sample going from the higher to the lower temperature. The receiving container may be adiabatic. That is, the dropped sample causes the container temperature to rise and this rise is measured. The container is surrounded by an adiabatic jacket which prevents heat loss to the environment. Much more common, however, is the use of an isothermal receiving container. In this case the container includes a solid/liquid mixture (ice and water, for example) and the heat released by the dropped sample alters the relative proportions of the two phases. The accompanying volume change is used to determine the heat lost by the sample.[40]

The drop technique has been in use for a long time. A very detailed survey of the state of the art up to about 1965 is given in reference 41. Few developments have been reported since then, though improvements have been made in maintaining more uniform furnace environments.[4]

The method is simple but has a number of drawbacks. All measurements must be made relative to established reference states otherwise it is difficult to compare results obtained in different experiments.

It is necessary to know that complete equilibration has occurred at the reference temperature. Samples likely to exhibit 'frozen in' disorder, glassification, supercooling, etc. have to be avoided.

It is difficult, using drop calorimetry, to make detailed studies over small temperature regions, and small transitions may go unnoticed, particularly continuous ones. The relative enthalpy changes resulting from even quite large transitions are small, as can be seen from enthalpy plots presented in this thesis. Having said that, however, it is worth noting that for some compounds, heat capacity and enthalpy data obtained by drop calorimetry are the best available. This is the case for the fluorite electrolytes mentioned in chapter 2. The calorimeter used for the fluorite studies is described in reference 43.

Low temperature studies

For work down to 4 or 5 K, helium baths with some means of reducing helium losses are satisfactory. If required, a cooler can be built into the system to liquefy coolant gas.[44]

For work below a few kelvin cooling is more difficult. By pumping on liquid helium, temperatures down to one kelvin can be reached. Further extension of the range is obtained by use of helium-3. Pumped helium-3 allows one to reach a few tenths of 1 K.

For work at still lower temperatures, adiabatic demagnetisation of a paramagnetic salt is commonly used. This method (in conjunction with a pumped helium bath) allows temperatures as low as a few millikelvin to be reached - though experiments at this lower limit are subject to difficulties additional to that of simply getting the coolant to the required temperature. The subject is reviewed by Hill et al.[37] Because of the necessity for pumped helium and for magnetic coils surrounding the calorimeter (for the adiabatic cooling process) samples for very low temperature work have to be small. Addenda(thermometer, heater, etc.) must be selected carefully otherwise their heat capacity may become large relative to that of the sample.

Since radiative heat losses become much less at lower temperatures, the distinction between isothermal and adiabatic shields becomes less significant. Generally therefore, isothermal shields are preferred because they are slightly simpler to operate. However, this does mean that processes involving long equilibration times are difficult to study. Finely powdered samples, which take a long time to come to thermal equilibrium, are not suited to the isothermal shield method.

At the lowest temperatures, heat exchange between the sample and its surroundings is so poor that it becomes extremely difficult to cool the sample. A thermal exchange gas - as

used in this work - would condense. A removable mechanical connection across the vacuum space is also unsuitable since at this temperature heat generated by vibration is significant. Kunzler et al.[45] got round these problems by supporting their sample in silicon powder. By correct choice of particle size a suitable rate of sample cooling can be obtained. On the time scale of one experiment heat loss from the sample to the supporting powder is small. Morin and Maita[46] have used a similar technique in measuring the heat capacity of a number of alloys. Their supporting medium was alumina powder.

Sample size and temperature increments

Adiabatic and isothermal calorimetry have provided enormous volumes of thermodynamic data. Samples may be bulk solids, powders, liquids or adsorbed gases. Measurements can be made over a wide temperature range (though only over a limited pressure range).

Traditionally the drawbacks have been the large mass of sample required (a few grams or more) and the size of the temperature increment produced by the heat input. The size of the increment is critically dependent on thermometer resolution since errors in measuring temperature have a large effect on the measured value of heat capacity. Typical temperature intervals are of the order of a few kelvin, although they may be as high as 50 K.[29] Very sensitive lightweight thermometers are now allowing these traditional problems to be overcome.[11,12]

The main advantage of adiabatic calorimetry is that it

provides absolute values of heat capacity by a simple and unambiguous calculation method.

What has not, in the past, been possible by traditional calorimetry is the detailed study of small regions of a heat capacity versus temperature curve - the determination of peak shapes and so on. For this sort of work we need uniform samples heated through very small temperature increments. Such studies have been made by adiabatic calorimetry,[11,12,47] but to a limited extent.

Further, if we wish to study the effects of stress,magnetic or electric fields, pressure, for example, on heat capacity it is often more convenient to use alternative experimental techniques.

Relaxation methods

These methods were developed for the study of small samples at very low temperatures. They rely, not on isolation of the sample, but on a link of known thermal conductivity to a heat sink of stable and known temperature. In the simplest case the sample is heated to a known temperature above that of the heat sink. The sample heater is switched off and the heat capacity can be determined from the slope of the sample temperature against time curve.[48,49] A more general discussion of relaxation methods is given by Bachmann et al.[50] Though these methods can be extended to 100 K,[49] their use at higher temperatures is limited.

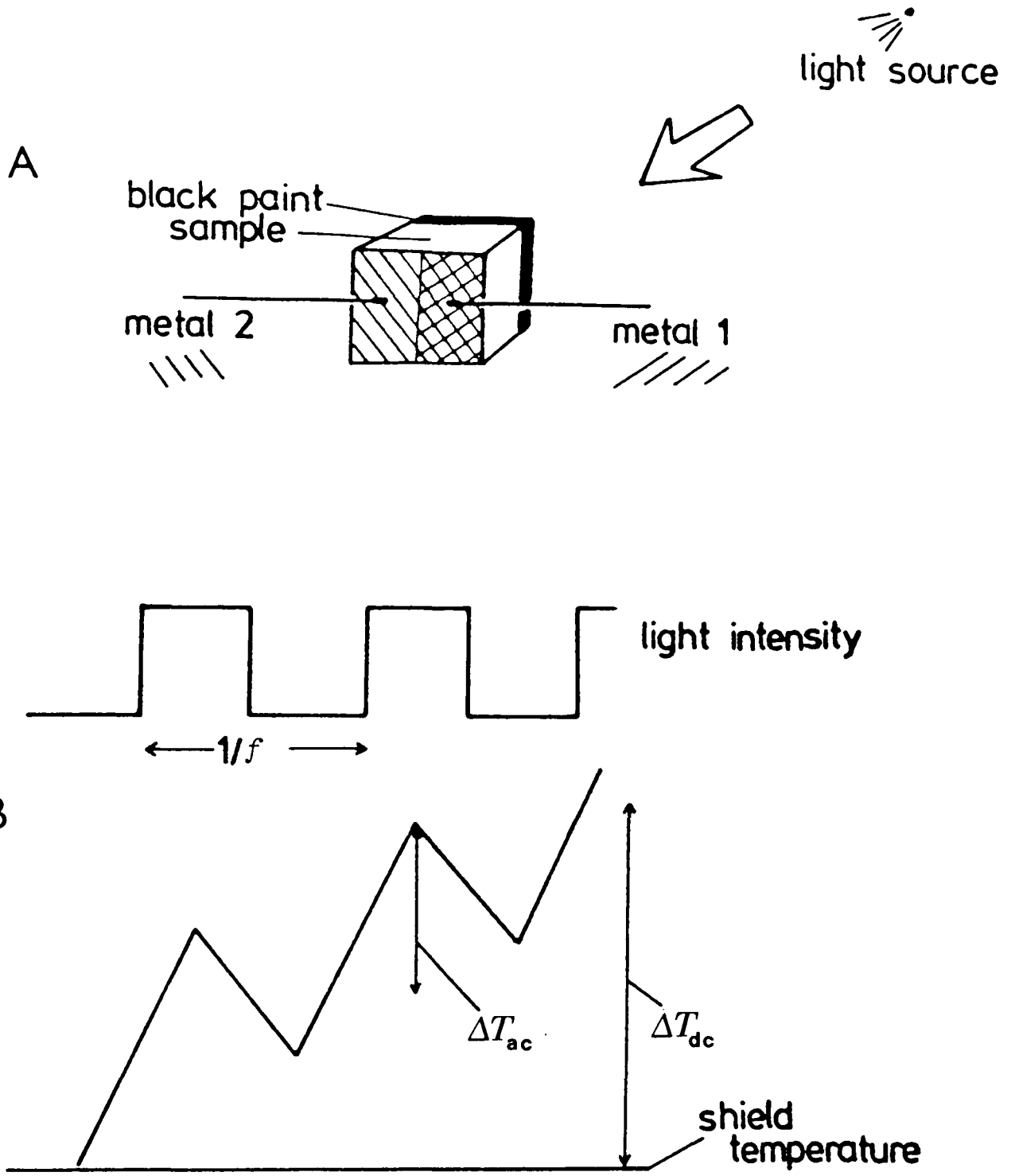

Figure 3.2 A, Sample arrangement for a.c. calorimetry in which the addenda are reduced to a minimum. The sample is a very thin film, pressed disc or crystal. The face is painted black to maximize energy absorption. ΔT_{ac} is recorded by the thermocouple on the sample back. ΔT_{dc} is recorded by a separate thermocouple close to the sample. B, Light pulses and their a.c. response. f is typically 1 Hz and ΔT_{ac} 15 mK.

A.c. calorimetry

In this method the sample is subjected to repeated small energy pulses, either electrical or radiative. The technique, though related to the relaxation methods,[50] can be extended to cover a far larger temperature range. Detailed descriptions of a.c. calorimeters, their theory and operation, are given by Handler et al.[51] and by Sullivan and Seidel.[52]

A particularly clear description of the experimental requirements is given by Stokka and Fossheim,[53] and the following description is based on their work.[53,54]

The sample is small and thin (0.1 - 0.5 mm). It is illuminated by chopped light ($\sim$ 0.2 - 2 Hz) and the temperature is measured by thermocouples. One couple measures the average, or d.c., temperature rise of the sample relative to that of a stable heat sink. The other measures the amplitude of the temperature oscillation produced by the pulsed heating. This amplitude may only be of the order of a few mK but its measurement is possible using expensive 'lock-in' amplifiers.[55] An idealised view of the temperature response is given in figure 3.2. Real traces are shown in reference 51. ΔT_{dc} may rise to between 25 and 250 mK before the sink temperature is adjusted.

Under suitable conditions [51-53] the sample heat capacity is proportional to ΔT_{ac}. These

conditions of heat loss, frequency, sample equilibration time, etc. are maintained during an experiment. Absolute measurement of heat capacity is extremely difficult. Very detailed relative heat capacity measurements can, however, be made. It is usual to refer the results to some known - from another method - heat capacity value for the same compound. This was the technique used by Vargas et al.[56] in making detailed studies of the transitions around 200 K in the family of solid electrolytes MAg_4I_5 (M= Rb, K, NH_4). Absolute values of heat capacity are available for $RbAg_4I_5$.[57] These are not available for KAg_4I_5 or $NH_4Ag_4I_5$ so the results of Vargas et al. for these compounds are subject to considerably more uncertainty in absolute terms.

The method has a very wide application [58] but there does not appear to be a calorimeter of this type operating in the U K.[54]

References to chapter 3

1 Experimental Thermodynamics Volume 1: Calorimetry of non-reacting systems, ed J P McCullough and D W Scott, IUPAC-Butterworths, 1968.

2 Chemical Thermodynamics Volume 1: Chemical Society Specialist Periodical Report, ed M L McGlashan, The Chemical Society, 1973.

3 E F Westrum, G T Furukawa and J P McCullough in reference 1, p 133.

4 D Moy and A C Anderson, *Cryogenics* , 1983, 23, 330.

5 D S Kyser and V O Jones, *Rev Sci Instruments*, 1977, 48, 1353.

6 Y Takahashi, H Yokokawa, H Kadokura, Y Sekine and T Mukaibo, *J Chem Thermodynamics*, 1979, 11, 379.

7 See for example J L Riddle, G T Furukawa and H H Plumb, Platinum Resistance Thermometry, National Bureau of Standards Monograph 126, 1973.

8 V Franke and E Hegenbarth, *Phys Stat Solid(a)*, 1974, 25, K17.

9 Cryogenic Linear Temperature Sensor CLTS, Data Sheet S35, Oxford Instruments.

10 S D Wood, B W Mangum, J J Filliben and S B Tillett, *J Res Nat Bur Stand*, 1978, 83, 247.

11 W Reese and L F May, *Phys Rev*, 1967, 162, 510.

12 T Matsuo, M Tatsumi, H Suga and S Seki, *Solid State Comm*, 1973, 13, 1829.

13 R L Powell, L P Caywood and M D Bunch in Temperature, its Measurement and Control in Science and Industry Volume III, Part 2, ed A I Dahl, Reinhold, 1962, p 65.

14 S Raman, N S N Murty, K S Roy, V V Rao and G Rangarajan, *Pramāna* , 1982, 19, 151.

15 E E Stansbury and C R Brooks, *High Temperatures-High Pressures* , 1969, 1, 289.

16 B B Benson and D Krause, *Rev Sci Instruments*, 1974, 45, 1499; F L Walls in Proc Workshop on Techniques for Measurement of Thermodynamic Properties, Albany, Oregon, 1979 (US Bureau of Mines Information Circular 8853, 1981).

17 B W Mangum in Proc Workshop on Techniques for Measurement of Thermodynamic Properties, Albany, Oregon, 1979 (US Bureau of Mines Information Circular 8853, 1981). This review also covers thermistors and germanium resistance thermometers.

18 R P Hudson, *Rev Sci Instruments*, 1980, 51, 871.

19 L G Rubin, *Cryogenics*, 1970,10, 14; L G Rubin, B L Brandt and H H Sample, *Cryogenics*, 1982, 22, 491.

20 M Mainard, J Kleinklauss and H Fousse, *Revue de Physique Appliquêe*, 1970, 5, 823.

21 C G Waterfield and L A K Staveley, *Trans Faraday Soc*, 1967, 63, 2349.

22 J W Edwards and G L Kington, *Trans Faraday Soc*, 1962, 58, 1313.

23 R C F Schaake, J C A Offringa, G J K van der Berg and J C van Miltenburg, *Recueil, J Roy Netherlands Chem Soc*, 1979, 98, 408.

24 W A Dench, *Trans Faraday Soc*, 1963, 59, 1279; O Kubaschewski, P J Spencer and W A Dench in reference 2, chapter 9.

25 D L Martin, *Phil Mag*, 1955, 46, 751.

26 F Grønvold, *Acta Chem Scand*, 1967, 21, 1695.

27 D Moses, O Ben-Aroya and N Lupu, *Rev Sci Instruments*, 1977, 48, 1098.

28 E Gmelin and P Rödhammer, *J Phys E* , 1981, 14, 223.

29 See for example H D Nussler and O Kubaschewski, *Trans J Brit Ceram Soc* , 1980, 79, 98.

30 D M Finlayson, G A Leiper and C A Vincent, *Solid State Comm*, 1980, 26, 261.

31 J T S Andrews, P A Norton and E F Westrum, *J Chem Thermodynamics*, 1978, 10, 949.

32 I S Williams, R Street and E S R Gopal, *Pramāna*, 1978, 11, 519.

33 E F Westrum, University of Michigan, personal communication.

34 K Arvidsson, B Falk and S Sunner, *Chem Scripta*, 1976, 10, 193; M Månsson, University of Lund, personal communication.

35 J W Stout in reference 1, p 215.

36 R Lagnier, J Pierre and M J Mortimer, *Cryogenics*, 1977, 17, 349; R Lagnier, Étude, Realisation et Essais d'un Dispositif de Determination de Chaleur Specifique en Mesure Dynamique de 4 à 300 K. Rapport CEA-R-4419, Centre d'Études Nucléaires de Grenoble Service de Basses Températures, 1973.

37 R W Hill, D L Martin and D W Osborne in reference 1, p 263.

38 E D West and D C Ginnings, *J Res Nat Bur Stand*, 1958, 60, 309; F L Oetting and E D West, *J Chem Thermodynamics*, 1982, 14, 107.

39 A Inaba, *J Chem Thermodynamics*, 1983, 15, 1137.

40 J C Southard, *J Amer Chem Soc*, 1941, 63, 3142.

41 E D West and E F Westrum in reference 1, p 333.

42 F L Oetting, *J Chem Thermodynamics*, 1978, 10, 941.

43 A S Dworkin and M A Bredig, *J Phys Chem*, 1960, 64, 269.

44 K Moriya, T Matsuo and H Suga, *J Chem Thermodynamics*, 1982, 14, 1143.

45 J E Kunzler, L R Walker and J K Galt, *Phys Rev*, 1960, 119, 1609.

46 F J Morin and J P Maita, *Phys Rev*, 1963, 129, 1115.

47 P C Lanchester and D P Baker, *J Phys E*, 1981, 14, 805.

48 E M Forgan and S Nedjat, *Rev Sci Instruments*, 1980, 51, 411.

49 B Cort and D G Naugle, *Phys Rev B*, 1981, 24, 3884.

50 R Bachmann, F J DiSalvo, T H Geballe, R L Greene, R E Howard, C N King, H C Kirsch, K N Lee, R E Schwall, H-U Thomas and R B Zubeck, *Rev Sci Instruments*, 1972, 43, 205.

51 P Handler, D E Mapother and M Rayl, *Phys Rev Letters*, 1967, 19, 356.

52 P F Sullivan and G Seidel, *Phys Rev*, 1968, 173, 679.

53 S Stokka and K Fossheim, *J Phys E*, 1982, 15, 123.

54 S Stokka, Rogalandsforskning, Stavanger, personal communication.

55 M L Meade, *J Phys E*, 1982, 15, 395.

56 R A Vargas, M B Salamon and C P Flynn, *Phys Rev B*, 1977, 17, 269.

57 W V Johnston, H Wiedersich and G W Lindberg, *J Chem Phys*, 1969, 51, 3739.

58 See for example I Hatta and A J Ikushima, *Jap J Appl Phys*, 1981, 20, 1995.

4

The Calorimeter:

Construction

It was decided that the control and measurement system should be based around a microcomputer and that as much of the associated electronic circuitry as possible should be built specifically for this project. In view of the amount of experimentation and testing that this would involve, it was thought best to base the calorimeter itself on a proven and well documented design. The design chosen was similar to that used at Oxford.[1,2]

Initially some reduction in size of the calorimeter vessel was considered.[3-5] However, we were fortunate enough to obtain a platinum resistance thermometer from Dr L A K Staveley (Oxford).[6] A good starting point for this work thus appeared to be the construction of a calorimeter around this thermometer. Once the control system had been proven, it would be possible in later projects to experiment with other calorimeter sizes, temperature ranges and temperature sensors.

The thermometer

Construction of the thermometer is described by Goalby.[6] His method was based on that recommended by the National Bureau of Standards.[7]

To avoid the lengthy and difficult process of calibration of this delicate item it was decided to accept the data of Bates [8] and recalibrate the thermometer only if this proved to be necessary. The only preliminary measurements made on the thermometer were therefore of its resistance at the triple point of water [9] and of the effects of self heating.

The thermometer current used during triple point cell measurements was 0.8 mA. Bates and Goalby mention the use of thermometer currents of up to 6 and 10 mA. However, it was felt that self heating at these currents was unacceptable (0.01 to 0.02 K in a few minutes in the triple point cell).

Table 4.1

Thermometer resistance (R/ohm) at 273.15 K

Goalby	this work [calculated from R(273.16 K)]
17.449 81	17.442 19[a]
	17.438 4[b]

[a] Tinsley - NPL type 5840 bridge; [b] Racal Dana and associated electronics

Temperature values are obtained from the Callendar - van Dusen equation [2,6,8]

$$t = (R-R_o)/\alpha R_o + \delta t[(t/100)-1]/100 + \beta[(t/100)-1](t/100)^3$$

where t is the temperature on the celsius scale (0 °C ≡ 273.15 K), R and R_o are the resistance values at t and 0 °C, and α, β and δ are constants [8]

$$\alpha = 0.003\ 913\ 16$$

$$\beta = 1.506 \qquad (0.0 \text{ if } T > 0\ ^{\circ}C)$$

$$\delta = 1.101\ 5$$

Temperatures reported in this work are thus based on the IPTS-48 of 1960 [10] rather than the more recent IPTS-68.[11] This is not uncommon in other work, see for example the experimental results from the laboratories of E F Westrum (Michigan) and H Chihara (Osaka). Data obtained using the different scales are interconvertible [12] but in view of the accuracy claimed for our temperature measurement, IPTS-48, IPTS-68 and thermodynamic temperature are indistinguishable.

Below 88 K the Callendar - van Dusen equation is not valid. No corrections have been made for this since the range involved (80 - 88 K) is small. Temperature measurement below 88 K is discussed at length by both Goalby [6] and Bates.[8] The problem does not arise if polynomial functions relating resistance and temperature are used (as currently recommended by the National Bureau of Standards [11]).

The inner vessel

The basic construction material is copper. This choice was made on the grounds of cheapness and the ease with which copper can be worked and soldered. It is also reasonably inert. All samples to be placed in the calorimeter were tested for reaction with copper by storing for several months with solder-jointed copper foil. This is particularly important with electrolyte samples as there is a significant possibility of galvanic corrosion.

It was not considered that plating the copper offered any

significant advantage. The only other serious contender as a construction material was nickel.

The sample container is required to be as light as possible. A wall thickness of 0.2 mm was considered to give sufficient mechanical strength. Since copper tube of the required dimensions was not available commercially, three construction methods were considered.

(i) The simplest, in principle, was to drill and shape the required cylinder from a solid copper rod.

(ii) The second alternative was to electroplate a cylinder onto a former which could then be dissolved away. I thank Dr R Dahm of this department for his advice on the practical aspects of this method and Dr J C van Miltenberg for comments on his experience with this method at Utrecht.

(iii) Finally, the vessel could be constructed from copper foil.

In fact method (i), though time consuming, proved practicable in the laboratory workshop so the other methods were not attempted.

The shape of the vessel is largely dictated by the size (about 6 cm long) and mass (7.7 g) of the thermometer. This is housed in a platinum cylinder with a glass bulb at the base.[6] A copper tube, placed centrally within the vessel, acts as a sheath housing the thermometer. This too was drilled from a copper rod. At room temperature the sheath is a very tight fit around the thermometer which was eased into place with a little apiezon N grease. Since the thermal expansion of

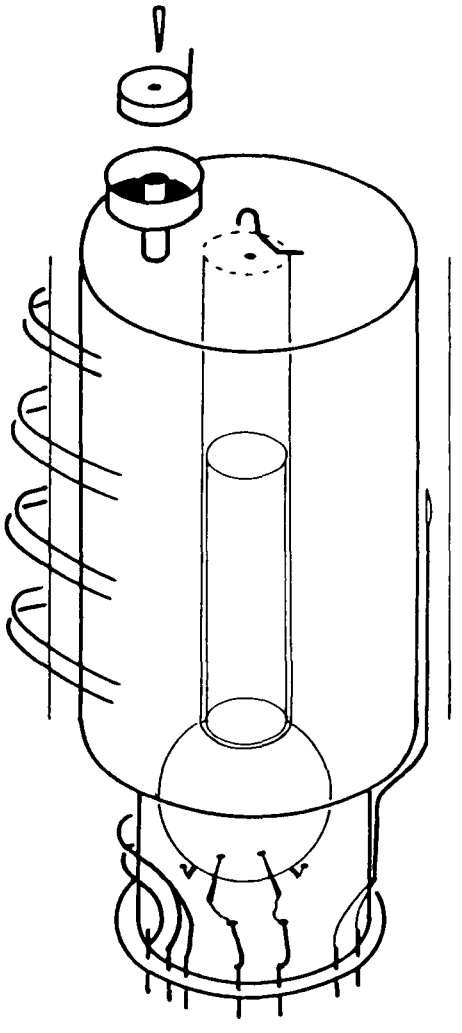

Figure 4.1 The sample vessel.

Table 4.2

Dimensions of the sample vessel

height	70 mm
diameter	25 mm
wall thickness	0.2 mm (cylinder)
	0.1 mm (base and top)
mass of copper and solder	22.5 g
total mass	42.1 g (including leads and shield base)

platinum is greater than that of copper, the thermometer will shrink slightly from the surrounding copper tube when the vessel is cooled. This ensures that no undue strain is introduced either in the thermometer wall or the surrounding tube.

The vessel end pieces were cut from 0.1 mm copper foil. All joints are silver soldered. A filling tube enters through the top. The top piece is shaped to ensure that no sample will be trapped inside the vessel during emptying (figure 4.1). The vessel is sketched in figure 4.1 and its dimensions given in table 4.2. The method used for sealing the filling tube is described later.

To the bottom of the vessel is attached a short cylinder of slightly smaller diameter than the body. This protects the glass bulb at the base of the thermometer. The bottom of this cylinder is flanged. The flange is used to anchor all electrical connections to the vessel. This prevents any tugging of the wires breaking the heater - to - lead or thermometer - to - lead solder joints. The mechanical strength of the thermal free solder is poor and the fine copper wires are brittle close to where they have been heated during soldering.

A copper constantan thermocouple junction is soldered directly to the vessel wall. The junction itself is formed by soldered twisted copper (32 swg) and constantan (33 swg) wires. Earlier tests had shown that these soldered junctions produce steadier voltage readings than spot welded or fused junctions.

The heater is wound round the vessel. It consists of 8.2 m 38 swg constantan wire (0.15 mm diameter, $\sim$25 ohm m^{-1}).

Constantan was chosen because it has a high resistivity and its resistance varies only slowly with temperature (see table 3.1).

The constantan is cotton covered but an extra layer of electrical insulation is provided between the windings and the copper body. This is lightweight paper (Rizla Green) that had been soaked in varnish (2 parts toluene, 1 part ethanol and 1 part GE 7031). The heater windings are held in place by a coat of the same varnish.

It should be noted that where enamelled copper wires touch the vessel surface, an extra layer of insulation proved to be essential. Occasional shorts to the vessel body occurred where enamelled wire crossed exposed copper (on the cylinder protecting the thermometer bulb).

A small hook is attached to the top of the vessel to receive the supporting thread.

Nine wires leave the base of the vessel. Two of these are the thermocouple wires and four are from the thermometer. The three remaining are from the heater; one end of the constantan winding is connected to two copper leads. The wires are formed into a bundle and varnished to bind them together. The bundle is coiled into a spring. Apart from the thermocouple leads, all the wires are 42 swg copper (about 0.01 mm diameter). Fineness is necessary to limit thermal conduction between the vessel and the shield base. Thermal conduction could be reduced further by using wires with poor thermal conductivity. However, this would also involve higher electrical resistance and possibly significant heat evolution in the leads.

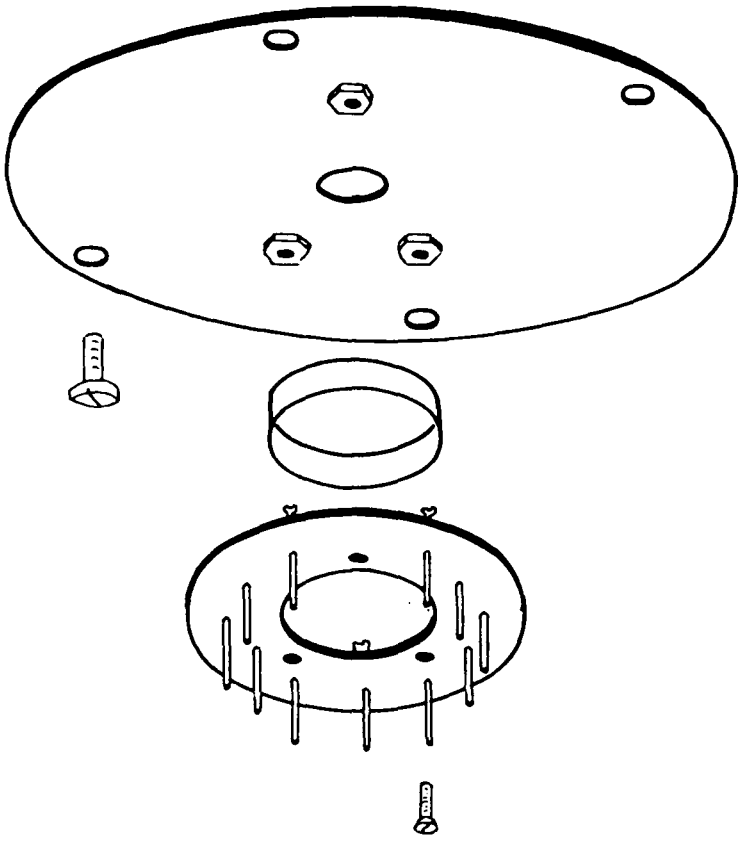

Figure 4.2 The shield base.

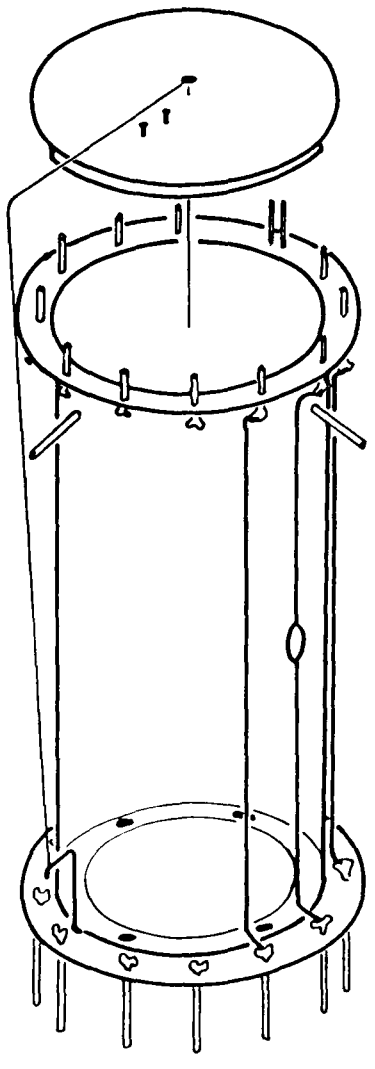

Figure 4.3 The shield body.

Table 4.3

Shield dimensions

height	180 mm
diameter	37 mm
wall thickness	0.3 mm
total mass	133 g

The wires pass to the shield base. This base is permanently attached to the vessel. It can be detached from the rest of the shield, and the vessel then removed through the bottom of the shield.

The shield base

This consists of two parts. A copper disc forms a continuation of the shield body. Four small bolts hold the base to the rest of the shield. The wire bundle from the vessel passes through a small hole in the centre of this disc. To the underside of the copper disc is bolted an insulating ring. The wires are soldered to pins fixed in this ring. The assembly is shown in figure 4.2.

Two of the base pins are connected to allow the single heater lead to be divided.

The point where the wire bundle passes through the copper disc has proved to be a constant source of trouble. Shorts between the enamelled wires and the shield base were frequent. A soft plastic ring within the hole would have been a good idea to prevent chafing between the wires and the copper. Varnish is used to hold the wires as firmly as possible, in an attempt to prevent chafing.

The shield

Like the central vessel, this is a cylinder drilled from a solid copper rod. Again the mass is kept low, this time to allow the shield to respond quickly to changes in sample temperature. Inside the cylinder, at the bottom, is a copper ring to which the shield base is bolted. Insulating rings surround the shield at both top and bottom.

In the bottom ring are pins for making electrical connections to the shield base. There are eleven pins, one of which is unused. In the top ring are thirteen pins, two more because extra are required for the shield heater.

Wires connecting the top and bottom pins run up the outside of the shield body (plastic coated, silvered copper, 0.2 mm diameter). The only exception is the thermocouple link which is part copper, part constantan. The junction is soldered to the shield body.

The bottom ring is divided into twelve segments, eleven of which contain a pin. The pins in the insulating ring beneath the shield base are similarly arranged so that positioning of the shield base with corresponding pins adjacent is quick and accurate.

The shield heater is of 36 swg constantan. It is wound non-inductively as two coils in parallel to give a total room temperature resistance of 175 ohm. Following usual practice, there is a slightly higher density of windings near the top and bottom of the shield.[2,13]

The shield has a tightly fitting copper lid. Through the centre is angled a small hole to take the vessel supporting thread (Bayer Perlon 1.1). When the vessel is in position, this thread is fixed to a hook near the bottom of the shield. Small pins on the lid allow minor adjustments to be made to the height of the vessel within the shield.

Three constantan wires are attached to pegs near the top of the shield wall. These join above the shield where they are attached to a nylon supporting thread (Bayer Perlon 2.2).

Twelve wires reach the shield from the outside world (thermometer 4, sample heater 4, shield heater 2, thermocouple 2). They are first cooled by being brought into good thermal contact with the outer (nitrogen cooled) can. Initially these enamelled copper wires were bound to a bolt inside the top of the can and held in place with varnish. However, repeated cooling cycles caused the wires to short, occasionally, to the outer can. This, since it could occur during a run, was troublesome. The leads are now therefore held free of the can by a plastic spacer. Cooling is effected by a coil of silver wire wrapped around the bundle of leads. The ends of the silver wire are attached to bolts in the can lid.

After connection to the pins at the top of the shield, the wires run down beneath the shield heater windings to be brought to the temperature of the shield and, in principle, to the temperature of the sample.

Except for repair, the shield need never be removed from its position suspended from the vacuum can lid. Details of the shield are shown in figure 4.3 and table 4.3.

Electrical connections

Electrical connections to pins at the top of the shield are permanent and made by means of thermal free solder (70.44 % Cd, 29.56 % Sn; Oxford Instruments). This solder proved difficult to work and had poor wetting ability and mechanical strength. The joints failed on a number of occasions, particularly during early runs. To make good joints, it was necessary to heat the solder to

a temperature above that attainable with an ordinary electrical soldering iron. This was done using an old fashioned copper soldering iron heated in a bunsen flame. The iron was filed clean before each use.

Failure also occurred as a result of the brittleness of the copper wire close to the solder joint. Fortunately a number of spare wires were included.

The links between the wires at the foot of the shield and the shield base are 'wire wrap' connections. The wire wrap pins and wires have proved extremely reliable and simple to use.

The vacuum can

The calorimeter assembly is completely enclosed in an evacuated brass can which is immersed in a liquid nitrogen bath. To prevent too rapid boil-off of the nitrogen, the tube to the pumping line is of glass. A short distance above the liquid nitrogen, therefore, is a brass/glass junction. A number of junctions were tried but failed as a result of the different expansivities of the two materials. Even when the junction included a resin supposedly flexible enough to allow for this, the glass cracked after a few heating and cooling cycles. The present junction, which appears to be successful, is a commercial glass/metal seal (Jencons copper/steel/glass) though it was necessary to resolder the copper/steel joint.

A similar problem arose in taking the electrical leads through the can lid. At first this appeared to be the easiest way of cooling the leads. This arrangement was shown in reference 14. However, again, differences in expansivities of the various materials caused cracks and leaks to form.

Table 4.4

Low melting solder compositions (proportions by mass)

Solder A (m.p. 55 °C)

Bi 49%; Sn 15%; Pb 18%; In 18%

Solder B (quoted m.p. 46.5 °C)

Bi 41.0%; Sn 10.6%; Pb 22.1%; In 18.1%; Cd 8.2%

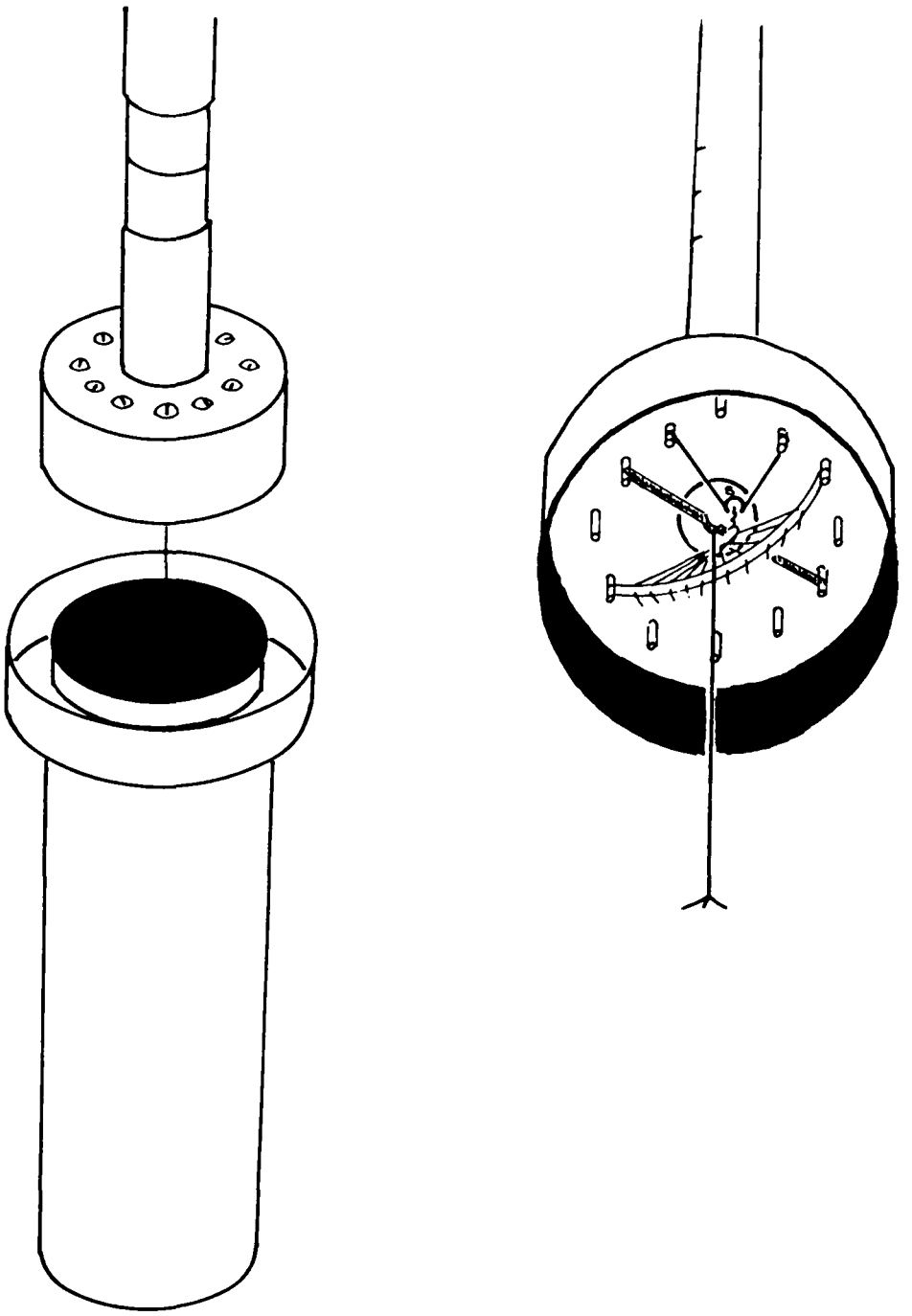

Figure 4.4 The vacuum can: the following features are visible beneath the can lid 11-1 silver cooling coil; 10-4 bar for attachment of shield support thread; 8-2 insulating spacer for electrical leads. The numbers represent the bolts that can be seen in the can lid, numbered as if they were digits on a clock face.

To overcome this, long leads are used which leave the vacuum system through the glass wall well away from the cooled region.

The vacuum can is sealed using low melting solder. Originally, a commercial solder (Apex Crafts, Leicester, m.p.88 °C) was used; however this did not flow freely until well above its melting point. Nor did it wet the brass easily. After frequent failures it was replaced.

Two other solders have therefore been prepared, though only solder A has so far been used (table 4.4). While failure of the joint still occurs when it is cooled in liquid nitrogen, it is no longer a difficult job to remelt the solder and reseal.

The solders were prepared by melting large lumps of the main ingredients (Bi, Sn, Pb) in a crucible (in a fume cupboard). The other metals were added as wire and the mixture cooled to just above melting point (solder A 65 °C, solder B 55 °C). The liquid was then poured off onto a watch glass to cool, any unmelted or oxidized material remaining behind.

The best solder flux was found to be $ZnCl_2$ in dilute HCl. 30% HCl solution was also used. Phosphoric acid, a common solder flux, tended to produce black deposits on the solder and can rim.

The vacuum line

Pumping is by means of a rotary oil pump and a silicone 704 oil diffusion pump. The layout is shown in figure 6.2. A helium gas line is included. Helium is used to improve thermal contact within the vessel, and to aid cooling of the vessel and shield at the start of a run. Pressures of about

1×10^{-5} Torr (1 Torr = 133.3 Pa) can be reached very quickly after beginning pumping (1 or 2 h). After pumping overnight the Penning gauge usually registers less than 10^{-6} Torr, though how reliable these values are at the extreme of the Penning's range is not certain.

References to chapter 4

1 C G Waterfield and L A K Staveley, *Trans Faraday Soc*, 1967, 63, 2349.

2 R G Linford, D Phil Thesis, Oxford, 1967.

3 K Arvidsson, B Falk and S Sunner, *Chem Scripta*, 1976, 10, 193.

4 K S Sukhovei, V F Anishin and I E Paukov, *Russ J Phys Chem*, 1974, 48, 937.

5 Conversations and correspondence, L A K Staveley (Oxford), E F Westrum (Michigan), M Månsson (Lund) and J C van Miltenberg (Utrecht).

6 B B Goalby, D Phil Thesis, Oxford, 1952.

7 J L Riddle, G T Furukawa and H H Plumb, Platinum Resistance Thermometry, National Bureau of Standards Monograph 126, 1973 (for the original work see Meyers, *J Res Nat Bur Stand*, 1932, 9, 807)

8 T R Bates, D Phil Thesis, Oxford, 1957.

9 C R Barber, R Handley and E F G Herrington, *Brit J Appl Phys*, 1954, 5, 41.

10 H F Stimson, *J Res Nat Bur Stand*, 1949, 42, 209; H F Stimson, D R Lovejoy and J R Clement in Experimental Thermodynamics Volume 1: Calorimetry of non-reacting systems, ed J P McCullough and D W Scott, IUPAC-Butterworths, 1968, p 15.

11 G T Furukawa, J L Riddle and W R Bigge, *J Res Nat Bur Stand A*, 1976, 80, 477; C R Barber, *Metrologia*, 1969, 5, 35; F D Rossini, *J Chem Thermodynamics*, 1970, 2, 447.

12 T B Douglas, *J Res Nat Bur Stand A*, 1969, 73, 451; J G Hust, *Cryogenics*, 1969, 9, 443.

13 J C van Miltenberg, *J Chem Thermodynamics*, 1972, 4, 773.

14 D A Armitage, P G Hall and R G Linford, poster presented at IUPAC Conference on Chemical Thermodynamics, University College, London, 1982.

15 Indium Solders Data Sheet, Preussag Metals.

5

The Calorimeter:

Control and Measurement

The controller selected to coordinate the necessary activities is a Commodore 3016 PET computer. (During the course of this work the memory size was enlarged to 32 k to allow curve fitting calculations to be performed on the same machine). The activities include: selecting the type of data required; communicating with a measuring instrument; accepting the data and performing calculations based on the data. In addition adiabatic conditions must be maintained at all times.

The possibilities of these computers in instrument control have been recognized for some time.[1]

The first priority was to obtain a working control system and to gain experience of its use. Once the system had been thoroughly tested, it was intended that provision be made for fully automatic running of the calorimeter. As far as the software and electronics are concerned this stage has been reached. However, for practical reasons, it has not been possible to test the automatic system fully. This is because it is not possible to leave the calorimeter unattended for long periods, say more than four or five hours: the longest period to date has been ten hours. One cause of this is loss of coolant, though a refilling system would not be difficult to arrange. A more serious problem results from electrical interference (see later).

Electrical measurements

Two sets of information are required for a heat capacity measurement:

(i) electrical energy input during the heating period

(ii) temperature rise resulting from this input.

Errors arising from non-adiabaticity must also be taken into account if they are considered to be significant.

Energy input is determined from three measurements:

(i) heating period

(ii) heater voltage drop

(iii) heater current.

Heating period

All timing is performed by the computer using its internal clock. This counts in units of one sixtieth of a second. This is therefore the limit of accuracy of determination of heating period. An error of one counting period in the shortest heating period (30 s for the empty calorimeter) introduces an error of only one part in two thousand (0.05%). Heating periods are more usually in the range five to ten minutes.

Comparison of the PET clock with other timers suggested that its accuracy is perfectly adequate for our purposes (agreement better than 1 part in 1000 over fifteen minutes).

Lanchester and Baker, whose calorimeter is described in reference 2, have suggested that the clock's accuracy is not high. However, they are concerned with precise measurements of much smaller time intervals.

Electronic delays, between setting the clock and switching

for example, are only of the order of milliseconds and can, in any case, largely be made to cancel by a suitable programming sequence.

The clock counts for 24 h from zero to 5 183 999 and then returns to zero. This would pose a problem if a heating period were initiated close to the end of a 24 h period. This is simply overcome. The PET is prevented from responding to an 'initiate heating' command if the clock plus heating period gives a total count of greater than 5 139 900.

Heater voltage drop

The voltage drop is measured using a voltmeter built during this project. With the present set up any heater voltage from 0 to 25 V can be selected manually. Generally four or five volts is suitable though the exact choice depends on the characteristics of the sample and the temperature range under investigation. The tendency in the latter months of this project has been to use even lower voltages as this allows for much improved automatic shield control during the heating period.

The semiconductor device chosen as the precision component in the voltmeter was a National Semiconductor ADC 3711 3¾ digit microprocessor compatible analogue to digital converter.[3] This chip is not itself a voltmeter but converts an analogue input voltage of 0 to ± 1.999 V into digital form.

The output digital information is in what is known as 'binary count decimal' (BCD) format. That is, the decimal information is output one digit at a time. Each digit is in binary form.

Other input lines to the chip indicate which digit is to be transmitted. The PET requires that first the sign is transmitted, then the most significant digit and so on down to the least significant digit. Part of the voltmeter circuitry provides suitably timed triggers to initiate and sequence digit transfer. Sequencing of digits is timed to suit the slowest item accepting the digits - a liquid crystal display. When the least significant digit is output, the voltmeter also signals to the PET that the voltage reading is complete (EOI line pulled low, see later).

The voltmeter display operates at all times, regardless of whether or not the voltmeter is communicating with the PET.

A liquid crystal display was chosen in preference to other types because of its low power requirements. Experience with the d.t.a. instrument had revealed problems associated with diode displays. The current surges due to digit switching were sufficient to cause electrical disturbances that were significant relative to very small signal inputs - such as those from thermocouples.

The BCD output is used directly to drive the liquid crystal display. The output is also electronically translated into ASCII which is the code understood by the PET computer. Communication between the voltmeter and the PET is via the computer's IEEE port (see later).

The voltmeter circuitry falls into two parts:

(i) the measurement section (the voltmeter itself)

(ii) the IEEE communication section.

The bulk of (i) is described in reference 3 and in the data

sheets of the associated components. To some extent this circuitry is straightforward but a number of unexpected problems did arise. Some of the difficulties were undoubtedly the result of my inexperience - having had no knowledge of electronics prior to this project - while others appeared to be associated with the ADC 3711 chip itself.

For example, initially the voltmeter was to be driven by its own mains derived 5 V power supply. This was to ensure that it had a stable power source unaffected by switching or power fluctuations elsewhere in the instrument. During testing this arrangement proved very satisfactory. Calibration, while somewhat tedious, was accomplished by means of a Weston cell, a variable resistor and the Racal Dana multimeter (see later). Unfortunately during subsequent use things were not so simple.

The calorimeter heater power is itself derived from an independent transformer. Measurements of the heater output with the Racal Dana multimeter indicated that this supply was extremely stable; better than ± 1 mV in 20 V. However, this stability was not apparent with the internal voltmeter. In fact it was observed that fluctuations of ± 10 mV occurred when measurements were made of any mains derived voltage. The problem did not arise if either the measured voltage came from a battery or the voltmeter was powered by a battery.

There appeared to be only three ways of overcoming this problem:

(i) a different voltmeter chip

(ii) a battery as the heater source

(iii) a battery as power source for the voltmeter.

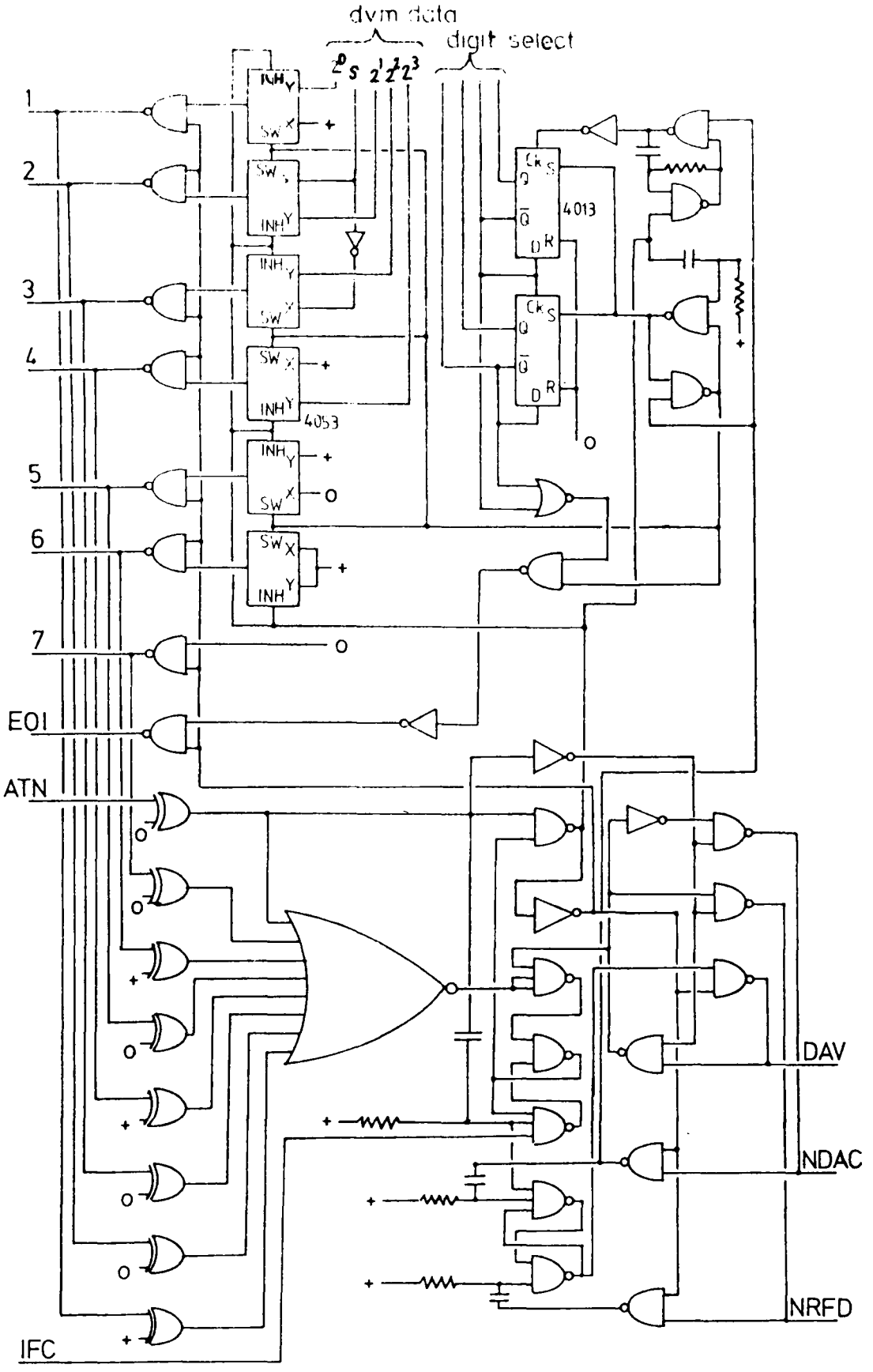

Figure 5.1 The IEEE logic circuitry for communication between the PET and the voltmeter built during this work.

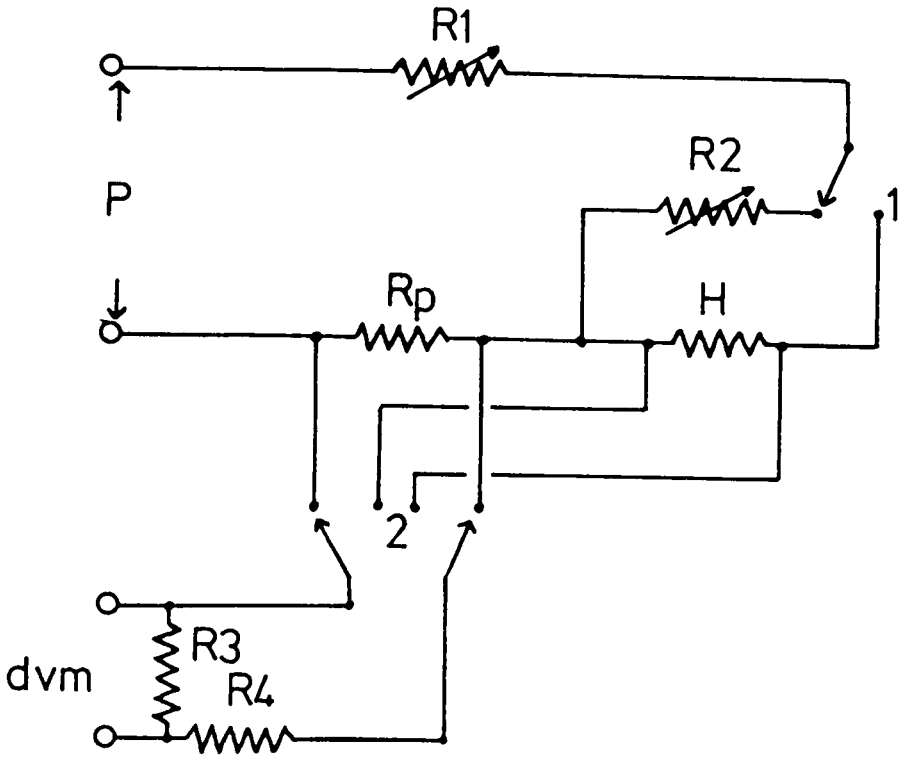

Figure 5.2 Arrangement used for the 12 V sample heater circuit: R1 1 kohm; R2 heater dummy max. 500 ohm; Rp precision resistor 50 ohm; R3 and R4 attenuating resistors 200 kohm and 1 Mohm, respectively. H heater; P 12 V d.c. power source; dvm internal voltmeter. The relays are shown in the off (zero) positions. The numbers are the user port signals required to change the latch positions: 1 PA0 high; 2 PA1 high.

The last appeared to be the simplest and has been adopted. A 9 V rechargeable battery replaces the transformer.

The ADC 3711 has a further refinement which at first appeared useful but which has since been abandoned. That is, it can read input voltages of either polarity, positive or negative. If the voltmeter is wired up to allow for this, stability is again adversely affected. The calorimeter voltmeter is thus restricted to measurements in the range 0 to +1.999 V. The only disadvantage of this is that it is necessary to check that the measurement input leads are connected with the correct polarity.

The IEEE circuitry was probably the most complex electronics project embarked upon during this work, despite the fact that the principle had been used previously in the department. The design was by Dr D A Armitage and construction and testing by myself. The interface logic is shown in figure 5.1.

Since the heater voltage is greater than the maximum acceptable by the voltmeter, some attenuation of the signal is necessary. This is simply performed using a pair of high stability fixed resistors, R3 and R4 in figure 5.2. R3 and R4 must be very large relative to the heater resistance. Initial values were R3 = 10^5 ohm and R4 = 10^6 ohm. By measuring the voltage drop across the heater directly with the Racal Dana multimeter, the attenuation was established at 11.05 : 1. The first runs (empty vessel, alumina, iodotungstate) were carried out with this arrangement. However, as the desirability of lower heater volages became apparent, attenuation was reduced by doubling the value of R3 (attenuation 6.02 : 1).

A further reduction in attenuation (R3 = 3 x 10^5 ohm) will be carried out when a suitable stable resistor is obtained.

A variation of one unit in the least significant digit of the heater voltmeter represents 1 mV in the attenuated signal; at worst say 1 mV in 500 mV. This produces an uncertainty of 0.2% in an individual voltage measurement. Comparison between heater measurements with the two voltmeters revealed no instance of our voltmeter differing by more than 1 mV from the true (Racal Dana) value.

The heater windings are of constantan; hence the resistance does not vary greatly with temperature (see table 3.1). However, it will vary slightly, particularly for large temperature increments, and this will affect the voltage drop and current flowing. To allow for this, a heat capacity measurement is not based on one voltage and current measurement, nor is it assumed that these values are constant during a heating period.

Instead, one pair of voltage and current measurements is made about every eight seconds. At least twice this frequency is possible but since the voltage drop rarely changes by more than 0.2% during a fifteen minute heating period, greater frequency was considered unnecessary. The voltage drop over the heating period is taken as an average of the individual readings.

Heater current

A precision resistor is wired in series with the heater. The current flowing through this resistor will be identical with that flowing through the heater. During a heating period

the voltage drop, V_p, across this resistor is measured. The current flowing can be obtained by application of Ohm's law.

A relay determines which of V_h(heater voltage) or V_p is measured by the voltmeter. The relay position is controlled by the PET.

Initially R_p was 20 ohm. However, with the use of lower heater power this was considered to be unsuitable and the precision resistor is now 50 ohm. The measured value at ambient temperature varies between 49.997 and 49.999 ohm over long periods. The assumption that this value is 50 ohm and stable introduces no significant uncertainty into the heat input determination.

At the end of a heating period the PET calculates the total heat input.

When the sample heater is off, the current is switched through a dummy heater. This can be adjusted such that the same current is flowing through the circuit as when the heater is on. This improves the stability of the heater power circuit. At different power outputs the voltage regulator runs at slightly different temperatures. Changes in temperature of the voltage regulator affect the voltage output slightly. The voltage regulator is therefore run at a steady temperature.

No switching transients ('on' or 'off' voltage surges) could be detected.

All voltage measurements are made by the 'four wire' method.[4,5]

Temperature rise

The thermometer is a platinum wire resistor of about 20 ohm at room temperature. For resistance measurements of very high

accuracy, d.c. or a.c. bridge instruments are usually employed.[5] These, even very expensive ones, often require manual balancing. This makes fully automatic measurement difficult. Such a d.c. bridge is in use elsewhere in the department (Tinsley NPL type 5840). It is manually balanced but does provide an 'out of balance' signal output. In principle, following manual setting, the out of balance signal could be used by the PET to calculate temperature change - albeit over a limited range. Reference 2 describes the use of this signal for an a.c. bridge.

However, for simplicity, it was decided to follow resistance changes using a multimeter, Racal Dana Series 6000. Similar instruments have been used elsewhere for temperature determination in calorimetric work (the authors of reference 6, for example, use a Yokogawa 2501 and those of 7 a Dana 5800).

Unfortunately, to perform resistance measurements, the multimeter drives a current of 10 mA through the resistor. The heat generated within the thermometer then becomes unacceptably high. It was therefore necessary to provide a current source of about 1 mA. This reduces power generation in the thermometer one hundredfold.

Such sources are commercially available or they can be constructed.[8] Experiments with electronic current sources built from relatively inexpensive components, however, proved unsatisfactory. The present system operates successfully with a 12 V lead-acid battery and high value precision resistors. Resistance values of 10 kohm and 15 kohm provide currents of around 1.2 and 0.8 mA. Strictly speaking this current source is not stable. As the sample temperature changes, the thermometer

resistance changes (about 1 part in 10^4 for a 1 ohm change in thermometer resistance, say 15 K). This in turn alters the current flowing. The thermometer current is therefore measured after each heating period. For the length of the following drift period the thermometer current is taken as constant.

The voltage drop across the thermometer is measured by the four wire method.[4,5]

The current is measured by determining the voltage drop across a precision resistor. Several types were tried. Small commercially available ones (RS Components) proved to be insufficiently stable except at much higher currents, about 3 to 7 mA. Boxed precision resistors (Tinsley, Cambridge Instruments), though more stable, were inconvenient as they had to be located outside the instrument. In the end, a resistor was constructed of manganin wire wrapped non-inductively around, and varnished to, a black heat sink. Manganin wire is the material of choice for resistors of high stability.[9]

The initial resistance of this resistor was 10.037 4 ohm. Following complete rewiring of the temperature measuring circuit (in an attempt to solve a problem discussed later), this value has been reduced to 10.028 0 ohm.

Provided that the instrument is allowed to warm up for several hours before measurements are made, this resistor is extremely stable (± 1 in the last digit over long periods).

The resistance value can be checked periodically by the PET setting the correct latch and instructing the multimeter to make a four wire measurement of resistance. Self heating of the resistor during continuous measurement of resistance can cause an apparent rise of about 0.2 mohm in a minute or two. The best estimate of

true or 'working' resistance is thus an average of a number of triggerred single resistance measurements. This proved to be more satisfactory than taking an average resistance based on continuous reading over a specified time (10 s, say). This was established by comparing Racal Dana and Tinsley-NPL bridge measurements of a number of resistors.

This problem may be eased by replacing the resistor with a similar one made of thicker grade manganin (at present 36 swg).

The IEEE port

The operation of this port, at the rear of the PET, is based on an American standard 'Institute of Electrical and Electronics Engineers Standard 488-1978'.

The port has 24 lines (8 are ground). Fifteen of the lines can be programmed as inputs or outputs and may transmit, or respond to, high (about +5 V) or low (about 0 V) signals.

The value of this port, however, lies in its ability to allow communication between the PET and external devices that understand the IEEE codes. Each IEEE device (several may be connected at the same time) has its own address. This enables the PET to select which device it wishes to communicate with.

There are eight lines for transmission of digital data between the PET and device. The other lines, driven high or low by the PET or the device (depending on the line's function) ensure an orderly sequence of events during data transmission. For example, the device will need to know when it has been addressed and when the PET is ready to accept data; the PET will need to know when valid data are on the data lines and to acknowledge receipt of those data so that new information may

be handled. A description of the operation of this port and some examples of its use are given in reference 10. Neither the home made voltmeter nor the PET comply exactly with the IEEE standard. The differences will only be mentioned where they affect the working of the calorimeter.

The Racal Dana series 6000

This is a 6½ digit multimeter. That is, it can display a seven figure reading of ohms or volts

0 or 1 XXX XXX.

Our instrument is fitted with three optional extras

(i) ohms measurement

(ii) 10 mV full scale amplifier

(iii) IEEE interface.

The maximum resolution on the 10 mV scale is 0.01 μV

0 or 1X.XXX XX mV

one decimal place better than the instruments of references 6 and 7.

At room temperature, with a thermometer current of 0.8 mA, the resistance of the thermometer can be measured with a resolution of about 0.01 mohm. However, the uncertainty in the last figure is considerable so, in practice, the resolution is taken to be about 0.1 mohm. This is about one order of magnitude less good than the department's d.c. bridge. Nonetheless, this is sufficient for the purposes of this work, and the multimeter has one other advantage over the bridge: it is more versatile as it is not restricted in its use to a thermometer resistance within a narrow range.

The Racal Dana has two sets of input terminals. One set is responsible for voltage drop measurements across the thermometer and its associated precision resistor.

With measurements of such high resolution, thermal e.m.f.s produced by dissimilar metal/metal junctions become significant. To reduce this problem, thermal-free solder (Cd-Sn, Oxford Instruments) is used for all connections outside the instrument. As far as can be determined using the Racal Dana, thermal e.m.f.s in this equipment are negligible.

However, there is another effect that produces similar results. This is instrument drift. After a period of time, the null or short circuit reading of the multimeter drifts slightly from zero. This is small but noticeable even after the instrument has been on for a long time. The instrument can perform internal recalibration routines that effectively set the null value to zero. This is time consuming (20-30 s) and is followed by a brief period of small but relatively rapid drift.

There are two ways of getting round this problem.

(i) The instrument measures the voltage drop across the thermometer. A relay is then closed (by the PET) and the voltage drop is measured with the input terminals short circuited. The true thermometer voltage drop is taken as the difference between the two. This difference calculation can be performed by the PET or the multimeter. Since the null off-set drifts only slowly, the null value need be updated only infrequently.

(ii) The current through the thermometer can be reversed. The true voltage drop is then taken as the average of the two.

The two methods produce, as far as could be determined, identical results. In the following chapters, most of the data have been obtained using the second method.

The multimeter is prevented from performing its internal calibration routines at critical moments during an experiment to avoid problems associated with sudden changes in the null value.

The authors of references 6 and 7 make no mention of drift and related problems.

An elaborate system for overcoming these problems and improving on the resolution of digital instruments has been produced by Beyer.[8]

All measurements made with the calorimeter described here must be with the multimeter on its most sensitive range. Mixing of ranges produces inconsistencies in the results, probably owing to the null value being different on different ranges (it is very much larger on the 100 mV range than on the 10 mV range).

PET-multimeter communication

There are two problems of communication between the PET and the multimeter. One relates to timing and the other to data errors. The PET normally waits for data from the IEEE lines for only 64 ms (this is non-IEEE-standard behaviour). If no data are forthcoming, the quantity or variable represented by those data is set at zero and the PET moves on through the program. For high accuracy work, the multimeter takes at least twice that time to perform one measurement.[4] It is therefore necessary for the PET to be instructed to keep returning to the data input statement until it finds data. This can be done in a number of ways, the simplest being to reject any zero value of a variable and to return to the input statement until a non-zero value is obtained.

However, since zero might occasionally represent valid data,

more reliable methods are available. If the PET has counted 'time out' after 64 ms, a particular 'status flag' is set within the microcomputer. The PET can check to see if this flag has been set. If it is set, it is assumed that the data are not valid. The flag is cleared and the data input statement is returned to. The process is repeated until data has been accepted without the flag having been set.

Alternatively the multimeter can be instructed to trigger the IEEE SRQ line when it has put data on the data lines. A program loop then ensures that the PET repeatedly returns to the data input statement and only accepts data when the SRQ line is set.

The transmitted data are numerical. Very occasionally errors occur in these data, though which instrument is responsible is not clear. If the PET is expecting numbers but receives an ASCII code corresponding to something non-numerical, it jumps out of the program and informs the operator that it has found an 'input data error'.

The PET is therefore instructed to look not for numbers but for 'strings'; that is, words that may be made up of any symbols, letters, numbers or punctuation marks. After the string has been input, it is evaluated. An ASCII code that does not correspond to a number is treated as if it were the nearest numerical code. If a data error does arise, it will not cause the PET to leave the program. The errors appear to occur in the sign of the input data. Calculations are arranged such that the sign does not enter into the temperature evaluation. Occasional sign faults in the thermocouple signals are not significant.

Multimeter operating modes

The multimeter can be instructed to operate in one of two modes, 'continuous' or 'triggerred'. In the first, readings are taken continuously and occasional readings are sampled by the PET. In the second mode, the instrument does nothing until it receives a 'trigger' signal from the PET. It then waits for what it considers to be a suitable settling time (or longer if instructed), spends a couple of hundred milliseconds taking a reading and outputs the data. This method makes it more difficult for the PET to obtain spurious values from the IEEE lines. This system was used in almost all the experiments described later.

Towards the end of this project, the second method began to appear less and less satisfactory, particularly when the multimeter was associated with a number of other switching functions. Sometimes considerable extra scatter appeared in the drift curves. This could be removed by not using the trigger mode and by not using current reversal through the thermometer. It was thought that the cause was a poor electrical contact in the thermometer circuit. However, following complete rewiring of this circuit (hence the slight change in precision resistor value described earlier), it now seems that this is unlikely unless the fault is within the thermometer. A more likely culprit is a sticking relay within the multimeter. The problem only arose during sections of two runs.

Temperature calculation

From the information it receives, the PET calculates the temperature corresponding to every reading, about one temperature value per 8-10 seconds during a drift period. The calculation is based on a simple iterative routine which in BASIC occupies no more than half a dozen program lines. However, this is fairly time consuming and calculations vary in the length of time required. Plotting and extrapolation of drift curves are much simpler if all calculations occupy the same length of time. Obviously a time delay could be inserted to ensure that this is the case.

In BASIC the calculations vary in length from about one second at 80 K to about one third of a second at 300 K. The variation between readings at temperatures close together is more than 0.1 s, this presumably being the time required for one cycle through the iteration.

The calculations were therefore performed using a machine code routine of about 250 program entries. The corresponding times are about 0.15 s (80 K) to 0.05 s (300 K) with a variation of no more than 0.015 s.

Shield control

The second set of multimeter inputs is used to record the shield-sample thermocouple difference signal. Temperature resolution, without further amplification of the signal, is better than 0.005 K even at 80 K.

Shield control is best considered in two parts. One is the PET's calculation that converts the voltage signal into a control signal. The second part is the electronic circuitry that translates the control signal into a heater voltage.

It is easier to describe the second part first since it dictates, to a large extent, the form of the control signals.

The user port

This input/output port of the PET consists of twelve lines, two of which are ground. There are eight data lines, PA0-PA7, which may operate as inputs or outputs. For the calorimetric work these operate only as outputs. Each may provide a signal of approximately zero or +5 V. This allows the output of binary signals equivalent to the numbers zero to 255. This is the control signal. Zero represents heater off and 255 shield heater full on.

The two other user port lines are the controls CA1 and CB2. CA1 is an edge sensitive input. That is, it can be programmed to respond to a signal change 0 to +5 V or +5 V to 0. This line is not used in the calorimeter control.

Line CB2 is more versatile. As an input it may respond to high (+5 V) or low signals. As an output it may produce these signals. In this work the PET switches the CB2 output from high to low or vice versa. This produces an edge which may be used in conjunction with edge sensing electronic logic circuitry. This point is discussed later under 'data latching'.

Shield power

The power source is a 1 A, -24 V regulator.

The PET's binary output is converted into analogue form using a digital to analogue converter (ZN 425). This signal, 0 to +2.55 V, has very low current driving ability. It is thus bufferred before being amplified and inverted, zero to -20 V. This voltage, applied to the base connection of a transistor allows the power source

voltage to be varied between zero and -20 V (see figures 5.3 and 5.4).

How then does the PET convert the temperature difference signal into a control number to drive the shield heater?

Control calculations

Commercial instruments used for adiabatic shield control generally operate on the basis of three terms:

(i) proportional; the shield power or voltage is proportional to the shield deviation from set conditions

(ii) integral; this adjusts the shield power according to the deviation from set conditions over a period

(iii) differential; this produces large increases or decreases in power in response to sudden changes in the shield-vessel temperature difference.

In this work, shield voltage has been controlled rather than shield power (proportional to voltage squared). This need not be the case, however.

Experience during this work suggests that proportional control is by far the most useful term. Integral control proved to be somewhat unmanageable so a contribution from this was not usually included. For a while it was replaced by a contribution based on average deviation of the shield from its set conditions. This term, when used, was always relatively small.

The most important contribution of the differential term is at the beginning of a heating period and immediately after the end of a heating period. In this project it was not used during drift periods.

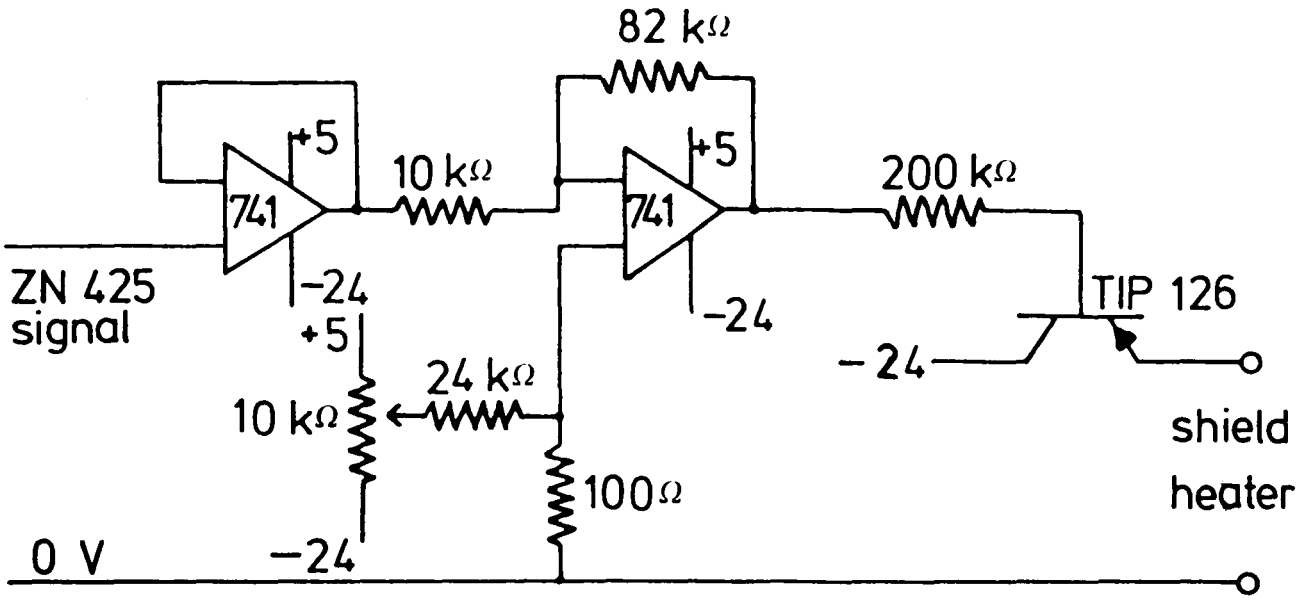

Figure 5.3 The shield heater control circuit. The ZN 425 (not shown) converts the digital user port signal (0-255) into a voltage (0-2.55 V). + and - numbers without units are voltages.

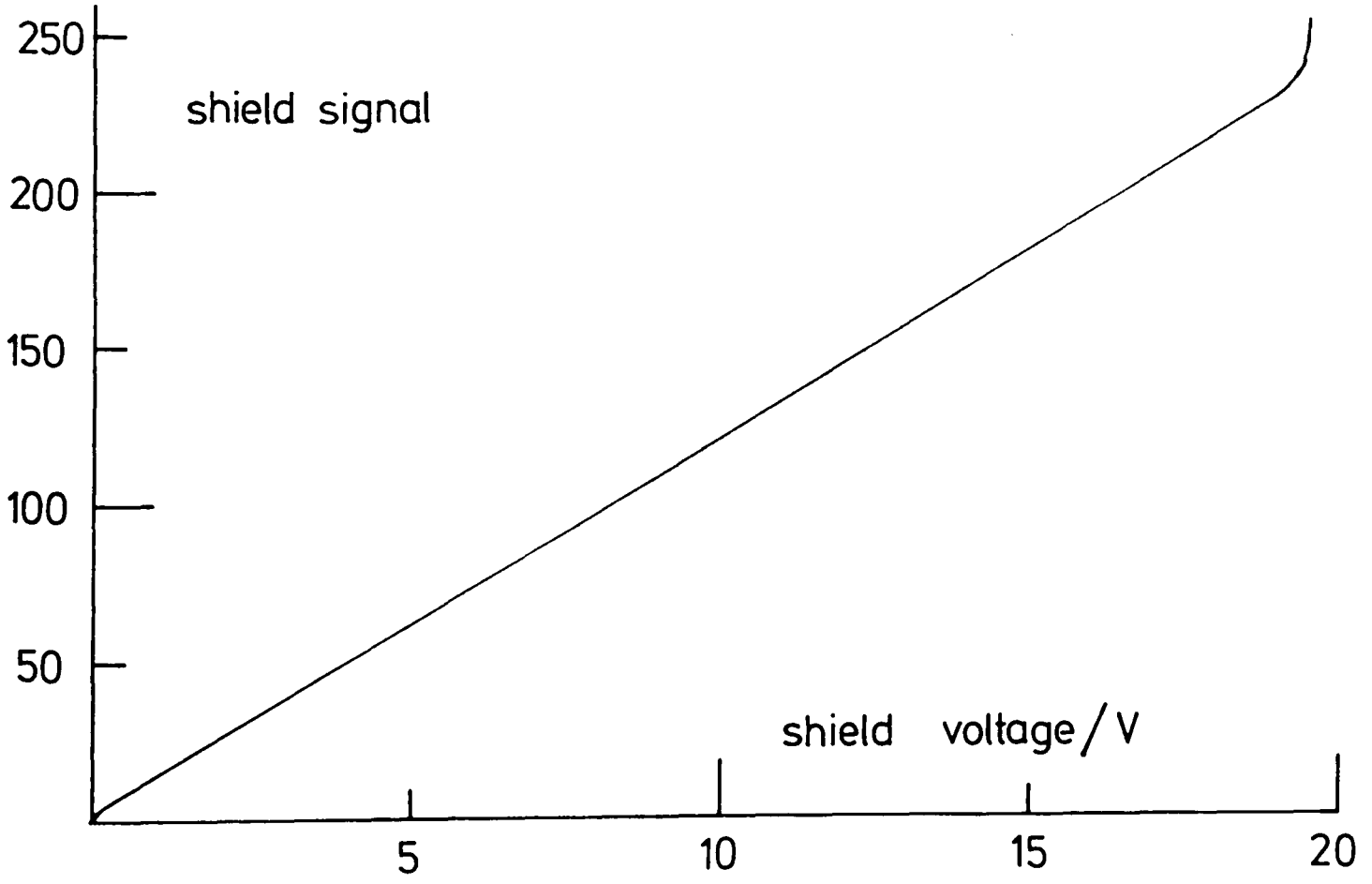

Figure 5.4 Shield voltage response (smoothed) to the user port control signal.

Control is based on a number of empirical parameters input by the operator at the beginning of a run. These are revised from time to time as the run proceeds. It is possible for the PET to perform this revision but this is so time consuming that manual adjustment has always been used.

Shield control during the initial drift period

Two parameters are necessary. One is an 'equilibrium' shield-vessel signal, V_c (in μV). The second is simply a multiplication term, M . The heater control signal is the product of M and the difference between the actual thermocouple signal and V_c. the parameter M, in this work, has varied between five and twelve. V_c varies from zero below 100 K to about - 30 μV at 300 K. For example, a run begins at 150 K. M is fixed at a value of seven. V_c is varied until a satisfactory drift curve is obtained; V_c = - 10 μV, say (minus represents shield warmer than vessel). Equilibrium is then established with a thermocouple signal of - 5 μV (shield about 0.2 K warmer than the sample).

For each drift period the PET prints the control conditions for reference when selecting suitable conditions at the beginning of a later run.

Shield control during a heating period

Two further terms are employed. One to increase M (5 times at 80 K to 2 times at 300 K) and a differential term. The differential term (usually 10 x M) operates on the difference between successive thermocouple inputs.

A variety of modifications were tried (M reducing slightly during the heating period and an additional term based on the

deviation of the thermocouple from the true equilibrium value) to make automatic control simpler. However, an optimum control function has not yet been established.

Manual intervention allows the operator to add or subtract up to 25% of the total heater signal at any time. This means a point is not lost if unsuitable values of the heating-period control parameters are chosen initially.

Shield control during the after-drift period

The differential term is continued for up to one minute into the after-drift period. V_c is adjusted slightly if necessary (by the PET or, more usually, manually) to maintain the shield-sample temperature difference the same as in the before drift period.

During the first few minutes after the heating period (while temperature measurement is not necessary) the PET can instruct the system to perform any necessary checks - voltage drop across the precision resistor, voltmeter null reading, etc.

Programming sequences for automatic running together with calculation of the molar heat capacity for each point have been produced. Each section has been tested separately. However, after the first sample for testing full automatic running (NMe_4I) had been loaded, a small leak developed in the calorimeter. Repeated cleaning and resealing of the cap suggests that this leak is not in the solder joint. Unfortunately the leak has not been traced. More substantial repairs (re-soldering of all joints) are likely to have a significant effect on the empty vessel heat capacity so remeasurement of the vessel heat capacity will be necessary.

Values of heat capacity, drift slope, etc. calculated by the PET have been produced and compared with values obtained by manual plotting of drift curves.

Data latching

As indicated earlier, a number of relays are required so that a particular measurement may be selected. These relays are under the control of the PET.

The following switching functions are available:

(i) between thermometer and precision resistor (1)

(ii) between heater and precision resistor (2)

(iii) Racal Dana null measurement (or resistor (1) resistance measurement)

(iv) thermometer current reversal

(v) heater on/off.

Control of these functions is via the user port. Clearly there must be some mechanism by which these signals can be distinguished from shield control signals. This is achieved by means of data latches. The user port output is fed in parallel to two eight bit latches. Each eight bit latch is made from two 74LS75 latches. Once the data are set on the user port lines a CB2 signal indicates which data these are. A falling edge signal from CB2 indicates 'relay signal'. A simple logic sequence converts this edge into a pulse which enables one eight bit latch (figure 5.5). These data are then transmitted by this latch and held until another pulse indicates that the relay data are to be changed (see figure 5.6).

A CB2 rising edge indicates 'shield signal'. This time a

pulse is produced which enables the other latch. The data will then be held as the shield signal and the relay data will be unaffected. Data latching is controlled by a short machine code routine. Whenever the shield signal is to be updated or some switching function performed the relevant data are transferred from BASIC to the machine code routine. No cross talk between signals has been noticed during calorimetric experiments.

The combination of eight high or low signals would allow us to operate a large number of relays. However, there are only five. The five lowest bits of the port user signal are used. Each of the five bits operates a relay via a transistor. The only major complication in this arrangement was in the selection of suitable relays. The best easily available to us - mercury wetted bounce free (RS Components) - were unsuitable. The relays were operated by 50 ohm coils. The current surges produced fluctuations in the zero volts line which upset some of the logic circuitry. The relays were therefore replaced by another type with 370 ohm coils.

These in turn posed another problem which had to be borne in mind in circuit design.

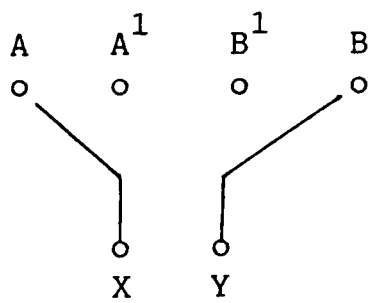

The off positions are represented by A and B. On switching the contact positions become X-A^1 and Y-B^1. During operation it was discovered that one on circuit 'made', X-A^1 for example, before the other 'off' circuit, Y-B, had broken. Relays from different manufacturers operated in the same way.

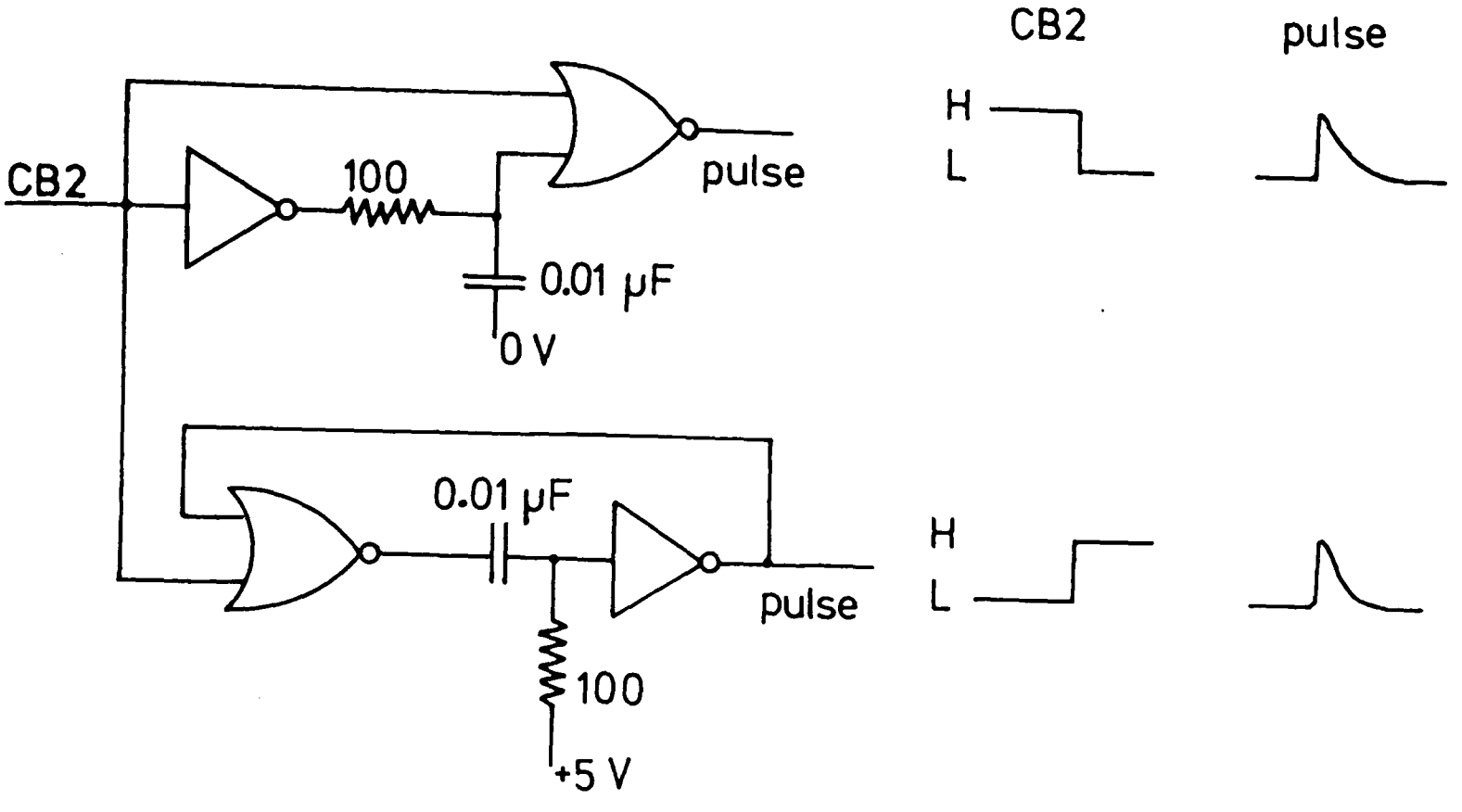

Figure 5.5 Logic associated with the CB2 line for producing pulses to enable the data latches.

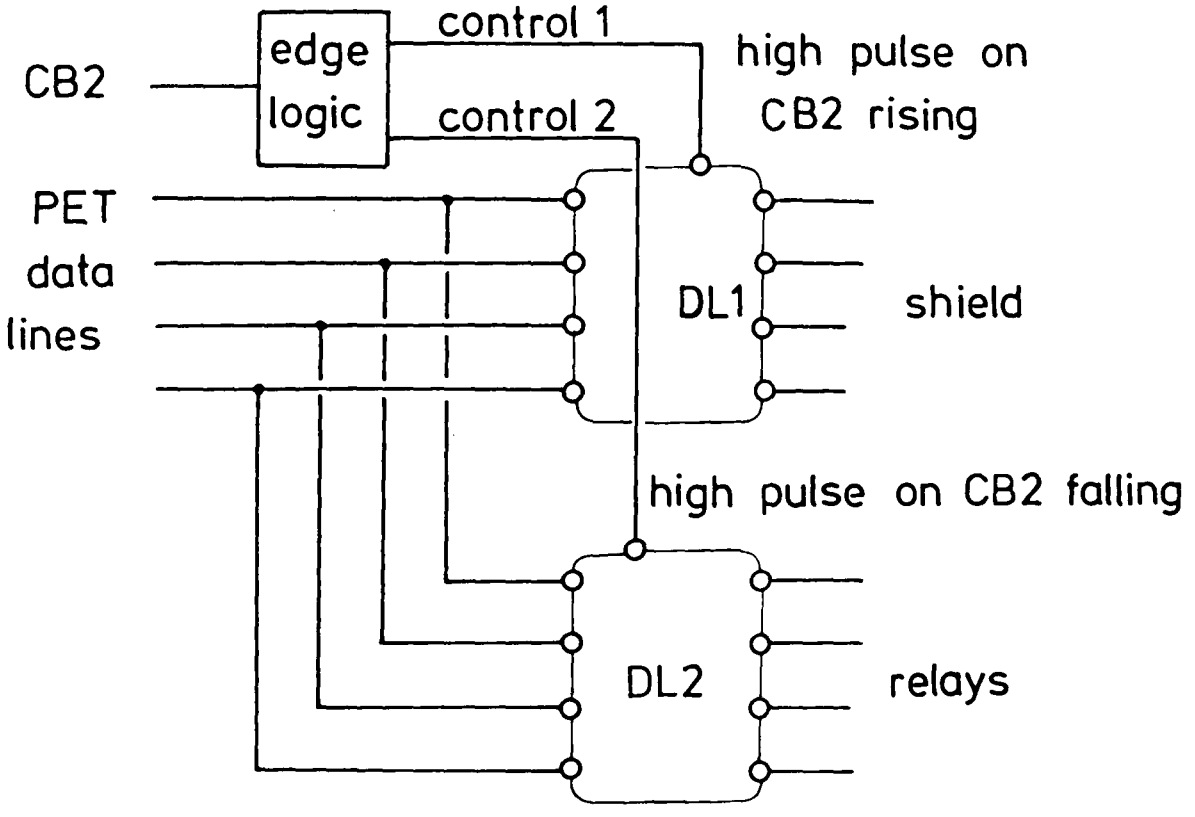

Figure 5.6 Operation of the data latches DL1 and DL2 using the logic circuitry of figure 5.5. For clarity only half of the data lines and latches are shown.

References to chapter 5

1 T M Jedju, *Rev Sci Instruments*, 1979, 50, 1077; and see for example H A Ashworth and R L Augustine, *Rev Sci Instruments*, 1981, 52, 105; R Shaw, J A Hardcastle, A R B Jusoh and M J Bongkik, *J Phys E*, 1981, 14, 301; N Collings, *J Phys E*, 1982, 15, 114.

2 P C Lanchester and D P Baker, *J Phys E*, 1981, 14, 805.

3 National Semiconductor Data Sheet ADC 3711, December, 1977 (available from Farnell, Leeds).

4 Series 6000 Microprocessing Multimeter Instruction Manual, Racal Dana, California.

5 See various articles in Experimental Thermodynamics Volume 1: Calorimetry of non-reacting systems, ed J P McCullough and D W Scott, IUPAC-Butterworths, 1968.

6 D Moses, O Ben-Aroya and N Lupu, *Rev Sci Instruments*, 1977, 48, 1098.

7 E Gmelin and P Rödhammer, *J Phys E*, 1981, 14, 223.

8 R P Beyer, US Bureau of Mines, personal communication; R P Beyer, M J Ferrante and R V Mrazek, *J Chem Thermodynamics*, 1983, 15, 827.

9 L Hartshorn and A G McNish in reference 5, p 59.

10 E Fisher and C W Jensen, PET and the IEEE 488 Bus (GPIB), Osborne-McGraw Hill, 1980.

6

The Calorimeter:

Operation

The vessel is designed to take samples in the form of small crystals, lumps or powders. Filling is via the filling tube shown in figure 4.1. A small paper funnel is used and this is discarded when filling is complete.

Before filling, the vessel is weighed. It is weighed again immediately after filling and the difference is taken as the sample mass. Weighings are performed with all vessel addenda - fixing bolts, cap, etc. - on the balance pan so that measurements obtained for different experiments may be compared.

The solder around the top of the filling tube is then melted with a fine tipped soldering iron. The cap is settled into place and the solder heated until it is completely fluid. A commercial solder m.p. 88 °C was retained for this seal after it had been rejected for the vacuum can seal. The reasoning behind this was that it would allow us (just) to observe the transitions in Ag_2HgI_4 around 50 °C. However, the problems with the commercial solder forced us to abandon it here too, in favour of a lower melting variety (see chapter 4).

Solder completely covers the copper cap. There is a 1 mm diameter hole through the cap and this is left exposed. At this point the vessel is weighed again and the total mass adjusted by addition or removal of solder. In this way no correction for heat capacity need be made for varying amounts

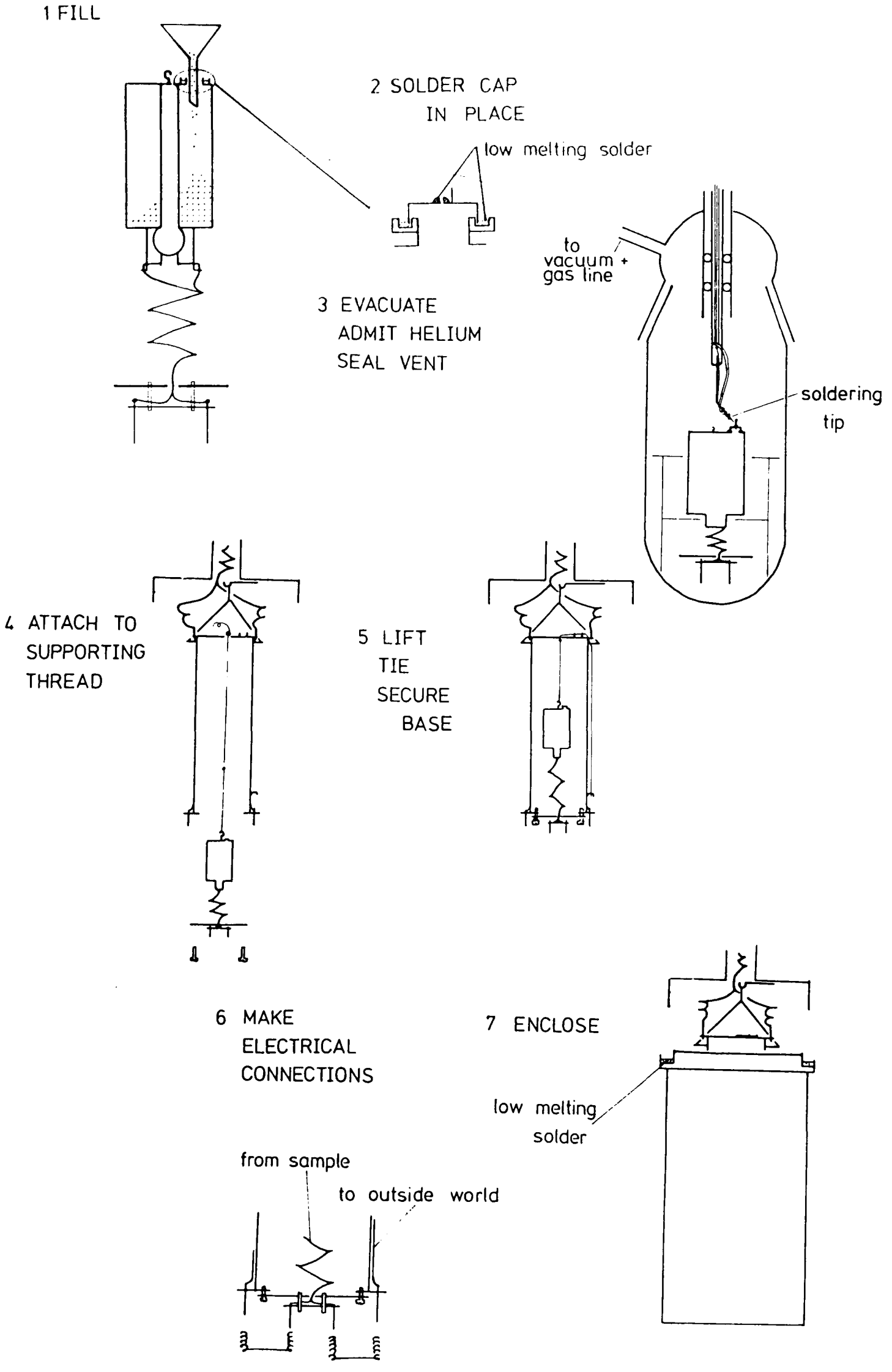

Figure 6.1 Filling and sealing the vessel.

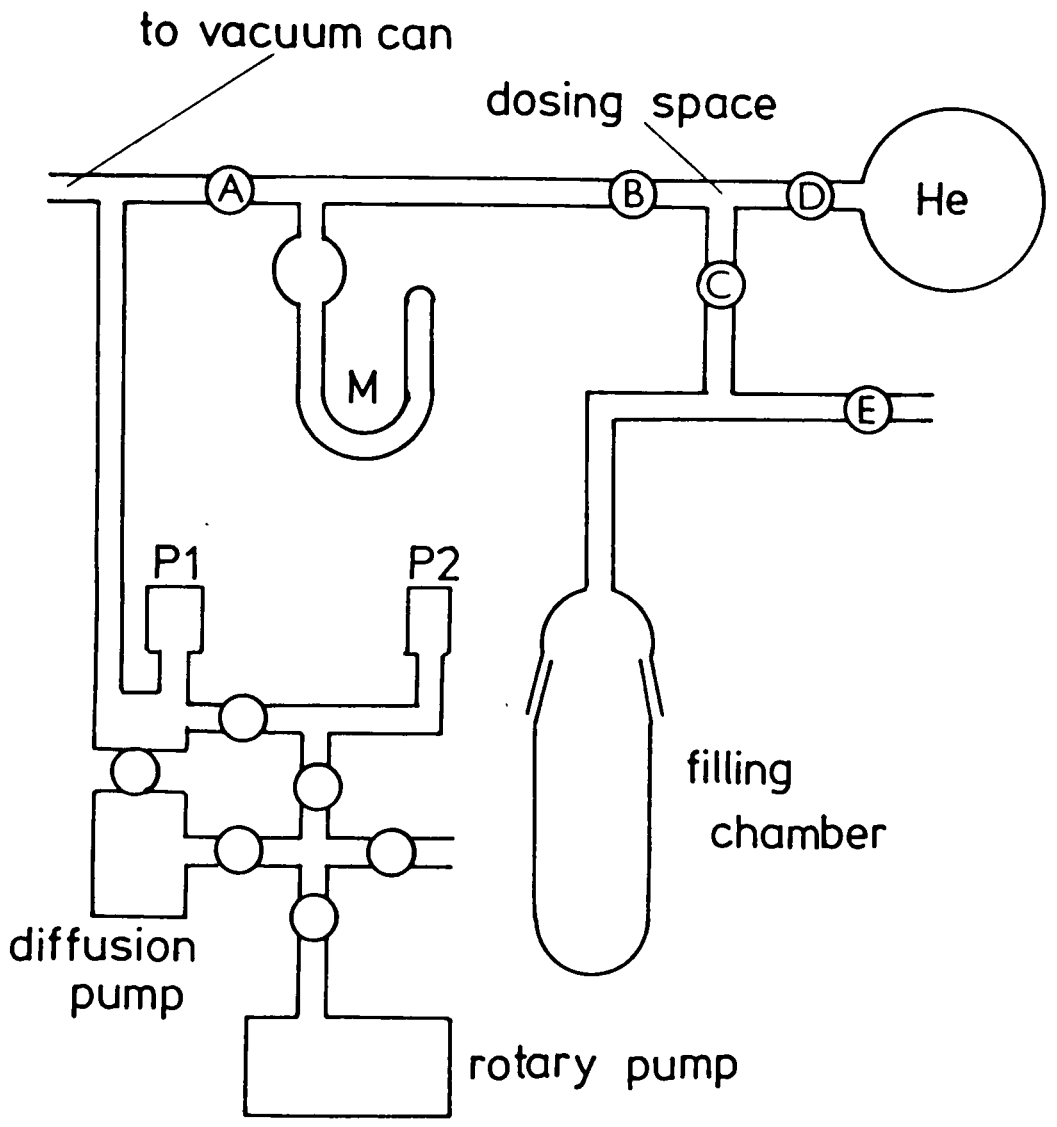

Figure 6.2 The vacuum system: M manometer; P1 Penning gauge; P2 Pirani gauge; A-E taps, see text; He helium gas bulb.

of solder. In cases where such an adjustment was difficult, small corrections were made using the data in an appendix to reference 2.

A separate chamber is attached to the vacuum line to allow the sample vessel to be evacuated and then filled with a small pressure of helium exchange gas. Small leaks during some runs gave an indication of just how vital this exchange gas is. The filling chamber is shown in figure 6.1 (part 3).

The base of the sample vessel is enclosed in a collar which allows it to be securely seated at the bottom of the chamber. A paper sleeve is put into the chamber before the vessel enters or leaves to ensure that no grease from the glass joint is rubbed onto the sample vessel. Once the vessel is in place the chamber can be evacuated. The sample is pumped for a few hours or overnight to ensure that any moisture is removed. The only exception to this was the sample containing NMe_4I since the volatility of the organic component under reduced pressure is not known. In this case pumping was restricted to less than one hour.

During pumping the soldering tip is outgassed at a temperature higher than that used for soldering.

After pumping, pressures recorded on the Penning are usually about 2×10^{-5} Torr though the pressure in the chamber will certainly be higher.

The chamber and helium line is now closed off from the pumping system (tap A figure 6.2). Taps B and C are also closed. One dose of helium is admitted to the dosing space by opening tap D. Tap D is closed. Tap C is opened to allow helium into the chamber. Tap B is then opened and the filling pressure can

be noted. Usually one dose (a few Torr) is sufficient but higher pressures (up to 35 Torr) have been used and are recommended for finely powdered samples.

The vessel can now be sealed by closing the hole in the cap. The soldering tip consists of a constantan winding (about 2.5 ohm) around a small, shaped brass bolt. The tip is solder wetted. Originally an aluminium screw was used to avoid removing solder from the cap. However, corrosion of the aluminium surface led to poor thermal contact between soldering tip and the solder. Movement of the soldering tip is limited so it is important that the vessel is well placed relative to the tip before evacuation. Covering of the 1 mm hole was not always easy. The system was improved by resting a copper pin in the hole. The solder proved far more willing to seal this than to cover an open hole - even a small one. The mass of the pin is only 0.04 g.

The vacuum in the filling chamber is released (tap E).

The vessel is weighed again. This mass is compared with that immediately before sealing. A reduction in mass of around 0.02 g indicates that the sealing operation has been successful. Following problems with very slow leaks, it is usual to leave the vessel on the balance for about an hour. If there is any significant increase in mass (more than a couple of milligrams) the vessel is left on the balance for much longer. If the mass continues to rise the seal is considered to be faulty.

Air is now admitted to the vacuum system and the vacuum can removed by warming the solder joint. The shield is clamped in place.

The sample vessel is attached to its support thread. When the vessel is not in place, the end of this thread is held clear of the shield bottom by a small weight. The vessel is raised by means of a thread while most of the weight is taken by a finger below the vessel. The thread runs down the outside of the shield and is attached to a hook near the foot of the shield wall.

The shield base (which remains attached to the vessel at all times,see chapter 4) is then attached to the shield using the four small bolts. The base will only fit when correctly oriented. This simplifies making the electrical connections.

Final adjustment of the vessel height can now be made. The vessel is lifted using the supporting thread. A knot on the thread inside the shield indicates when the correct position is reached. The thread is looped over one or two posts on the shield lid to maintain this position. Occasionally the thread breaks. It is in any case stretched and weakened by repeated use so it must be replaced from time to time.

At this point it is wise to checkthat all pins on the shield base are in fact insulated from that base. The vessel wires pass through a small hole in the base before being soldered to the pins. Shorts between these enamelled wires and the base were a very annoying problem. Wire-wire shorts were never noted. Varnish is not sufficient protection against chafing between wires and copper, even if the wire movement is very limited (see chapter 4).

It is now possible to make the electrical connections

between the vessel (pins on the shield base) and shield (pins on a flange surrounding the shield). Wire-wrap links are made between adjacent pins. Pin-pin connection is checked (about 0.3 ohm or less). No failures or problems with these connections have been noted.

The wrapping wire used is silver coated copper. During cooling-warming cycles severe cracking of the silver coat is apparent both to the eye and under a microscope. This cracking in no way affects the performance of the junctions. The cracked surfaces tarnish very rapidly in air.

The shield clamp is replaced and the resistance of the shield-vessel thermocouple is checked. A value less than eight ohms suggests that the vessel is touching the shield wall. The usual cause of this is that the vessel height within the shield has not been adjusted properly.

A visual check is made of all the connections at the top of the shield. Each wire is given a gentle tug with a pair of flat ended tweezers.

The solder in the rim of the vacuum can is cleaned by scraping away any oxidized material. The can is lifted around the shield until it presses against the top rim. The solder is melted with a small bunsen flame. Again any debris is removed and any material that is not completely fluid. If it appears necessary more solder is added or the surface is re-fluxed (dilute HCl or slightly acid $ZnCl_2$ solution).

Pumping can be started once the solder has solidified. All pin-pin resistances are checked at the point where the wires leave the vacuum system. It is particularly important

to check that there is no electrical link between the pins and the vacuum can or piping at earth potential. It is necessary to unplug the heaters to perform this check.

Once the vacuum in the system registers less than 10^{-4} Torr, the vacuum seal is tested by surrounding the can briefly with liquid nitrogen.

The instruments are now switched on and a check made that the control program functions correctly.

The system is pumped overnight or longer before the can is again immersed in coolant.

Cooling

The vacuum can is surrounded by a large dewar flask of coolant. Generally this is liquid nitrogen which is suitable for runs up to about 280 K, though shield control becomes difficult above 260 K. During the first few runs (empty vessel, alumina and, to some extent, silver iodotungstate), liquid nitrogen proved unsuitable above about 200-240 K. This probably was a result of the higher sample heater currents used in early runs and the difficulty of following the rapid temperature rise with the shield. Some early work was therefore carried out using methanol slush baths (about 180 K) and solid carbon dioxide in methanol (about 200 K). Results obtained where the different bath ranges overlap were identical.

However, these baths are no longer used. The range 270-300 K is covered using a coolant of part frozen salt water (260 K).

The sample is brought to the temperature of the coolant using helium exchange gas. The vacuum chamber can be closed off from the pumps and helium gas introduced. A few Torr

pressure of helium is sufficient to take the sample from room temperature to 78 K in two or three hours. Pressure of less than 10^{-5} Torr is obtained within minutes of restarting pumping.

The sample is allowed to equilibrate at the required temperature for at least a couple of hours before any measurements are made. The first measurement of a particular series is generally considered to be of less good quality than the others and is not tabulated in the later chapters unless no other data close to that temperature are available.

Since helium was already available on the vacuum line, the alternative method for rapidly cooling the sample - a mechanical link between the sample and can wall - was not considered.

Removing the sample

Once the diffusion pump has cooled, air is admitted to the vacuum system. The vacuum can is lowered and the shield is clamped in position.

The wire-wrap connections are removed followed by the retaining bolts. At this point it is important that the vessel be supported from below at all times. The support thread is unhitched from the posts on the shield lid and from the retaining hook near the foot of the shield. The vessel is lowered and removed. To prevent the thread disappearing back into the shield a small weight is attached to it.

The vacuum can is replaced.

Before removing the cap, the vessel is brought to atmospheric pressure either by drilling through the solder over the hole in

the cap (now abandoned) or by removing the copper pin.

The cap can then be removed and the sample gently shaken out.

The vessel is weighed (1) before removing the pin; (2) after removing the pin; (3) after removing the cap; (4) after removing the sample.

The inside of the vessel is cleaned with water and acetone and is dried by evacuation in the helium filling chamber.

Heat capacity measurement

Construction of the calorimeter, particularly the sample vessel, took much longer than expected. Therefore, once the system was complete and tested, it was decided that the first priority lay in data acquisition rather than in optimizing the control program to allow for automatic running.

The initial equilibrium drift curves are obtained by selection of control parameters. These are adjusted until a suitable drift is obtained (usually less than 1 mK min^{-1}). The Racal Dana is then instructed that it must not perform any calibration functions. The voltage drop across the precision resistor in series with the thermometer is checked.

Drift is then maintained until a linear plot has been obtained for about the length of the heating period to be used.

The operator or the PET then initiates a heating period. The PET screen displays shield-sample temperature difference (as μV) and the shield control parameters. If control is not considered satisfactory manual adjustment of the shield heater power is possible using the keyboard numerical keys. Heating may be stopped at any time and the PET will display the total heat

input and beginning, end and mid-points of the heating period. It is possible to obtain total shield deviation from equilibrium conditions (in units of μV s) but this is not normally done. A number of tests have indicated that corrections to the heat capacity resulting from shield errors are negligible (see the 'worst case' example later).

At the timed end of the heating period the PET produces the heat input and timing information given above. It is now necessary to wait for re-establishment of the same shield-sample temperature difference as existed in the pre-heating period. Usually this is rapid and again no correction for shield errors is necessary.

There is now a period of equilibration during which time frequent temperature measurement is not necessary. This allows various parameters to be checked (voltmeter null reading, voltage drop across the precision resistor, etc.) or adjusted (new heating period, heater power, heating period control parameters etc.).

The length of time required for equilibrium to be reached varies from sample to sample from a few minutes to an hour or more. Drift temperatures are measured at 10 s intervals. Extrapolation of these curves (which are linear) is usually to the mid-point of the heating period. The temperature rise is the difference between the extrapolated values. The mid-point is taken as the temperature of the heat capacity determination.

At the end of the heating period the shield temperature rises relative to that of the sample, sometimes by as much as 0.2 or 0.3 K. At low temperatures this is a problem since

cooling of the shield is very slow. In these cases therefore the after-drift period is arranged with the shield warmer, relatively, than it was during the before-drift or heating periods. Since, during the heating period, the shield has followed the conditions set in the before-drift period, extrapolation is now to the end of the heating period, not to the mid-point. The temperature of the heat capacity determination is still taken as the mid-point.

Some examples of drift curves are shown in figure 6.3.

In the caption to that figure a list is given of data available from the heat capacity calculation program. Drift points were stored on tape and input separately for the calculation.

Electrical interference

It soon became apparent from the drift curves that the instruments were very sensitive to electrical disturbances elsewhere in the building - the most dramatic of these disturbances being when the earth line was struck by lightning.

To minimize this interference all instruments were fitted with mains filters. While this eases some problems concerned with switching of other instruments nearby - such as a kettle in the adjoining office - most of the effects remained. One bad example is the Xpelair fan in the laboratory. Switching on or off the fan crashes the computer program. The PET must be switched off and the program reloaded from tape.

As a precaution, before loading a program, all instruments

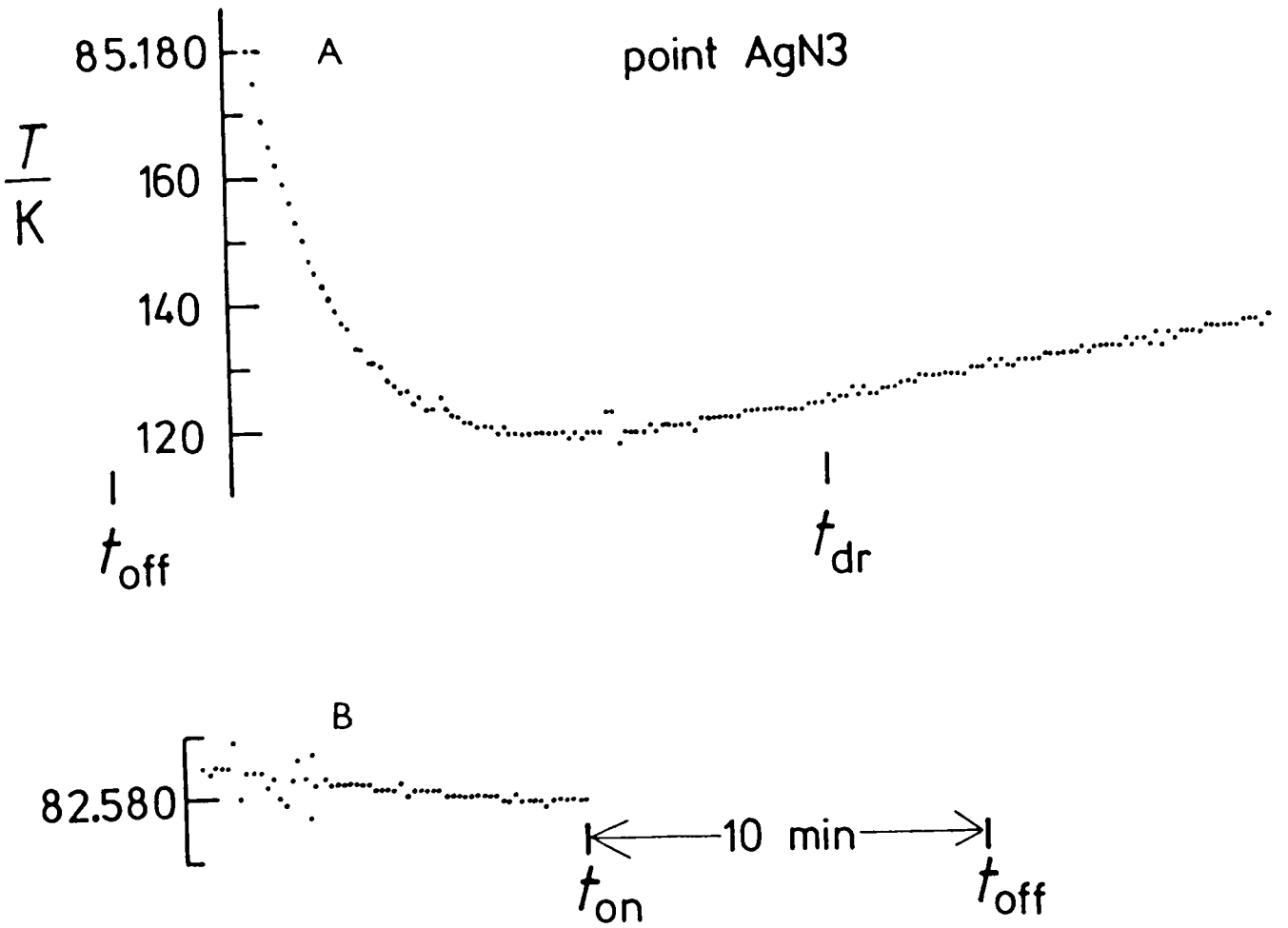

Figure 6.3 Examples of drift curves obtained during this work (hand plotted): B before drifts; A after drifts.

Alternatively the heat capacity may be calculated by the PET. A linear curve fit is produced for a part of the drift chosen by the operator (number of points up to last point). Sample name, heat input, heating time, average temperature, temperature increment and total heat capacity are printed. Curve fit data are displayed on the screen.

attached to the PET, even if they are not going to be used immediately, are switched on. Switching on the printer, for example, after the program has been loaded often damages the program.

The best quality drift curves are obtained at night. Bad interference is experienced at 10.20 a.m. (tea break), 12 a.m., 3.30 p.m. (tea break) and at about 4.45 p.m. However, the scatter produced is not serious enough to affect adiabatic control or heat capacity measurements significantly. Drift curves are extended over slightly longer periods. An example of such scatter is visible in figure 6.3.

Unfortunately there is a further source of interference which causes enormous problems. On the roof of the building is a short wave radio transmitter which, when in use, generates spurious signals several hundred microvolts in magnitude. The transmitter is used by a radio club and by the Electrical Engineering Department. At some times of the year the radio was operated every tea break, lunch time, most evenings and some Saturday mornings. The Electrical Engineering Department was very unwilling to restrict the use of the transmitter and we were not informed in advance when transmissions were to take place. The Electrical Engineering Department did suggest extensive measures for screening all equipment and filtering of signals to the Racal Dana. About 4-6 weeks was spent in experimenting with these filters with no significant reduction in interference. Fortunately examinations and summer holidays arrived to provide a respite. Short of removing the transmitter or the calorimeter to another building it is difficult to visualize a solution to

this problem.

Other instruments in the building are also affected.

Shield error corrections

Having selected a set of control parameters it is possible to maintain the shield-sample temperature difference constant to within 0.01 K at 80 K (better at higher temperatures as the thermocouple sensitivity increases). Good linear drift curves can be obtained.

During a heating period control may be slightly less good, perhaps within 0.02 K for the bulk of the heating period. At the beginning of the heating period, however, deviation from the equilibrium conditions may occur to the extent that the shield temperature may fall by as much as 0.2 K below the required value for a few seconds. A similar effect, but in the opposite direction occurs when the sample heater is switched off.

The first deviation will cause the sample to lose energy to the shield. The second will cause the sample to gain energy.

To balance this sort of effect, in principle, it is possible to run the shield deliberately either too hot or too cold for an equivalent length of time. In this way it should be possible to cancel errors arising from shield deviations from equilibrium.

However, this technique is viewed with some suspicion. Experience suggests that heat losses to a cold shield are greater than gains from a hot shield if imbalance temperatures are equal (but opposite). This is noticeable above about 200 K.

This is probably the result of the shield ends being at a slightly lower temperature than the body.

Alternatively the heat errors produced by shield deviation from equilibrium can be calculated from the area under the deviation-time curve. The heat equivalent of this area is determined by measuring the area under drift curves with the shield deliberately offset. Temperature drift can be equated with area under the (deliberate) deviation-time curve.

An example of such a calculation is given. This is a 'worst case' example. It represents a very early point with poor shield control. Such shield control would now be considered unacceptable.

Alumina: point 5 19/2/83 at about 83 K

It was established from a number of drift curves that zero drift corresponded to a shield-sample signal of about - 1 μV (shield about 0.05 K warmer than sample). From the drift curves it was observed that heat loss or gain was directly proportional to shield offset from equilibrium. An area of 60 μV min under a shield-cold drift curve represented an energy loss from the sample (as determined from the temperature drop and approximate total heat capacity) of 0.1 J.

$$+ 60\ \mu V\ min \equiv 0.1\ J \text{ lost from sample}$$

For the 5.5 min period between the start of the heating period and re-establishment of the shield-sample temperature difference at a steady value equal to that of the before-drift period, the shield error amounted to + 20 μV min or about 0.03 J lost from the sample.

For this 40 s heating period the energy input was 9.91 J. The error in energy input resulting from the shield error is thus 0. 3%.

This is several times larger than any error determined since the calibration runs. Later corrections have been small and very difficult to evaluate precisely. As a result no corrections for shield errors were made in this work. Any point during which shield control is considered poor is either abandoned or marked as uncertain (see the tabulated results in later chapters).

In general shield error effects are considered to be less than 0.1%.

Precision and accuracy

It was hoped that overall accuracy of the calorimetric measurements would be better than 1%. Only comparison of results obtained with published data allows us to evaluate this. In view of the results obtained with alumina, this aim appears to have been achieved, particularly in view of the fact that control was fairly crude for the early measurements. Certainly, alumina was an extremely easy sample to work with; on the other hand the empty vessel proved to be a very difficult subject.

The results obtained suggest that precision is far better than 1%. Reproducibility of results obtained under different conditions and the lack of scatter of the points about smoothed curves are evidence of that.

In many respects the calorimeter is therefore comparable with other instruments constructed recently.[3] My one reservation lies in the absolute value of the temperature determined using

a multimeter. This should be borne in mind when reading the data tabulated in later chapters. Temperatures are quoted to two decimal places. However, the second place is probably only significant relative to adjacent values, and absolute significance is not claimed.

Induction effects

It has been assumed that heater-induced effects in the thermometer and thermocouple are negligible. Deliberate rapid changes in shield heater power do not appear to affect the thermometer, and thermocouple effects are certainly less than a microvolt. Effects resulting from sample heater switching are more difficult to detect since they will be superimposed on relatively much larger real temperature changes. Thermometer effects will in any case not be important because the absolute temperature during and shortly after the heating period is not used in the calculations. In fact, once confidence had been gained in the system, temperature was not measured during that time.

Problems with temperature measurement while heating is taking place have, however, been reported.[4] Induced e.m.f.s in thermocouples used in the d.t.a. instrument built during this work are very large even though heaters are non-inductively wound. It should be noted, however, that these heat powers are three orders of magnitude greater than the calorimeter sample heater power.

References to chapter 6

1 I Kh Aopyan and B V Novikov, *Sov Phys Solid State*, 1982, 24, 332; B Baranowski, M Friesel and A Lunden, Paper SC17-P3/33, 4th International Conference on Solid State Ionics, Grenoble, 1983.

2 R G Linford, D Phil Thesis, Oxford, 1967.

3 See for example J C van Miltenburg, Thesis, Utrecht, 1972; R Burriel, Thesis, Zaragoza, 1979; K Arvidsson, B Falk and S Sunner, *Chem Scripta*, 1976, 10, 193; Z Jianyao, F Yangpu, H Zhixin, L Chuyun and S Dunrong, *Acta Phys Temp Humilis Sin (China)*, 1983, 5, 76 (*Phys Abs*, 1983, 86(1215), entry 79333).

4 J Garcia, J Bartolomé, D Gonzalez, R Navarro and W J Crama, *J Chem Thermodynamics*, 1983, 15, 1109.

7

The Calorimeter:

Calibration and Testing

The heat capacity of the empty vessel is much smaller than that of the vessel when full of sample so the operating characteristics in the two situations may be very different. A few preliminary experiments early in 1983 indicated that empty vessel measurements might prove difficult. The sample heater was too powerful for the shield to follow.

The first run was thus on alumina. Alumina was chosen as it was expected to show a heat capacity variation more in line with that of the samples to be studied than benzoic acid, the standard material recommended for this range.[3]

If the empty vessel measurements then proved difficult, measurements would be made on the vessel containing benzoic acid. The empty vessel heat capacity could then be calculated by the difference

vessel heat capacity = total heat capacity minus known heat capacity of sample

As it happened this was not necessary.

Despite what has been said above the results are presented in the more logical sequence with the empty vessel first.

A very high density of points, with extensive areas of overlap between runs,allowed a comparison to be made between results obtained with different control parameters (long versus short heating periods, etc.). Results obtained under different conditions appeared identical, though no measurements were made with small temperature increments (less than 1 K).

Heat capacity of the empty vessel

Calorimeter total mass with all addenda (unsealed) 42.069 g

(sealed with 10 Torr helium) 42.042 g

In early runs it was not possible to use liquid nitrogen as coolant over the whole temperature range (78 - 315 K). In part this was a result of the high sample heater power. With the empty vessel, it was necessary to replace nitrogen with a methanol slush at about 200 K. On the basis of later results, it also appears possible that vacuum conditions in early runs were not as good within the experimental chamber as suggested by the Penning gauge (less than 10^{-6} Torr). The methanol slush became unsuitable at about 270 K. With the empty vessel it proved difficult to make measurements above 280 K, even with ice as coolant. Drift curves were often steep.

This problem may lead to errors in the calculation of sample heat capacity above about 270 K. However, provided that the vessel has no anomaly in the region 270-300 K the errors should not be serious.

At a later date (see chapter 10) a few heat capacity measurements were made on the empty vessel in the range 270-290 K. These measurements suggest that the original results in this range may be slightly low. This conclusion is supported by the experimental data for alumina.

The experimental values of the heat capacity are listed in table 7.1. These values, except those marked with an asterisk, were fitted to a five term function using the PET computer.

All permutations of terms from T^{-2} to T^{5} and ln T were tried.

Table 7.1

Experimentally determined heat capacity of the empty vessel

T/K	C_p/J K^{-1}	T/K	C_p/J K^{-1}	T/K	C_p/J K^{-1}
78.44	6.11	114.08	8.31	192.79	10.55
78.50	6.20	115.56	8.35	195.76	10.51*
79.77	6.24	119.05	8.54	196.54	10.57
81.81	6.32	120.87	8.58	198.41	10.54
82.79	6.39	122.67	8.64	200.48	10.61
83.41	6.53	126.51	8.82	201.03	10.65
84.79	6.57	128.61	8.91	202.32	10.59
85.15	6.59	130.67	9.00	203.65	10.67*
85.67	6.64	132.71	9.09	204.30	10.68
85.90	6.62	134.73	9.16	206.45	10.73
86.33	6.66*	134.94	9.09	208.58	10.75
87.05	6.67	138.41	9.27	211.06	10.82
87.63	6.76	142.10	9.30*	213.75	10.86
88.15	6.79	144.60	9.38	216.10	10.87
89.20	6.92	147.56	9.48	216.54	10.87
92.49	7.07	150.48	9.56	218.23	10.89
94.78	7.21	153.38	9.65	218.64	10.92
95.89	7.28	156.25	9.74	220.30	10.94
96.99	7.35	159.10	9.82	220.35	10.95
97.39	7.36	161.93	9.89	222.40	10.98
98.09	7.40	164.72	9.95	226.56	11.03
99.00	7.46	167.49	10.02	228.61	11.07
99.14	7.47	170.26	10.04	230.66	11.05
100.15	7.53	173.01	10.14*	232.71	11.08
101.27	7.60	175.52	10.12	234.75	11.12
102.51	7.64	175.74	10.18	236.78	11.15
103.72	7.74	178.45	10.24	238.79	11.14
104.89	7.82	181.15	10.28	239.58	11.19
106.09	7.87	183.84	10.34	240.83	11.21
107.41	8.01	183.98	10.37	241.53	11.19
108.77	8.05	185.71	10.44	242.86	11.23
110.12	8.13	186.50	10.40	243.54	11.25
111.44	8.21	189.50	10.48	245.56	11.23*
112.77	8.23	191.72	10.47	246.14	11.24*

Table 7.1(continued)

Experimentally determined heat capacity of the empty vessel

T/K	C_p/J K^{-1}	T/K	C_p/J K^{-1}	T/K	C_p/J K^{-1}
248.61	11.29	268.18	11.50	284.10	11.60*
251.08	11.31	270.57	11.46	284.53	11.59*
253.54	11.33	273.23	11.50	287.38	11.80*
256.00	11.37	275.87	11.63*	294.17	11.82
258.45	11.40	278.49	11.56*	296.87	12.08*
260.91	11.44	280.85	11.55		
263.27	11.45	281.11	11.56*		
265.72	11.46	282.58	11.56		

Points marked with an asterisk (*) were omitted from the curve fitting procedures because of poor after-drift curves - either they were steep or too short (usually a result of electrical interference caused by short wave radio signals).

Table 7.2

Some comparisons with Bates' calorimeter[2]

T/K	C_p/ J K^{-1}	
	Bates	this work
88.00	8.76	6.80
120.81	11.24	8.57
150.11	12.63	9.59
197.79	14.04	10.60
253.34	15.10	11.33
298.08	15.75	11.81

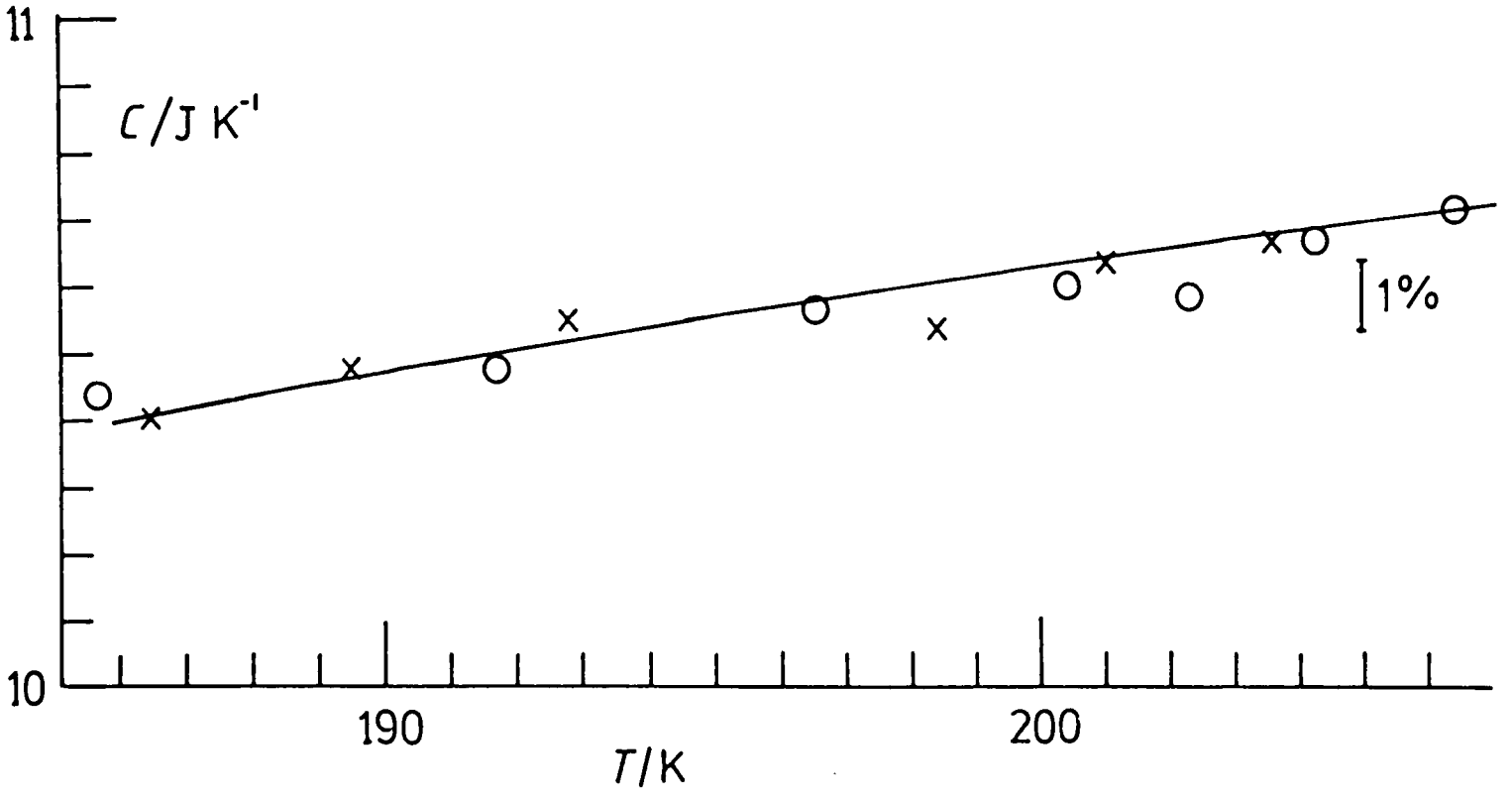

Figure 7.1 Part of the heat capacity curve for the empty vessel: solid line equation (7.1); x liquid nitrogen coolant; o methanol slush coolant.

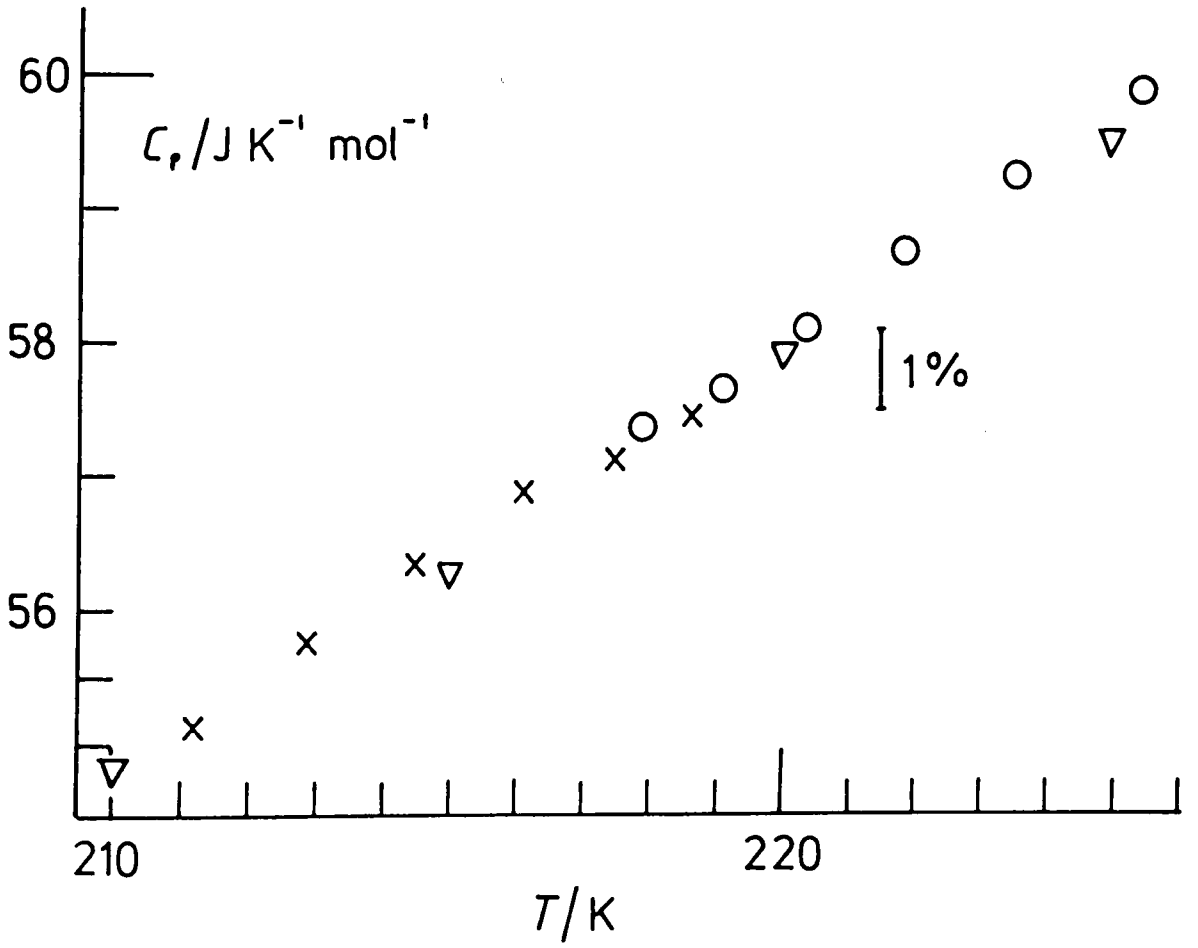

Figure 7.2 Part of the molar heat capacity curve for alumina: x liquid nitrogen coolant; o methanol slush coolant; ∇ from the curve fit of reference 3.

The best fit (123 points, standard deviation 0.03) was obtained with

$$C_p/\mathrm{J\ K^{-1}\ mol^{-1}} = -49.024 - 0.085\,99(T/\mathrm{K}) + 8.534\,6\times10^{-5}(T/\mathrm{K})^2 + 6\,160(T/\mathrm{K})^{-2} + 13.833\times\ln(T/\mathrm{K}) \qquad (7.1)$$

A section of the heat capacity curve is shown in figure 7.1. This shows the overlap region between two coolant baths, liquid nitrogen and methanol slush. Also shown is the function (7.1). In table 7.2 a few values derived from equation (7.1) are compared with the results of Bates.[2] His calorimeter was of approximately the same dimensions, was of copper and contained the same thermometer.

Despite the fact that the quality of the results above 280 K is poor, equation (7.1) is taken as valid up to 315 K. The very bad scatter of points above 282 K made it tempting to ignore these in the curve fitting. However, if this is done, the fitted function begins to curve down slightly beyond 290 K. Some of the high temperature points were thus retained to prevent this.

Alumina

The alumina used was a National Bureau of Standards Calorimetry Conference sample[3] kindly loaned by Dr N G Parsonage of Imperial College. It was in the form of small lumps.

The alumina was sealed in the vessel with approximately 10 Torr pressure of helium exchange gas. No correction to the heat capacity was made for this helium. The mass of the vessel was recorded as (in air)

1st series 42.080 g

2nd series 42.052 g

Solder corrections were thus negligible (less than 0.02 g in 42 g; 0.05% by mass).

Table 7.3

Experimental values for the heat capacity of aluminium oxide

T/K	C_p/J mol^{-1} K^{-1}	T/K	C_p/J mol^{-1} K^{-1}	T/K	C_p/J mol^{-1} K^{-1}
78.27	6.65	115.11	18.36	152.71	32.97
79.36	6.87	116.37	18.78	154.79	33.73
80.51	7.15	117.77	19.28*	156.84	34.65
80.74	7.18	121.28	20.48	158.86	35.44
81.67	7.32	122.43	20.94	160.85	36.21
82.52	7.60	123.71	21.46	163.17	37.07
82.73	7.61	125.18	22.07	165.47	38.03*
83.53	7.71	126.63	22.59	167.07	38.54
83.77	7.90	126.75	22.67	168.94	39.38
84.57	8.07*	128.06	23.22	170.79	39.74
84.77	8.16	128.37	23.31	172.97	40.91
85.56	8.57*	129.46	23.72*	175.46	41.87
85.76	8.43	130.11	23.49*	177.92	42.86
86.61	8.76	130.84	24.25	180.34	43.82
87.28	8.93	131.83	24.61*	182.71	44.78
88.88	9.41	132.20	24.77	185.07	45.67
89.80	9.65	133.56	25.28	187.38	46.48
90.71	9.87	133.59	25.28*	189.74	47.47
91.60	10.18	134.88	25.83	192.04	48.36
92.49	10.47*	135.24	25.93	194.31	49.27
93.40	10.73	136.19	26.36	196.53	49.99
94.26	10.90	136.87	26.53	198.46	50.88
95.82	11.48	137.48	26.89	199.97	51.12
96.72	11.67	138.63	27.37	201.80	51.84
97.53	11.96	139.61	27.68	207.94	54.00
98.04	12.03	140.52	28.04	211.24	55.13
98.53	12.29	141.01	28.28	212.87	55.75
108.31	15.58*	142.37	28.81*	214.50	56.35
109.17	15.97	144.19	29.56	216.11	56.88
110.18	16.35	145.98	30.28	217.50	57.12
111.27	16.81	147.74	31.16*	217.95	57.37
112.56	17.22	148.80	31.41	218.67	57.43
113.83	18.13	150.60	32.15	219.10	57.63

Table 7.3(continued)

Experimental values for the heat capacity of aluminium oxide

T/K	C_p/J mol^{-1} K^{-1}	T/K	C_p/J mol^{-1} K^{-1}	T/K	C_p/J mol^{-1} K^{-1}
220.39	58.11	252.26	68.02	284.25	76.54
221.89	58.69	255.92	69.03	286.63	76.80
223.59	59.25	259.53	69.97*	288.65	77.67
225.50	59.89	263.11	71.15	289.96	77.93
229.63	61.31	266.65	72.07	293.02	78.87
231.65	61.99	270.69	73.17	293.26	78.56
233.64	62.59	275.27	74.35	296.52	79.45
235.68	63.12	279.30	75.14	299.79	80.03
237.84	63.74	279.78	75.46	303.06	80.77
240.94	64.73	280.67	75.75	306.28	81.54
244.77	65.84	282.37	76.11	309.46	82.60
248.54	66.92	284.06	76.42		

* Points not included in the curve fitting procedures.

Following heating periods, equilibrium was re-established within a few minutes and drift periods of 15-20 minutes were sufficient. The heater power used was about 0.3 W which is now considered to be too high for good shield control. An example of the possible size of the error introduced was given earlier.

Heat capacity of alumina

The alumina results were obtained in two stages. In the first, with liquid nitrogen coolant, measurements were continued until shield control became difficult, above about 220 K. As pointed out earlier, this probably resulted from the use of a relatively high heater power which the shield was unable to follow.

The sample was removed and experiments then performed on the empty vessel over the whole temperature range.

In the second stage, alumina was again sealed in the vessel and results obtained up to 310 K. Some low temperature measurements were duplicated. The masses of alumina in the two stages differed slightly

mass of alumina, stage 1: 42.466 g, 0.416 5 mol

stage 2: 42.389 g, 0.415 7 mol

The experimental results for the molar heat capacity are tabulated together in table 7.3. Results in the overlap region are shown in figure 7.2 together with some National Bureau of Standards' data for the same standard alumina.[3]

These experiments provided far more confidence in the calorimeter than had the work with the empty vessel. The results, plotted out on a very large scale, fell close to a smooth curve up to 310 K. A plot on the scale required for this thesis would show no useful features.

The molar heat capacity data were fitted to the function

$$C_p/\mathrm{J\ K^{-1}\ mol^{-1}} = 234.143 + 1.552\,96(T/\mathrm{K}) - 2.481\,1\times10^{-3}(T/\mathrm{K})^2 + 1.523\,9\times10^{-6}(T/\mathrm{K})^3 - 76.734\times\ln(T/\mathrm{K}) \qquad (7.2)$$

(121 points, standard deviation 0.1). The use of higher powers of temperature did not improve the fit, nor did fitting as two curves, one for each sample mass. Three quarters of the experimental points lie within 0.2% of the fitting curve, 85% within 0.3%.

Results obtained from equation (7.2) are compared with the National Bureau of Standards' values in table 7.4. The measurements above 250 K are not as good as we would have liked. However, our aim was for an accuracy of better than one per cent and this has been achieved. Further, it was achieved on the first runs with the calorimeter. In view of the early difficulties involved in shield control, these results were very encouraging.

The initial samples to be studied were to be solid electrolytes produced by solid state reactions. Since it is difficult to determine the exact stoichiometries of these, it is not thought that an absolute error of one per cent is serious. The high precision of the instrument is sufficient to allow us to observe, reliably, small anomalies in the heat capacity.

I am confident that, as a result of improvements to the control system, accuracy of far better than one per cent will be demonstrated in a future project. At this stage of the work, however, further optimization of calorimeter accuracy did not seem to be justified.

Table 7.4

Smoothed molar heat capacity of alumina: this work and National Bureau of Standards[3]

T/K	C_p/J K^{-1} mol^{-1}		% deviation
	this work	NBS	
80	7.03	6.90	+1.8
85	8.25	8.25	0.0
90	9.64	9.69	-0.5
95	11.15	11.22	-0.6
100	12.78	12.84	-0.4
105	14.50	14.54	-0.3
110	16.29	16.32	-0.2
115	18.14	18.16	-0.1
120	20.04	20.06	-0.1
125	21.98	21.99	0.0
130	23.94	23.96	-0.1
135	25.92	25.95	-0.1
140	27.92	27.96	-0.1
145	29.92	29.97	-0.1
150	31.92	31.98	-0.2
155	33.92	33.99	-0.2
160	35.90	35.99	-0.2
165	37.88	37.97	-0.2
170	39.84	39.94	-0.2
175	41.78	41.88	-0.2
180	43.70	43.79	-0.2
185	45.59	45.68	-0.2
190	47.46	47.53	-0.1
195	49.31	49.35	-0.1
200	51.12	51.14	0.0
205	52.90	52.89	0.0
210	54.66	54.60	+0.1
215	56.38	56.28	+0.2
220	58.06	57.92	+0.2
225	59.71	59.53	+0.3
230	61.33	61.10	+0.3
235	62.91	62.63	+0.4
240	64.46	64.13	+0.5
245	65.97	65.59	+0.6
250	67.44	67.01	+0.6
255	68.88	68.40	+0.7
260	70.28	69.76	+0.7
265	71.65	71.08	+0.8
270	72.98	72.37	+0.8
275	74.27	73.62	+0.8
280	75.53	74.84	+0.9
285	76.75	76.03	+0.9
290	77.93	77.19	+0.9
295	79.09	78.31	+1.0
300	80.20	79.41	+1.0
305	81.27	80.47	+1.0

References to chapter 7

1 D C Ginnings and G T Furukawa, *J Amer Chem Soc*, 1953, 75, 522.

2 T R Bates, D Phil Thesis, Oxford, 1957.

3 G T Furukawa, T B Douglas, R E McCoskey and D C Ginnings, *J Res Nat Bur Stand*, 1956, 57, 67; see also D A Ditmars and T B Douglas, *J Res Nat Bur Stand A*, 1971, 75, 401; D A Ditmars, S Ishihara, S S Chang, G Bernstein and E D West, *J Res Nat Bur Stand*, 1982, 87, 159.

8

The Crystalline Electrolytes

$Ag_{13}I_9W_2O_8$ and $Ag_6I_4WO_4$

The first electrolyte studied was $Ag_{13}I_9W_2O_8$. It was known that this compound undergoes at least two, and probably three, phase transitions between 100 and 300 K. Conclusions concerning the order of these transitions were originally based on spectroscopic studies,[1,2] though these conclusions are now known to be erroneous. The most recent study from the same laboratory suggests that there are two first order transitions and a lambda anomaly.[3]

The purpose of this investigation was to confirm - or deny - the presence of the third transition and to investigate the shape of the heat capacity curve, particularly above the first order transition at 246 K.

By coincidence, at about the same time as our heat capacity results appeared,[4] an x-ray study confirmed the presence of four phase regions between 77 and 300 K.[5]

There is some disagreement about which transition is associated with the onset of conductivity. This point will be returned to later.

Preparation of $Ag_{13}I_9W_2O_8$

Chan and Geller[6] report some difficulty in producing phase pure material for their crystallographic study. Their suggested preparation method involves prolonged solid state reaction in an

oxygen atmosphere, and they report that on heating in vacuum slight decomposition of the electrolyte occurs with loss of oxygen. However, no indication of the extent of decomposition is given. It is not visible by d.t.a. or t.g.a. (this work).

It was therefore decided to investigate the solid formed from cooling of a melt of Ag_2WO_4 and AgI in the required proportions.

An intimate mixture of the components was produced by coprecipitation from Ag NO_3 solution using the quantities of KI and Na_2WO_4 required by stoichiometry. Both AgI and Ag_2WO_4 are extremely insoluble. The yellow precipitate was very fine, and it was necessary to heat the solution nearly to boiling point. Filtration of the cooled solution could then be carried out through grade 50 paper. The precipitate was washed with water until the washings were free from Ag^+, WO_4^{2-} and I^-.

As much of the preparation as possible was carried out in the dark.

The sample was dried at 380 K. Heating in an oven to 575 K produced a completely fluid dark red melt. The melt was allowed to cool slowly in air, 24 h at about 560 K, just below the melting point, followed by cooling over a period of three days to 470 K. The sample was maintained at this temperature for four days. At this point the sample was removed, crushed and thouroughly ground. It was then reheated to just above the melting point (570 K) and the cooling process repeated.

The sample was examined by x-ray powder diffraction and thermal analysis. On the basis of their work on single crystals, Chan and Geller describe how best to assess the purity of polycrystalline material from powder patterns. In our sample

we could detect no evidence for the presence of either of the starting materials, AgI or Ag_2WO_4. Nor, following Chan and Geller's recipe, is there any evidence of the phase $Ag_5IW_2O_8$. However, we will return to this composition later.

It should be borne in mind that x-ray photographs are not very satisfactory for detecting small quantities of impurity phases. The problems are further aggravated with $Ag_{13}I_9W_2O_8$ by two additional factors. First, the parent compound has a very large number of lines. Secondly, most of the lines are not sharp, and there is also a certain amount of diffuse background to the photograph making it difficult to detect very weak lines. The presence of line broadening and a diffuse background is characteristic of this class of solid electrolytes. These features result from uncertainty in the position of the mobile Ag^+ ions.

D.t.a. traces (only at scan speeds greater than 20 K min^{-1}) showed some evidence of a thermal effect around 430 K. If this is the result of the presence of unreacted silver iodide, the amount is very small. A number of d.t.a. runs with unreacted mixtures suggest less than one or two per cent of the original starting material.

Further annealing at about 500 K over the Easter break (about five days) produced no change in the x-ray or d.t.a. behaviour.

The sample melts incongruently, beginning near 560 K, to form a red melt. It has been suggested that preparation of a pure compound from this melt may be difficult due to phase separation at the solidification temperatures.[6] However, the melt supercools very readily. D.t.a. traces with a wide range of scan speeds all showed only a single solidification peak (see figure 8.1).

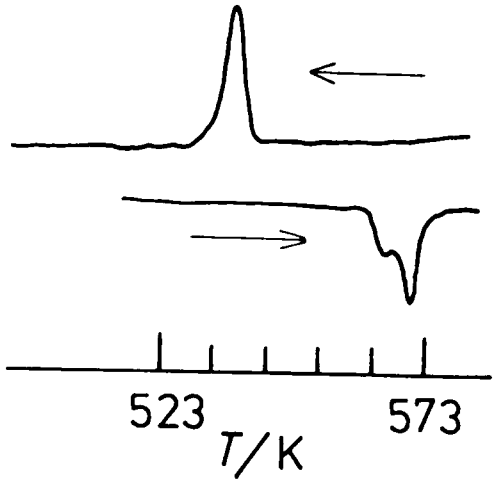

Figure 8.1 Melting and solidification of crystalline $Ag_{13}I_9W_2O_8$ as shown on a d.t.a. trace (both heating and cooling about 20 K min^{-1}). It is possible to supercool the liquid well below the melting point before solidification occurs.

The sample was coarsely crushed for loading into the calorimeter.

Heat capacity of $Ag_{13}I_9W_2O_8$

Calorimeter mass (empty)	42.071 g
Sample mass	48.133 g

No solder corrections were made.

Since there was clear evidence of hysteresis and non-equilibrium behaviour, the heat capacity results are listed in chronological order rather than in order of increasing temperature (table 8.1). This also allows some indication to be obtained of the temperature increments employed. It should be noted that the accuracy of the final three points above 295 K is considered to be poor as the drift curves obtained were steep (7-8 mK min^{-1}).

The results are shown in figure 8.2. The two first order transitions are clearly visible, as is the continuous transition near 275 K.

Estimation of the latent heats associated with the first order transitions is difficult since there is evidence of pre-transition effects; in the higher temperature case the choice of a base line heat capacity is somewhat arbitrary.

However, to make comparison with other work simpler, we restrict ourselves to to the temperature region close to the transition. Baseline heat capacity curves were drawn by hand. Points from these curves and the experimental points from series 1 and 4 were used to estimate the 'excess' heat capacity in the transition region. The latent heat data are given in table 8.2.

A second measurement was made of the enthalpy change associated with the lower first order transition. This involved a single heating period of one hour (385.4 J, 16.36 K), giving

$$\Delta H(\text{single point value}) = 880 \text{ J mol}^{-1}$$

Agreement with the value given in table 8.2 is good.

If we include a contribution to the lower transition from the region 172-192 K, the transition enthalpy change can be increased substantially (to 1080 J mol^{-1}).

In reference 4 we gave an estimate of what we believe would be the maximum effect visible by the d.s.c. technique near 275 K, 250 J mol^{-1}. Greer et al's value is 105 J mol^{-1}. Considering their extremely small d.s.c. event (equivalent to less than 2.5 μg water on the sample pan), Greer et al's conclusions concerning the nature of the transition are very impressive.

The total molar enthalpy of the solid, relative to that at

Table 8.1

Heat capacity of the electrolyte $Ag_{13}I_9W_2O_8$

T/K	C_p/J K^{-1} mol^{-1}
series 1	
79.53	546
81.42	551
82.77	553
84.61	556
86.42	560
88.21	563
89.76	565
91.37	569
93.12	572
94.85	577
96.56	579
96.66	582
98.24	586
98.33	586
99.95	586
101.60	591
103.78	596
106.46	601
109.12	606
111.73	610
114.33	615
116.88	620
119.41	624
121.91	629
125.01	634
129.37	644
134.35	651
146.81	668
151.59	674
156.30	682
160.96	690
162.81	694*
165.56	697
167.42	699
171.89	708
176.40	714*
180.85	723
185.26	733
189.59	741
193.89	751
196.68	800
197.93	1137
199.04	1087
200.28	807
201.66	764
203.06	758
204.46	755
series 2	
197.50	905
200.17	803
201.56	767
202.99	758
205.87	753
207.28	762
210.33	766
211.69	768
213.04	769
215.79	778
219.91	783
224.06	784
228.16	794
232.25	802
236.34	810
240.34	818
series 3	
208.66	782
212.85	796
217.07	792*
series 4	
227.47	800
231.49	803
235.47	810
239.44	817
242.70	831
244.66	839
247.16	911
248.20	1273
248.96	1273
250.34	906
251.60	877
252.86	875
254.13	873
255.39	877
256.65	874
series 5	
270.61	896
271.86	882
273.10	892
274.45	897
275.54	898
276.78	870
278.03	850
279.30	842
280.58	845
281.86	843
283.13	839

Table 8.1(continued)

Heat capacity of the electrolyte $Ag_{13}I_9W_2O_8$

T/K	C_p/J K^{-1} mol^{-1}	T/K	C_p/J K^{-1} mol^{-1}	T/K	C_p/J K^{-1} mol^{-1}
284.39	843	268.00	881	series 7	
285.64	839	269.25	884	282.38	844
286.88	839	270.49	890	286.18	849
series 6		271.74	891	289.54	844
257.91	875	272.98	894	293.83	846
259.80	879*	274.22	900	297.55	839*
262.34	865*	275.46	906	301.09	835*
264.86	875	276.70	874	304.84	832*
266.75	880	277.97	856		

Points marked with an asterisk are considered to be poor; either after-drift curves were very steep or they had to be cut short.

Table 8.2

Enthalpy changes for the first order transitions in $Ag_{13}I_9W_2O_8$

T/K		$\Delta_t H$/J mol^{-1}	
this work	Greer et al.	this work	Greer et al.
198.5±0.2	199	890 (192-203 K)*	674
248.6±0.2	247	980 (241-251 K)*	711

* Temperature interval over which the excess heat capacity was estimated.

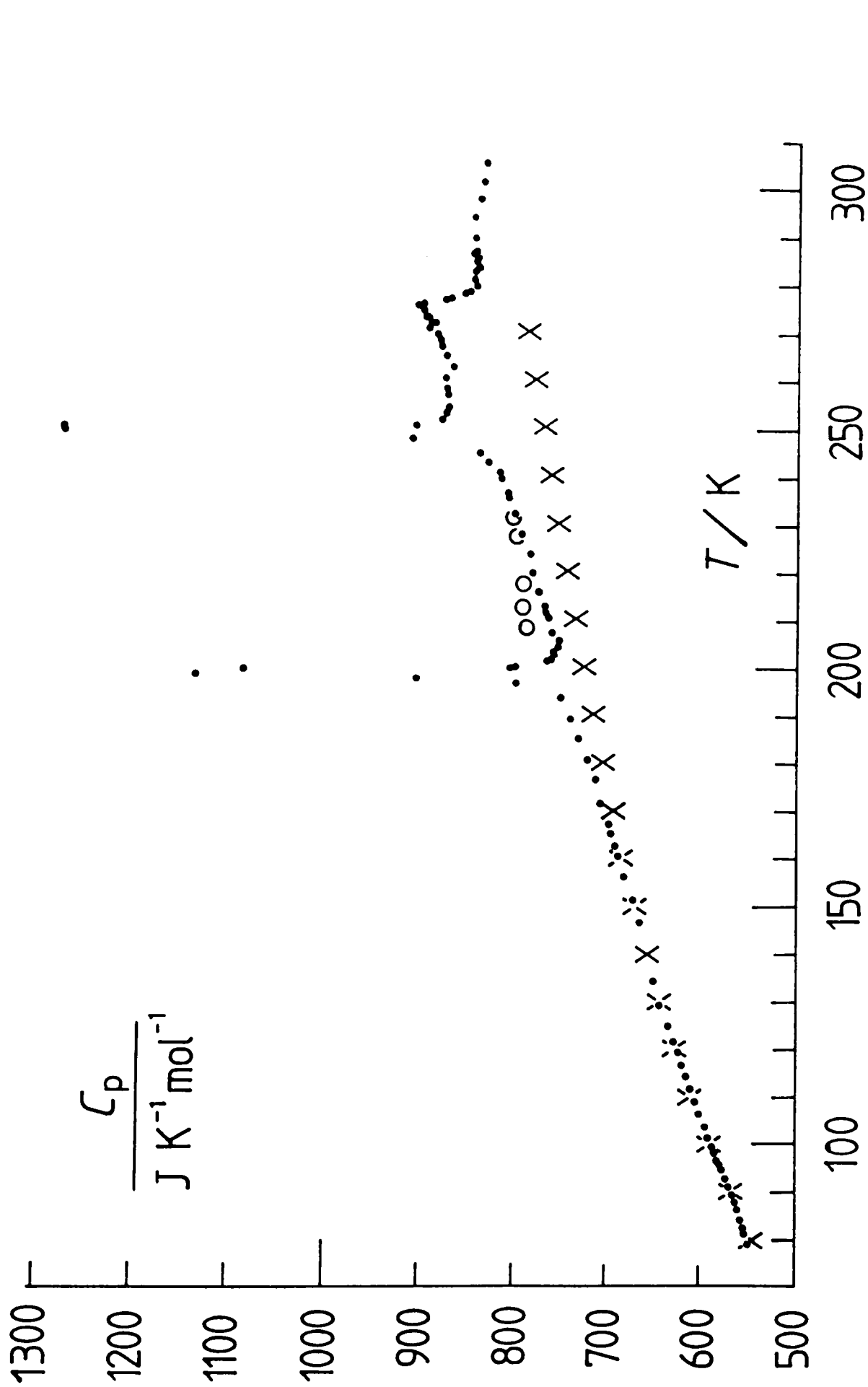

Figure 8.2 Molar heat capacity of the electrolyte $Ag_{13}I_9W_2O_8$:
o points observed for a sample cooled only to 202 K;
x heat capacity of the mixture $9AgI+2Ag_2WO_4$ (see chapter 10).

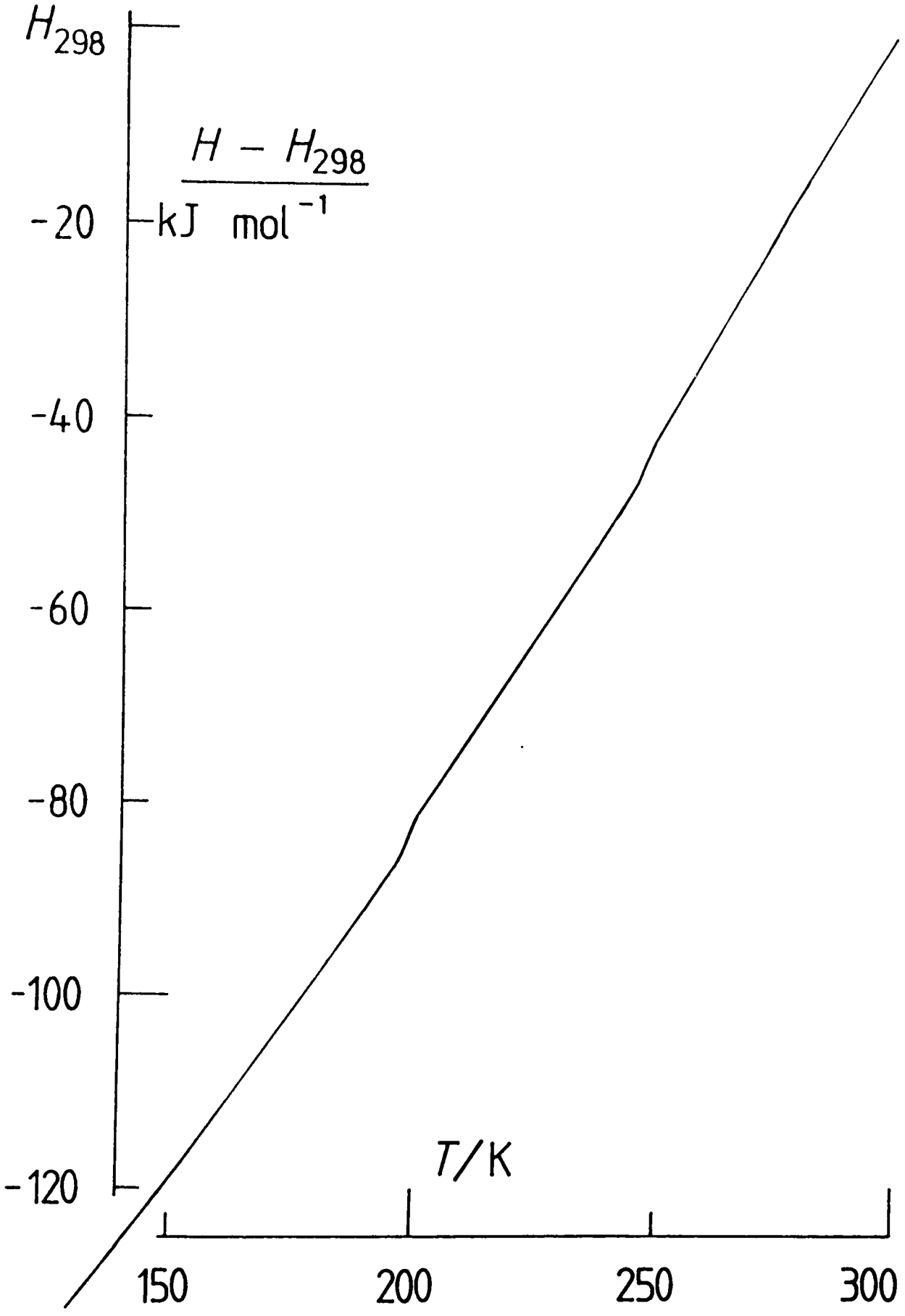

Figure 8.3 Total molar enthalpy of crystalline $Ag_{13}I_9W_2O_8$ in the range 140-300 K, relative to that at 298.15 K. The first order transitions are visible as small steps.

298.15 K, is plotted against temperature in figure 8.3. The steps resulting from the first order transitions are visible.

Just above the transition at 198 K there is evidence of non-equilibrium behaviour. This is visible in figure 8.2. A continuous run, from below the transition, indicates the formationof a metastable state which exists over a temperature range of about 20 K. If the sample is annealed at room temperature and then returned to a temperature of 202 K (above the transition) a new heat capacity curve is produced which does not coincide with the first. This sort of behaviour is not altogether unexpected for a first order transition.

A second run was thus made through the transition and longer drift periods allowed for points just above the transition. The results, with drift curves of about 1 h, were marginally higher than expected on the basis of the first run. For the point at 207 K heat capacity values based on extrapolation back (to the mid-point of the heating period) from sections of the drift curve after about 30 min, 60 min and 90 min increased slightly from 765 to 770 J K^{-1} mol^{-1}. In view of the uncertainty introduced by long extrapolation back this is not considered to be a very suitable way of determining the equilibrium heat capacity. The equilibrium value is assumed to be that defined by the upper points in figure 8.2.

After our heat capacity work on this system had been completed, Mr P D Hatton (SERC Daresbury) offered (time permitting) to provide us with a variable temperature x-ray powder study of this compound. However, since that time a paper has appeared[5] describing temperature dependent x-ray studies of a single

crystal of $Ag_{13}I_9W_2O_8$. The structure of the low temperature phases is not determined, only the relationship between their symmetry and that of the room temperature phase (whose structure has been described in detail)[6].

In a caustic footnote to reference 5 Professor Geller makes clear the disagreement between himself and the authors of reference 3. The two groups disagree on the temperature at which the material may be considered to be a 'fully disordered three dimensional silver ion conductor'. In fact Professor Geller even objects to the use of the term 'fully disordered' since only a fraction (44.5%) of the silver ions are involved in conduction[5].

Habbal et al., on the basis of conductivity and Raman studies, originally concluded that two transitions occur in $Ag_{13}I_9W_2O_8$. Conductivity results from the second of these, a broad 'Faraday' transition between 200 and 280 K. Over this range gradual silver ion disordering occurs, the disordering being completed around 280 K. The d.s.c. study caused them to modify their conclusions concerning the nature of the transitions (confirmed by this adiabatic calorimetry study[4]) but not their belief that disordering became complete at just below 280 K. Their conductivity studies do indeed show a very sharp inflection near 280 K.

The most detailed conductivity studies are those of Geller et al.[15] On the basis of their results, Geller et al. concluded that the material undergoes first order transitions at 197 and 246 K. There is a step in conductivity at the higher first order transition. This step is relatively broad (about 10 K) but the change is complete by 247 K.

There is no inflexion or discontinuity whatsoever visible on their conductivity plots above 250 K.

This work[4] and Geller's recent crystallographic study[5] confirm that the high temperature transition does exist. De Boer and Geller label the room temperature phase α and that stable between 246 and 277 K α'. Their crystallographic study does not, however, allow them to draw many conclusions regarding the changes taking place in the range 246-277 K. They assume, however, that changes do not involve Ag^+ disordering - at least not of mobile Ag^+ ions. On the basis of the allowed symmetry relations between phases separated by a continuous transition (a property of Landau theory[7]) they state that the transition α to α' involves the loss of two-fold symmetry in a unit cell which is otherwise little changed.

The slight curvature in the $\log(\sigma T)$ versus $1/T$ plot observed by Geller et al. in the conducting region is interpreted as due to a slight fall in activation enthalpy with rising temperature. Both sets of authors emphasise this curvature,[3,15] though this is by no means surprising in view of the number of factors entering into the conductivity equations and the assumptions made about them.[8]

To resolve the dispute between the two groups it would be desirable to have an independent set of conductivity data. It is hoped to perform such a study in this department.[9] It is interesting to note that a very recent study of conductivity in the $AgI+Ag_2WO_4$ system[10] is in marked disagreement with both of the earlier sets of conductivity data. I have asked Dr Antonin for further details of his results but these have not so far been forthcoming.

A more satisfactory resolution of this dispute would be by independent determination of the nature of the changes taking place during the high temperature transition. In this connection it is worth noting that silver tungstate itself undergoes a continuous transition at about the same temperature (see later).

Also shown in figure 8.2 is the heat capacity of the mixture $9AgI+2Ag_2WO_4$. At temperatures below the lowest transition the two sets of heat capacity data are very similar. At higher temperatures, however, the heat capacity of the compound is higher than that of the constituents. This is true even at 300 K where the heat capacity of the compound is no longer rising significantly. This may suggest that Ag^+ ion disordering is still occurring even though this is not visible in x-ray studies. Note that de Boer and Geller do not rule out some further Ag^+ disordering beyond 246 K. They merely state that it does not contribute significantly to the conductivity. They also comment that the curvature of the conductivity plot cannot result from an increase in the number of charge carriers, as this, other things remaining constant, would lead to a steepening of the curve rather than to a levelling off, as is in fact observed. Such a view is in line with the conductivity equations given in reference 8.

The solid electrolyte $Ag_6I_4WO_4$

The solid electrolyte in the system $AgI+Ag_2WO_4$ was identified by Takahashi et al.[11] as $Ag_6I_4WO_4$, and much work has been carried out on a solid of this composition.[12-14] The material is used

in a commercial memory cell by Sanyo.

Chan and Geller[6] suggest that material made according to Takahashi et al. is two phase, consisting of $Ag_{13}I_9W_2O_8$ and $Ag_5IW_2O_8$. This claim is made on the basis of x-ray powder diffraction results. However, it appears quite possible that the materials $Ag_6I_4WO_4$ and $Ag_{13}I_9W_2O_8$ represent different compositions within the same solid phase.

A heat capacity study of the composition $Ag_6I_4WO_4$ has been made to see whether any difference in behaviour is observed. It may be that the transitions are significantly affected by the presence of a higher proportion of tungstate in the solid. If so then we would expect there to be differences in electrical behaviour as well.

Preparation of $Ag_6I_4WO_4$

The electrolyte was prepared by the fusion of the required proportions of $Ag_{13}I_9W_2O_8$ and a material of composition $Ag_5IW_2O_8$ (see later). The cooling process was the same as that described earlier except that the final five day annealing was omitted.

A d.t.a. trace showed no evidence of unreacted AgI. The melting behaviour was the same as for $Ag_{13}I_9W_2O_8$ except that the broad melting peak near 560 K could not always be resolved into a clear doublet.

The x-ray powder photograph is very similar to that of $Ag_{13}I_9W_2O_8$. There are, however, some differences in line intensities, and the diffuse background is considerably stronger. These x-ray data are compared with those of Takahashi et al. in table 8.3.

Heat capacity of $Ag_6I_4WO_4$

Calorimeter mass(empty)	42.257 g
Sample mass	36.545 g

A small correction was made for the increased heat capacity of the empty vessel. It was assumed that the excess mass (0.2 g) was all solder, though in fact 0.04 g was the copper closure pin.

Once the vessel had been connected to the electrical system it was discovered that serious shorts had appeared between two of the vessel wires and the shield base. Slight adjustments to the position of the cable could be made to remove these shorts. However, since the same thing had happened before, it was decided to dismantle the shield base, clip off the offending section of cable and clean and reconstruct the base. This time the wires through the metal shield base were rigidly held in place using several liberal doses of varnish close to the hole through the base. It was assumed that this would not affect the heat capacity of the empty vessel. The total mass of the vessel and addenda was reduced by almost 0.1 g. This was determined from the vessel full and empty weighings at the end of the $Ag_6I_4WO_4$ run.

The heat capacity was determined only in the range 160-310 K. No attempt was made to examine the non-equilibrium behaviour described earlier for $Ag_{13}I_9W_2O_8$.

The molar heat capacity results are listed in table 8.4 and plotted in figure 8.4. In the same figure is plotted the heat capacity of the mixture $4AgI+Ag_2WO_4$ to highlight any differences in behaviour between $Ag_6I_4WO_4$ and $Ag_{13}I_9W_2O_8$.

Table 8.3

Silver iodotungstate x-ray d values

This work		Takahashi et al.
$Ag_{13}I_9W_2O_8$	$Ag_6I_4WO_4$	$Ag_6I_4WO_4$
d/Å	d/Å	d/Å
11.5(100)		
8.8(10)		
7.6(10)		
4.62(5)		
4.35(5)		4.44(w)
		4.25(vw)
4.09(5)		4.13(vw)
3.72(60b)	3.68(10b)	3.68(mb), 3.79(mwb)
3.44(70b)	3.45(100)	3.48(msb)
3.15(20b)	3.18(10), 3.12(10)	3.18(mb)
	2.99(5)	2.96(mb)
2.94(15b)	2.93(10)	2.92(m)
2.86(2)	2.86(5)	2.87(m)
2.75(35b)	2.74(10)	2.71(sb)
2.69(2)	2.70(5)	
2.62(5)	2.63(8)	
2.56(30)	2.56(30)	2.56(wb)
2.44(1)		2.46(w)
2.37(3)	2.38(5)	2.38(wb)
2.30(15)	2.29(5)	2.31(mb)
2.15(20)	2.14(20)	2.18(mb)
2.03(3)		
2.00(3)		
1.91(10)		1.93(wb)
1.80(5)		
1.73(3)		

Figures and letters in parentheses represent relative intensities: s strong, m moderate, w weak, vw very weak, b broad.

The heat capacity behaviour of the two compositions is very similar. Both are likely to be unsuitable as electrolytes at low temperatures.

The enthalpy changes for the first order transitions are given in table 8.5. The uncertainties in these are slightly greater than for $Ag_{13}I_9W_2O_8$ since fewer experimental points were determined.

The enthalpy changes are slightly smaller (both per gram or per mole Ag^+) than for $Ag_{13}I_9W_2O_8$ but the differences are small.

There are slight differences between the 'peaks' near 275 K, though whether these are significant is questionable. The $Ag_6I_4WO_4$ 'peak' is rounded giving the appearance of a smaller area under the curve. This may result, however, from the relatively larger temperature increments used in that work.

The excess heat capacity 'per mole Ag^+' is plotted for both samples in figure 8.5. The 'base line' heat capacity is derived, in both cases, from the results between 215 and 245 K and 280 and 300 K.

On the basis of the heat capacity results there should be no significant differences in the electrical properties of the electrolytes of composition $Ag_{13}I_9W_2O_8$ and $Ag_6I_4WO_4$.

Table 8.4

Heat capacity of the electrolyte $Ag_6I_4WO_4$

T/K	C_p/J K^{-1} mol^{-1}	T/K	C_p/J K^{-1} mol^{-1}
166.62	321	243.96	383
170.07	323	245.42	390
173.51	326	246.85	412
176.93	329	248.11	607
180.33	332	249.33	471
183.70	336	250.70	410
187.05	339	252.83	403
190.37	342	257.14	401
193.64	352	262.89	404
196.68	460	268.59	408
199.68	366	272.47	410
202.88	352	275.33	410
206.10	352	277.50	393
209.30	354	278.95	397
212.48	357	280.41	393
215.64	360	282.59	393
219.28	363	285.47	396
223.87	367	289.78	397
228.46	370	295.47	397
232.70	371	301.14	397
235.75	375		
238.77	378		
241.75	382		

Table 8.5

Enthalpy changes for the first order transitions in $Ag_6I_4WO_4$

T/K	temperature interval	$\Delta_t H$/J mol^{-1}
198	192-201 K	380
248	245-253 K	430

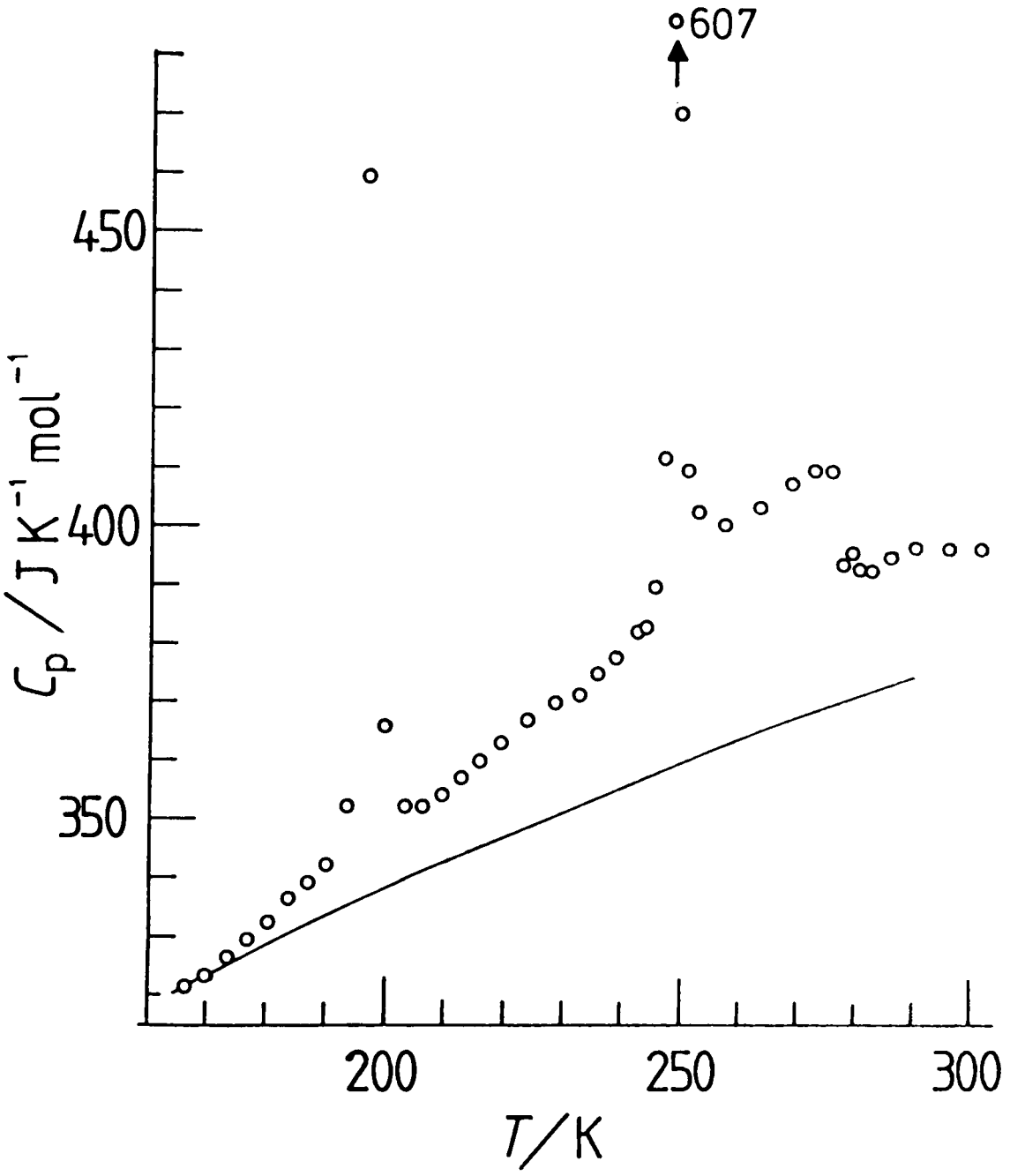

Figure 8.4 Molar heat capacity of the crystalline electrolyte $Ag_6I_4WO_4$. The solid line represents the heat capacity of the mixture $4AgI+Ag_2WO_4$ (see chapter 10).

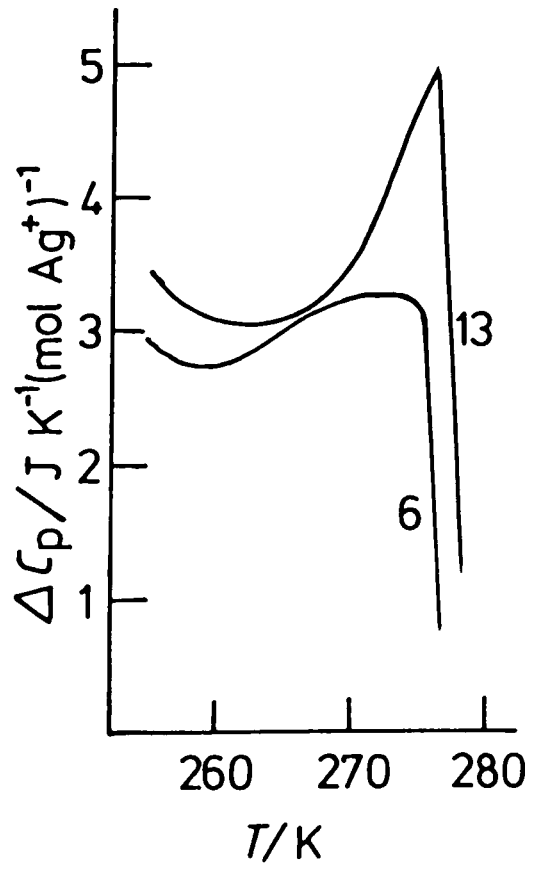

Figure 8.5 Comparison of the excess heat capacities in the region of the continuous transition: 13, $Ag_{13}I_9W_2O_8$; 6, $Ag_6I_4WO_4$.

References to chapter 8

1 F Habbal, J A Zvirgzds and J F Scott, *J Chem Phys*, 1978, 69, 4984.

2 J F Scott, F Habbal and J A Zvirgzds, *J Chem Phys*, 1980, 72, 2760.

3 A L Greer, F Habbal, J F Scott and T Takahashi, *J Chem Phys*, 1980, 73, 5833.

4 P G Hall, D A Armitage and R G Linford, *J Phys C*, 1983, 16, L835.

5 M P de Boer and S Geller, *J Solid State Chem*, 1983, 48, 121.

6 L Y Y Chan and S Geller, *J Solid State Chem*, 1977, 21, 331.

7 W Cochran in Structural Phase Transitions and Soft Modes, ed E J Samuelsen, E Andersen and J Feder, Universitetsforlaget, Oslo, 1971, p 1.

8 L D Barr and A B Lidiard in Physical Chemistry, An Advanced Treatise, Volume 10, ed H Eyring, D Henderson and W Jost, Academic Press, 1970, p 151; B C H Steele and G J Dudley in Solid State Chemistry, International Review of Science (Inorganic Chemistry), Series 2, Volume 10, ed L E J Roberts, Butterworths, 1975, p 181.

9 E Speers, Leicester Polytechnic, unpublished results, 1983.

10 V Antonin, *Coll Czech Chem Comm*, 1983, 48, 430.

11 T Takahashi, S Ikeda and O Yamamoto, *J Electrochem Soc*, 1973, 120, 647.

12 R D Armstrong, T Dickinson and P M Willis, *J Electroanal Chem*, 1974, 53, 389.

13 K Shahi and S Chandra, *Phys Stat Solid(a)*, 1975, 28, 653.

14 M V Šušić and S V Mentus, *Electrochim Acta*, 1983, 28, 35.

15 S Geller, S A Wilber, G F Ruse, J R Akridge and A Turković, *Phys Rev B*, 1980, 21, 2506.

9

The Glassy Electrolyte $Ag_{13}I_9W_2O_8$

The number of crystalline oxysalts with electrolyte properties similar to the mixed tungstates is limited. However, a very large number of papers have appeared describing conducting glasses formed by silver iodide + silver oxysalt systems. The oxo-anion may be based on a range of elements from boron[1,2] to the heaviest so far used, tungsten.[3] Oxygen within the large anion may be replaced with another group VI element and in a few cases bromide or chloride ions may be substituted for iodide.[4]

The great interest in these glasses stems from some of their favourable physical properties; it is easy to produce thin films and to cast solid pieces of electrolyte, thus reducing the grain boundary impedance effects[5] associated with electrolytes made from compressed powders.

The heat capacity of one glass, of composition $Ag_7I_4AsO_4$, has been reported and the results are shown in figure 9.1.[6]

I thank Dr C A Vincent for providing an enlarged version of the heat capacity plot.

A study of the heat capacity of a glass of a composition $Ag_{13}I_9W_2O_8$ was made during this work. This allows a comparison to be made between the arsenate and tungstate glasses, and between crystalline and glassy tungstate electrolytes.

Preparation

Samples of the glass were prepared by quenching from the

melt at 673 K into a dewar of liquid nitrogen (78 K) or liquid/solid n-pentane slush (140 K). The melt was poured slowly, with vigorous stirring, into the coolant to ensure that all droplets were small. No difference between the two samples was observed either in appearance or d.t.a. and x-ray properties. n-Pentane slush was the coolant used for the calorimetric material.

The x-ray diffraction photographs indicated the presence of some γ-AgI in the glass. However, the lines were weak and only the three strongest γ-AgI lines appeared. It was not possible to prepare a sample of this composition completely free of AgI (this point is also discussed in reference 1).

For reasons outlined later, it is not possible to estimate the amount of unreacted AgI present by thermal methods.

Experimental heat capacity

The glassy droplets were lightly crushed for loading into the calorimeter. This was necessary since, though the droplets were small, some had been flattened or elongated during cooling.

Calorimeter mass(empty)	42.102 g
Sample mass	32.885 g

No solder corrections were made.

The results are listed chronologically in table 9.1 and displayed in figure 9.2 together with a plot for $9AgI+2Ag_2WO_4$. No trace of the peaks characteristic of the crystalline solid is apparent.

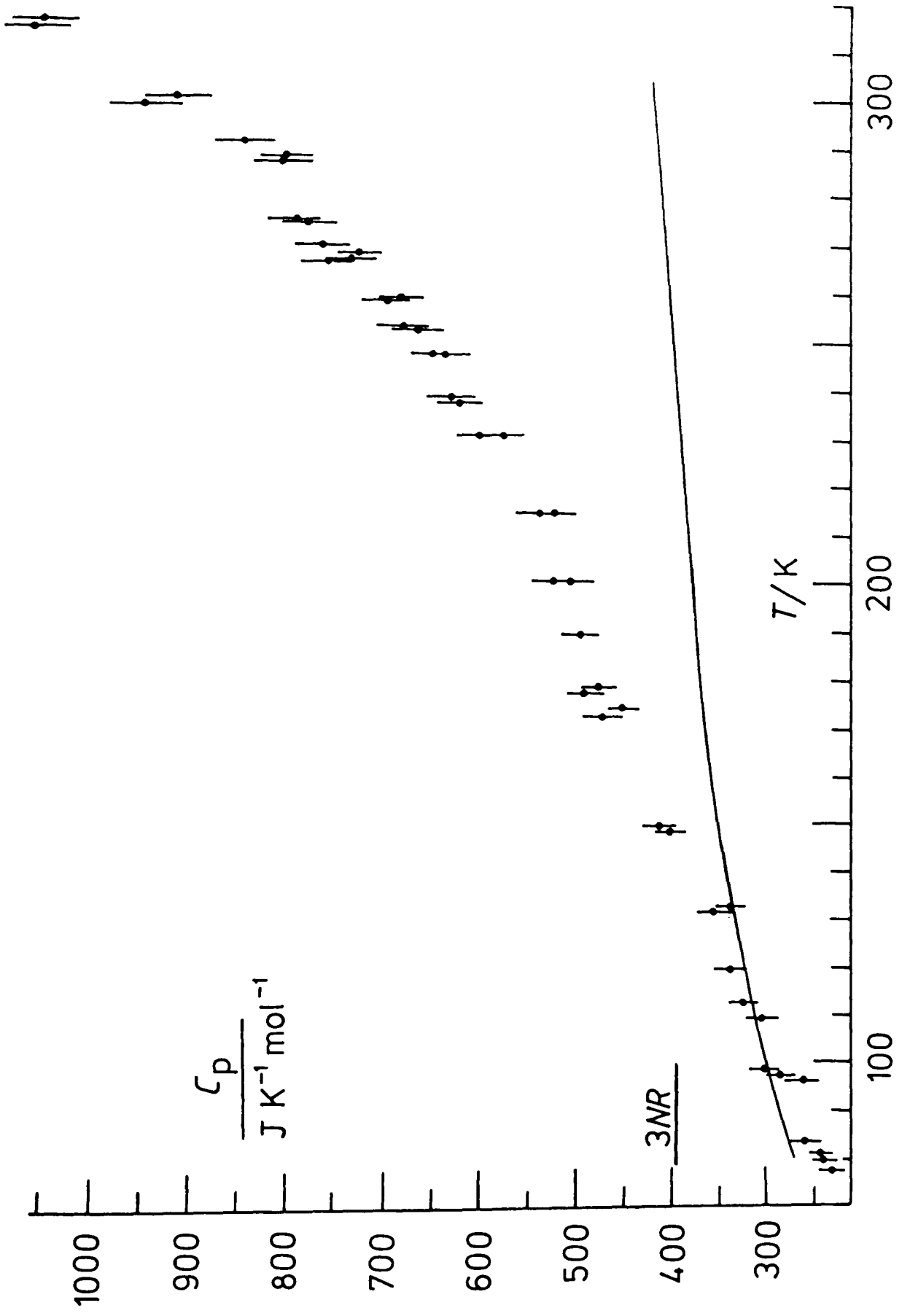

Figure 9.1 Molar heat capacity of the glass $Ag_7I_4AsO_4$ (adapted from reference 6). The solid line is for the glass $Ag_{6.5}I_{4.5}WO_4$ (this work). Both have the same classical limit, $48R$.

Table 9.1

Heat capacity of the glassy electrolyte $Ag_{13}I_9W_2O_8$

T/K	C_p/J K^{-1} mol^{-1}	T/K	C_p/J K^{-1} mol^{-1}	T/K	C_p/J K^{-1} mol^{-1}	
series 1		126.61	648	276.93	815	§
155.20	696	130.62	655	277.20	814	§
160.78	702	134.58	663	278.47	823	
166.28	709	138.49	670	278.60	809	§
171.71	715	142.34	675	278.75	815	§
176.56	725	146.15	680	281.86	818	
177.08	725	149.91	685	283.23	820	
181.88	730	153.63	691	283.41	809	§
187.13	736	series 3		284.92	814	
192.33	742	223.90	772	series 7		
196.63	747	228.85	776	221.69	765	
200.03	751	233.80	782	223.71	770	
203.42	755	240.23	790	226.12	774	
207.73	759	250.03	786	228.52	777	
212.79	760	254.63	787	230.92	780	
217.81	766	series 4		233.31	781	
222.78	769	236.87	779	235.65	783	
series 2		241.74	783	238.06	786	
79.50	544	246.58	787	240.42	789	
82.65	551	251.38	788	242.77	790	
85.74	557	256.14	789	series 8		
88.77	563	series 5		212.38	770	
91.74	571	284.63	825	214.84	775	
94.65	578	292.39	832	217.29	777	
97.50	585	296.96	835	219.72	781	
100.12	591	310.37	833	221.76	787 (764)†	
103.17	594	314.89	838	225.06	792	
106.16	600	series 6		229.96	798	
109.10	609	270.57	811	234.82	804	
112.00	616	272.12	812	239.63	805	
114.86	623	273.66	814	244.42	789	
118.37	630	273.95	822 §	247.59	800	
122.52	641					

† The value in parentheses is that obtained following a step in the drift curve.

§ To give some idea of reproducibility, some points were duplicated.

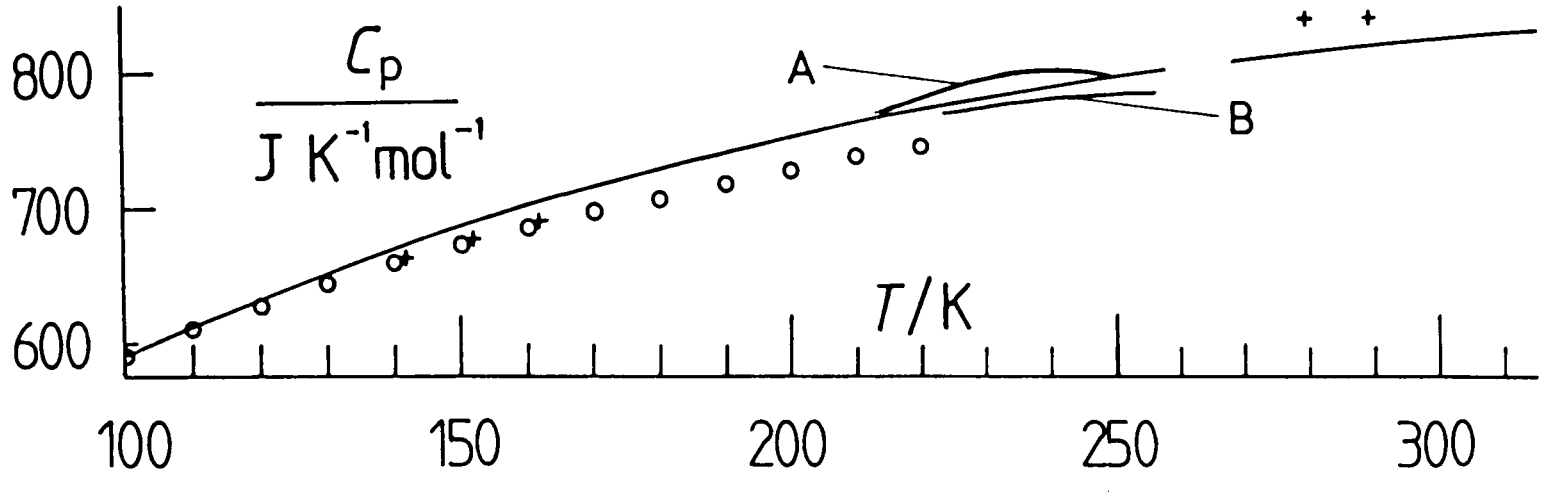

Figure 9.2 Molar heat capacity of the glass $Ag_{13}I_9W_2O_8$. O represents the heat capacity of the mixture $9AgI+2Ag_2WO_4$; + some heat capacity values for the crystalline $Ag_{13}I_9W_2O_8$. A and B represent extremes of non-reproducibility discussed in the text.

Below 200 K, the heat capacity measurements were straightforward. However, at higher temperatures non-reproducible behaviour is clearly visible in the figure. In addition, in the temperature region 250-270 K, it proved difficult to make any reliable measurements of the heat capacity. Steps of the order of 0.01 K sometimes occurred in the drift curves producing anomalously low heat capacity points.[19]

I attribute this behaviour to the crystallization of some γ-AgI from the glass. In view of the fact that the local environment of Ag^+ in the glass and crystalline phases may be similar, it is probably not surprising that this behaviour becomes most marked in the temperature region in which the Ag^+ ions are becoming highly mobile. No crystallization of $Ag_{13}I_9W_2O_8$ is evident in x-ray photographs. These x-ray powder

diffraction photographs, taken of the sample after its removal from the calorimeter, still show γ-AgI lines. On the basis of the intensities, it is not possible to say whether more γ-AgI is present although it is now possible to see more than three AgI lines. No other features are present except diffuse 'glass' bands.

An alternative explanation for the curious behaviour is that cracking or sintering of the glassy particles is allowing the release of strain energy trapped in the solid.[20]

In their study of the iodoarsenate glass, Finlayson et al.[6] comment that no thermal hysteresis appears in their heat capacity results. However, within their quoted precision, ±5%, hysteresis in the iodotungstate would not be visible either.

Other properties of the glassy electrolytes

The tungstate glass appears to be stable for long periods in air at ambient temperature. An x-ray photograph of a sample stored for several months showed only the three γ-AgI lines.

Atmospheric moisture does not cause rapid deterioration of the glass structure. Devitrification, and probably some cation exchange, occur immediately on contact with aqueous ionic solutions or with ionic solids (such as KBr) in air. A number of authors have commented on this.[1-4]

It is thought that the glasses contain discrete anions rather than chain structures, as is common in silicate glasses.[4] In addition, only a fraction of the Ag^+ ions in the glasses contribute towards ionic conduction, as is also the case for crystalline $Ag_{13}I_9W_2O_8$. It would be expected, therefore that the conductivity of the glassy and crystalline tungstate

materials would be similar. This has been found to be the case.[8] Work in this department has in fact suggested that the tungstate crystalline material may have a higher ionic conductivity than the glass.[9] The same is not true in other systems as crystalline conductors are not formed.[8]

Although conductivity studies have not formed part of this work, preliminary results suggest that the conductivity of the calorimetric glass is similar to that reported for other glassy systems, about 10^{-2} S cm^{-1} at room temperature.[4,10]

The conductivity of the glasses is about an order of magnitude less than that of crystalline materials like $RbAg_4I_5$ but, as mentioned earlier, their useful mechanical properties more than make up for this.

Below about 110-120 K, the heat capacity curves of glassy and crystalline $Ag_{13}I_9W_2O_8$ and the mixture $9AgI+2Ag_2WO_4$ are almost identical. Above 120 K, the glass curve begins to rise above the other two, suggesting that Ag^+ ion disordering or movement is possible.

If this is the explanation for the excess heat capacity then we would expect no low temperature step in the conductivity curve, as is found, for example, in crystalline AgI; nor would we expect a linear Arrhenius plot until the Ag^+ current carrying system had become 'saturated'. In crystalline $Ag_{13}I_9W_2O_8$, the Ag^+ disordering occurs over a limited temperature range and a step appears in the conductivity plot (at 246 K or up to 277 K depending upon whose results one accepts).

Gradual disordering in the glass will cause the current carrier concentration to rise with temperature. This will lead

to a conductivity plot rising above linear with increasing temperature [when plotted in the usual way as $\log(\sigma T)$ against $1/T$]. After saturation a decrease in slope will occur followed by a more nearly linear curve.

Unfortunately, for the glasses, there are few low temperature studies of conductivity as a function of temperature. Generally temperature ranges are too short for changing slope to be detected. Above room temperature, complications arise due to glass transitions and crystallization. Again it is hoped that this shortcoming will be remedied by future work in this department.[9]

An extensive set of measurements has been made on the arsenate glass.[13] On the basis of the formula $Ag_7I_4AsO_4$ (compare $Ag_{6.5}I_{4.5}WO_4$), it would appear to be similar to the tungstate. The heat capacity results are, however, dramatically different.(figures 9.1 and 9.2).

The enormous excess heat capacity in the arsenate cannot result solely from disordering or promotion of Ag^+ ions into new sites; it is too large.[6] Conductivity studies above room temperature reveal a downward curve to the conductivity plot with increasing temperature. This suggests that the Ag^+ carrier concentration is no longer increasing significantly. The change in slope is also in line with a decreasing activation energy with rising temperature. In this point, Ingram et al.[13] agree with Geller et al.'s conclusions for the crystalline tungstate, though the two sets of workers use slightly different arguments (see also reference 8 of chapter 8).

Ingram et al.[13] consider that 'normal' behaviour for these

glasses is represented by a'linear Arrhenius plot'. They obtain such plots for glasses annealed at 25 °C but not for those annealed at higher temperature. Long periods of annealing are necessary and further annealing does not occur on the time scale of conductivity measurements. It is probable that annealing allows some relief of the large strain energies locked into these glasses on quenching (see later). It is the less strained glasses, annealed at the higher temperatures that have the lower conductivity and most curved plots.[13]

I agree with Ingram et al. in their conclusion that the falling activation energy for conduction may result from cooperative local motion of the anions allowing, presumably, readier (less activated) movement of the conducting species. In view of the large Debye-Waller type factors observed in crystalline electrolytes for the non-mobile anions,[14] this local motion may also operate in crystalline systems, possibly to a lesser extent. This would explain the curvature in Geller et al.'s conductivity plot for the crystalline iodotungstate (see chapter 8). Ingram et al.[13] describe the motion as 'quasi-liquid local motion' but it does not seem necessary to invoke this concept.

The lower conductivity of their annealed samples may be a result of movement of Ag^+ ions into lower energy sites where they are no longer mobile.

Ingram et al.[13] consider that below 180 K, the heat capacity represents the expected behaviour for a salt with a complex anion. Extrapolation of this almost linear curve then represents 'normal behaviour'. They do not comment on the fact that performing this extrapolation takes the heat capacity way beyond the classical limit.

They then consider the 'excess' heat capacity between the observed curve and the linear extrapolation. The excess is interpreted as a 'pre-melting' phenomenon (hence their use of 'quasi-liquid' mentioned earlier) involving either formation of anion Frenkel defects or rotational disordering of arsenate ions.

A d.t.a. trace published earlier by the same group[15] shows no sign of the large endothermic event suggested by the heat capacity study. The trace does show an endothermic peak beginning just above 330 K, and it may be that the adiabatic study is revealing a pre-transition region. The 330 K transition is considered by Grant et al.[15] to be the glass transition. This is in line with the conclusions of other authors except that glass transition peaks in related systems are generally exothermic.[8,16]

Dr Vincent has commented to me[17] that the failure to find an excess heat capacity in the tungstate glass is in accord with his group's views on the structural relaxations peculiar to the arsenate system.

I remain unconvinced. Heat capacity studies are needed to confirm the differences between these two systems and to extend the data to other glasses. Conductivity data are also needed for other glasses subjected to the same treatment as the arsenates.[13] In particular, I wonder whether it is true to say that 'linear Arrhenius plots represent normal behaviour' for these systems. My doubts are only strengthened by the curvature observed in Arrhenius plots for crystalline $Ag_{13}I_9W_2O_8$ (see the discussion and references in chapter 8).

At present it appears that the feature peculiar to St Andrews'[6,13,15]

arsenate glass is the endothermic glass transition. It remains to be seen whether this is a function of the material or the preparation method.

Glass transitions and crystallization

Most of the glassy electrolytes show two exothermic effects in d.t.a. or d.s.c. studies. The first (330-350 K) is considered to be the glass transition, and the second (390-480 K) to represent crystallization from the glassy melt or supercooled liquid.[8] Exceptions (other than the arsenate) were said to be the borate glass (stable to much higher temperatures)[2] and the tungstate glass (one exotherm at about 460 K).[8,16]

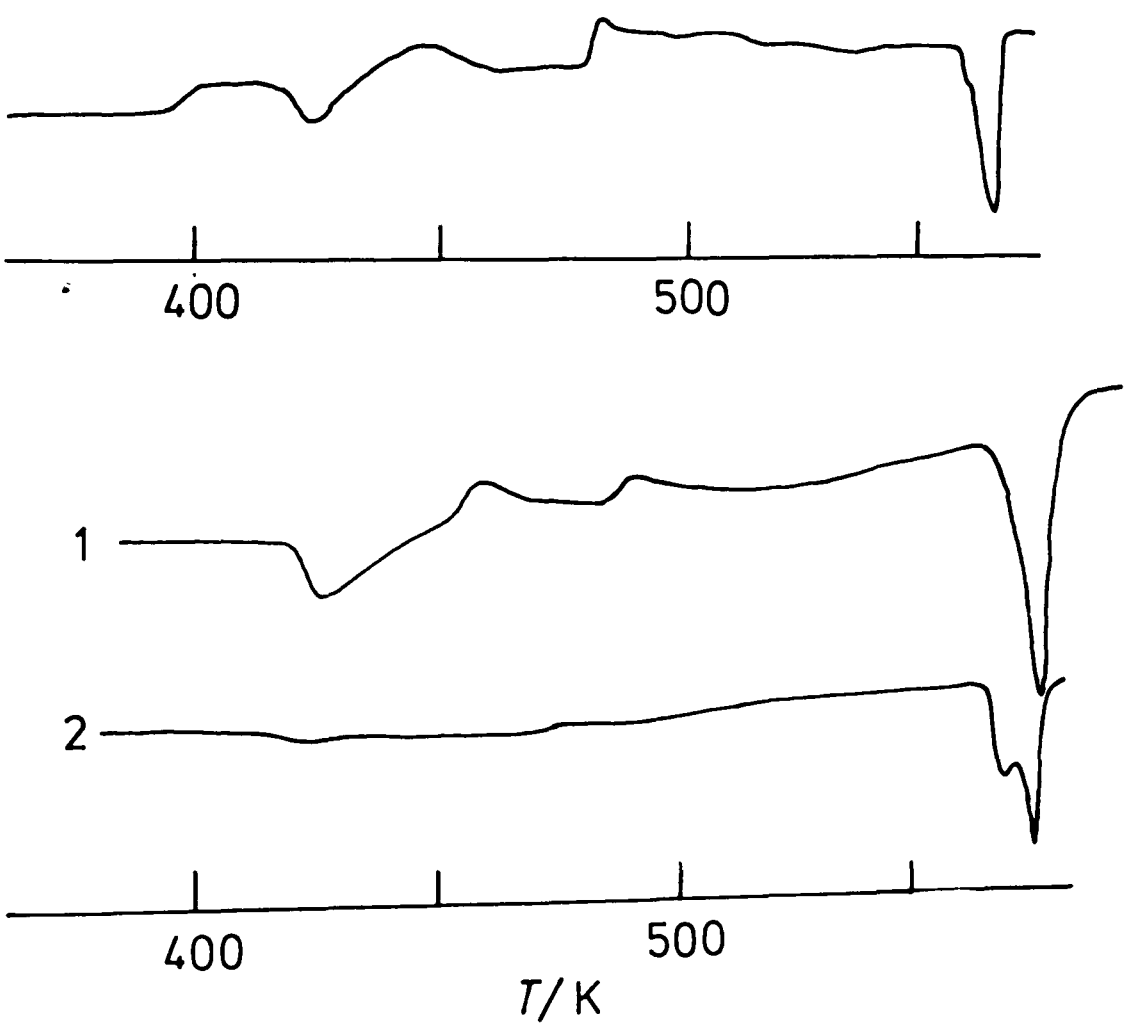

Figure 9.3 D.t.a. behaviour of the glasses $Ag_{13}I_9W_2O_8$ (top) and $Ag_6I_4WO_4$ (bottom 1 and 2); 1, first heating cycle; 2, second heating cycle.

To check the latter statement, a d.t.a. study was carried out on three iodotungstate glasses of composition $4.5AgI:Ag_2WO_4$, $4AgI:1Ag_2WO_4$ and $2AgI:1Ag_2WO_4$. The results for the first two systems are shown in figure 9.3. The tungstate glasses do, therefore, exhibit behaviour similar to that observed in, for example, chromate and molybdate glasses. Why the authors of reference 16 failed to observe this is not clear. Probably the peak was obscured by the relatively larger endotherm at 415-430 K.

The d.t.a. behaviour is not reversible. Subsequent runs show a reduction in all thermal events (except that at the melting temperature). Crystallization, though not apparent by d.t.a., begins immediately above the glass transition (see later).

The behaviour of the 4:1 glass is interesting. Despite the fact that x-ray examination indicates that no γ- or β-AgI is present, a large endothermic peak appears near 420 K. A possibility is that AgI is crystallizing from the glass during heating. In fact, Minami et al.[7], in studies of tungstate and molybdate glasses, have suggested that the glass structure is closely related to that of γ-AgI (this is not inconsistent with the comment that the Ag^+ environment in the glass is locally very similar to that in crystalline $Ag_{13}I_9W_2O_8$). They go on to say that segregation of γ-AgI is rapid at temperatures above 373 K. This is in contrast to observations made during this work. X-ray diffraction photographs taken of glasses annealed at various temperatures above ambient have not indicated any increase in AgI content.

The size of the 420 K endotherm does not appear to be dependent on sample heating rate. If segregation of AgI is

taking place it would be expected that slow heating of the sample would produce more AgI.

An alternative explanation may be that while γ- or β-AgI is soluble in the glassy matrix, α-AgI is not. The thermal event at 420 K thus represents phase separation and, according to the x-ray results obtained in this work, reaction of α-AgI with the matrix to produce $Ag_{13}I_9W_2O_8$.

The glass transition at 390 K in the 4.5:1 glass has been confirmed by means of thermomechanical analysis (t.m.a.). A softening of the glass is revealed by an apparent contraction near 390 K followed by further contraction at 420 K. Softening is noticeable since the t.m.a. plunger marks the surface of samples heated to 400 K and beyond. X-ray diffraction photographs of 4.5:1 glass specimens heated to 420 and 470 K show the presence of the crystalline phase $Ag_{13}I_9W_2O_8$, in the former case accompanied by glass-like diffuse rings. As commented earlier, this contrasts with the finding[7] that AgI is the crystalline phase formed on heating. However, further studies on samples annealed at between 350 and 400 K are needed to confirm this.

No studies have been reported on the stability of these glasses subjected to cooling-warming cycles below or around room temperature.

Powder diffraction photographs of the 2:1 glass indicate that no crystalline phases are present. The d.t.a. trace exhibits very shallow broad peaks in the region 415–475 K. Annealing at 425 K for 15 min induces crystallization of a phase (or phases) whose x-ray pattern has not been reported previously. The pattern does not correspond with that reported

by Takahashi et al. for the single phase crystalline material of composition $2AgI:1Ag_2WO_4$ (see chapter 10).

The fact that the glass transitions are usually seen as exotherms does not seem to have aroused comment in the literature. At first glance the transition

$$\text{glass} \longrightarrow \text{glassy melt}$$

might, by analogy with other melting processes, be expected to be endothermic. However, in an ideal glass, it is questionable whether the process would be seen in a d.t.a. trace at all. The transition would be continuous (see chapter 2).

It is possible that softening at the glass transition allows the release of strain energy stored during quenching, and it is this that is visible on the d.t.a. trace. This seems reasonable on the basis of similar behaviour in polymer systems.[18] The exotherm could also result from an early crystallization effect, on the particle surface or other high energy sites, for example.

No indication of why the arsenate system should be different emerges from the work on that glass.[6,10,13,15] It is known, however, that the thermal effects visible at glass transitions are very sensitive to the thermal history of the sample.[21]

References to chapter 9

1 A Magistris, G Chiodelli and A Schiraldi, *Electrochim Acta*, 1979, 24, 203.

2 G Chiodelli, G Campari Vigano, G Flor, A Magistris and M Villa, *Solid State Ionics*, 1983, 8, 311.

3 G Chiodelli, A Magistris and A Schiraldi, *Electrochim Acta*, 1974, 19, 655.

4 T Minami, *J Non-cryst Solids*, 1983, 56, 15.

5 R D Armstrong, T Dickinson and K Taylor, *J Electroanal Chem*, 1977, 78, 45.

6 D M Finlayson, G A Leiper and C A Vincent, *Solid State Comm*, 1980, 36, 261.

7 T Minami, H Nambu and M Tanaka, *J Electrochem Soc*, 1977, 124, 1659.

8 A Schiraldi, *Electrochim Acta*, 1978, 23, 1039.

9 A Jelfs, Leicester Polytechnic, unpublished work, 1983.

10 M Lazzari, B Scrosati and C A Vincent, *Electrochim Acta*, 1977, 22, 51.

11 T Takahashi, *J Appl Electrochem*, 1973, 3, 79.

12 B B Scholtens, A Brouwer and G H J Broers, *J Appl Electrochem*, 1978, 8, 165.

13 M D Ingram, C A Vincent and A R Wandless, *J Non-cryst Solids*, 1982, 53, 73.

14 S Hoshino, *J Phys Soc Japan*, 1957, 12, 315.

15 R J Grant, M D Ingram, L D S Turner and C A Vincent, *J Phys Chem*, 1978, 82, 2838.

16 A Magistris, G Chiodelli and G V Campari, *Z Naturforsch*, 1976, 31a, 974.

17 C A Vincent, University of St Andrews, personal communication, 1983.

18 M D Glasse, Leicester Polytechnic, personal communication, 1983.

19 Exothermic temperature drift effects in metastable solid-solution systems have been assigned to phase separation: K Moriya, T Matsuo and H Suga, *J Phys Chem Solids*, 1983, 12, 1121.

20 For other discussions of the effects of non-equilibrium behaviour on drift curves, see for example H Suga and S Seki, *Faraday Discussions of the Chemical Society*, 1980, 69, 221; R H Beaumont, B Clegg, G Gee, J B M Herbert, D J Marks, R C Roberts and D Sims, *Polymer*, 1966, 7, 401.

21 A Q Tool, *J Amer Ceram Soc*, 1948, 31, 177.

10

Silver Iodide and Silver Tungstate

To produce the 'mixture' heat capacity curves drawn in the previous chapters, it is necessary to know the molar heat capacities of the components, silver iodide and silver tungstate. In the former case sufficient data are available. There is no heat capacity study of silver tungstate reported in the literature so such a study was undertaken in this work.

Silver iodide

The low temperature studies of Leduc and Coleman[1] and of Pitzer[2] were described in chapter 2. Pitzer's work covers the whole temperature range of interest here (figure 10.1). For this work, Pitzer's data were converted into joules and fitted to the polynomial

$$C_p/\mathrm{J\ K^{-1}\ mol^{-1}} = -126.602 - 0.5577(T/\mathrm{K}) + 1.2046\times10^{-3}(T/\mathrm{K})^2 - 9.93\times10^{-7}(T/\mathrm{K})^3 + 47.198\times\ln(T/\mathrm{K}). \quad (10.1)$$

The heat capacity is well in excess of the classical limit ($6R$) and rises particularly steeply beyond about 250 K. This should be borne in mind when examining the mixture heat capacities drawn earlier. The curves are not, in any case, extended beyond about 240 K. The problem of what to use as a mixture heat capacity is returned to in chapter 11.

The silver iodide $\beta,\gamma \longrightarrow \alpha$ transition

Silver iodide undergoes a first order transition at 419 K to the solid electrolyte phase α-AgI. The properties of silver

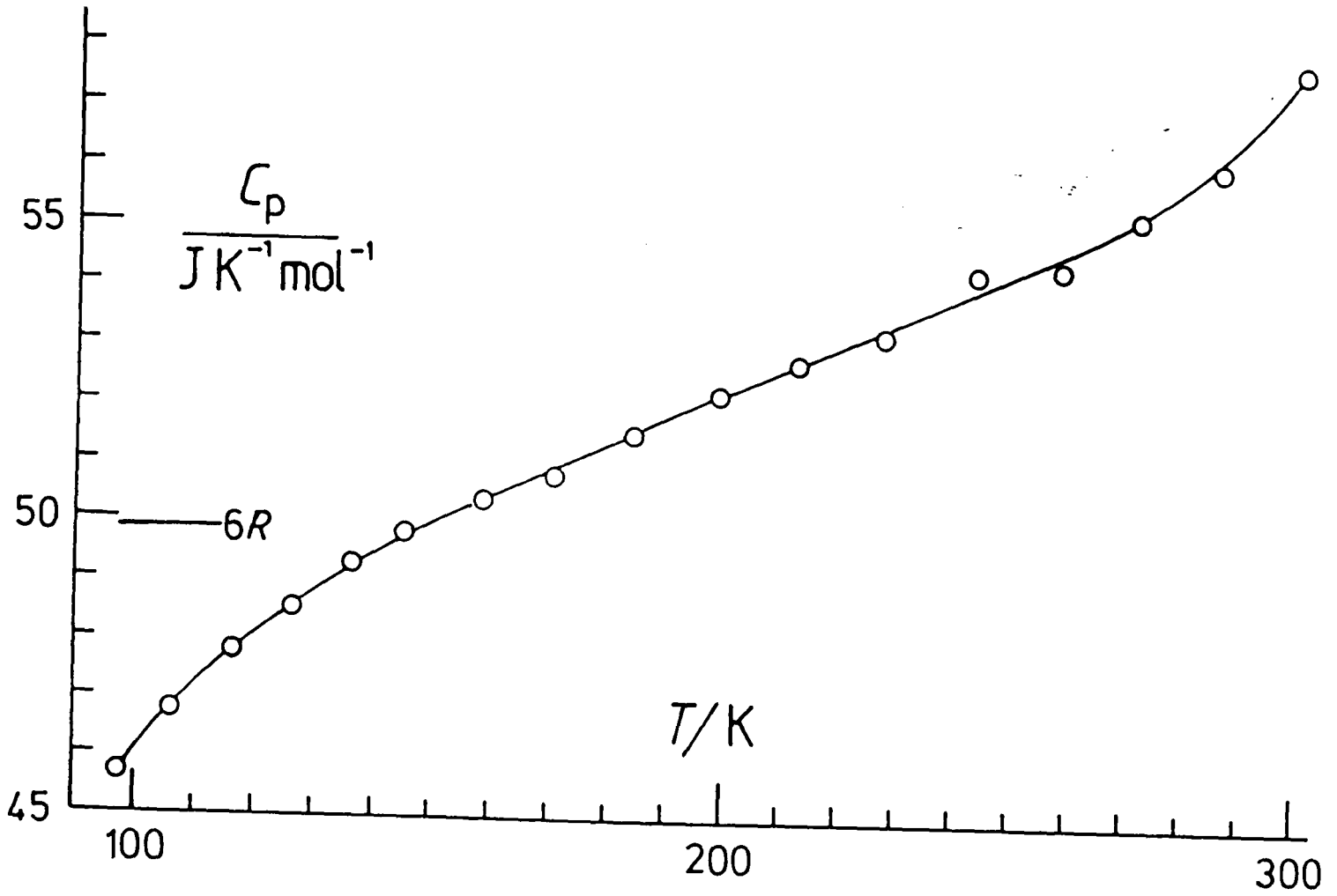

Figure 10.1 Part of Pitzer's heat capacity data for silver iodide. The solid line represents equation (10.1).

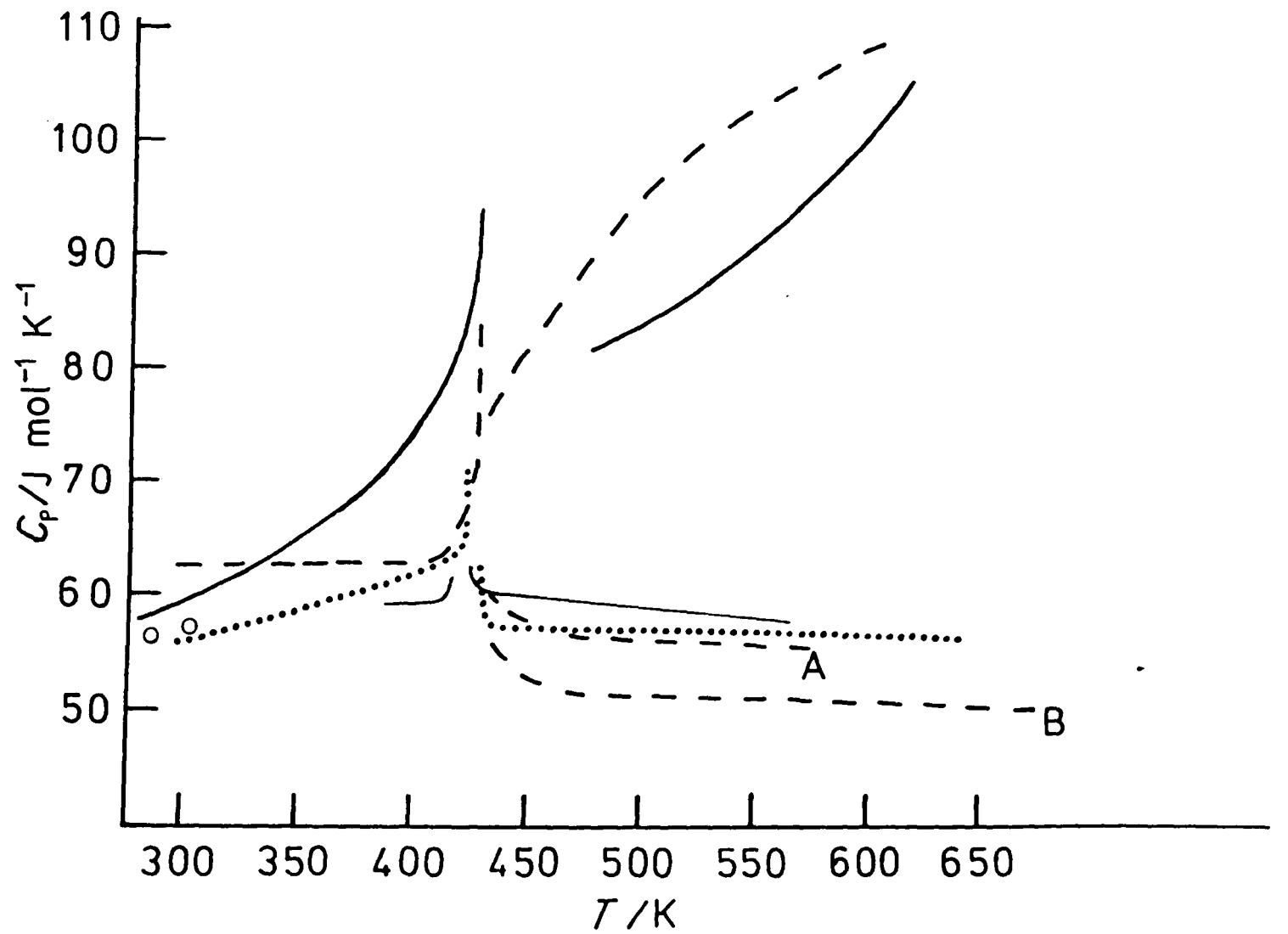

Figure 10.2 Heat capacity of silver iodide close to the transition: o ref. 2; ··· ref. 9; — Leiser[11]; — Hoshino[11]; - - ref. 8. A and B curves for non-stoichiometric materials.[8]

iodide and its relatives (Ag_2S,[3] $RbAg_4I_5$, etc.) have been reviewed many times.[4,5] The compound is interesting, not only because it is the simplest solid electrolyte, but also because it is considered to have bonding on the borderline between ionic and covalent.[6,7]

Heat capacity studies through the transition have been reported.[8-11] There is disagreement about the shape of the heat capacity curve following the transition, and the argument has been pursued in the literature.[10] The heat capacity curves are illustrated in figure 10.2.

According to Perrott and Fletcher[8], stoichiometric α-AgI retains considerable Ag^+ order above the transition. Disordering takes place over an extended range until a high temperature continuous transition is reached at about 700 K.

Nölting and Rein,[9] on the other hand, find no evidence for this behaviour. They conclude that stoichiometric and non-stoichiometric α-AgI are fully disordered after the transition. Heat capacity curves similar to those of Nölting and Rein have been obtained by Perrott and Fletcher but only for samples that are slightly non-stoichiometric. No satisfactory resolution of this dispute has appeared. This is unfortunate since silver iodide has been the subject of considerable theoretical work. Generally the data of Nölting and Rein appear to have been accepted[5] and O'Reilly[12] has used their results for comparison with his theoretical work. Other theoretical work has attempted to explain the heat capacity differences.[13]

From Raman studies,[14] one group of workers claim to have obtained evidence for an order-disorder transition in α-AgI

near 700 K. They clearly have their reservations about the results of Perrott and Fletcher, but do comment that they found considerable differences between samples.

A similar dispute surrounds silver sulphide.[15]

There is clearly scope for a reinvestigation of the heat capacity of silver iodide above 400 K.

There are disagreements about the interpretation of other silver iodide results. Where, for example, are the Ag^+ ions located, and can they be considered to be 'liquid like'?[16,17] There are also unresolved problems concerning the thermal expansion[18] and microwave conductivity.[19,42]

Silver tungstate

The crystal structure of silver tungstate, empirical formula Ag_2WO_4, has been described by Skarstad and Geller.[20]

The structure contains planar $[W_4O_{16}]^{8-}$ anions which, apparently, are not centrosymmetric. The structure is interesting, not only because of the presence of these large ions, but also because it contains silver in a wide variety of coordination environments. Silver is very versatile in this respect, and this property - together with the unusual relationship between silver and iodine - is thought to be important in allowing silver ion mobility.[21]

The unit cell is orthorhombic (*Pn2n*, a = 10.89 Å, b = 12.03 Å, c = 5.92 Å) and contains two $Ag_8W_4O_{16}$ formula units.

It should be noted that in fitting this structure to their data, Skarstad and Geller neglect about one hundred strong diffraction points because of 'streaking'. Some reservations have been expressed to me concerning the effect of this on the

Table 10.1

Silver tungstate x-ray d values

This work d/Å	Bottelberghs d/Å	McKechnie et al. d/Å	Takahashi et al. d/Å
1.61(10)	1.61(w)	1.61(w)	
1.66(10)	1.66(w)	1.65(w)	
1.68(30)	1.68(m)	1.67(m)	
		1.97(w)	1.96(w)
2.00(40)	2.01(m)	2.00(m)	2.01(s)
2.14(5)	2.16(vw)	2.15(w)	2.16(vw)
			2.20(vw)
			2.37(vw)
2.41(10)	2.42(vw)		2.44(vw)
		2.62(vw)	
2.64(1)	2.63(vw)	2.64(vw)	2.65(w)
2.72(30)	2.73(m)	2.70(m)	2.72(m)
2.83(100)	2.85(vs)	2.81(vs)	2.85(vs)
2.95(50)	2.96(m)	2.98(m)	2.96(m)
	3.08(vw)	3.08(w)	
			3.14(w)
			3.28(w)
3.50(3)	3.48(vw)	3.45(w)	3.49(vw)
3.76(5)	3.78(vw)		3.80(w)
4.07(5)	4.04(vw)	4.04(w)	4.08(w)
		4.35(w)	
5.31(40)	5.35(m)	5.22(m)	
8.12(20)			

Figures and letters in parentheses represent relative intensities: vs very strong, s strong, m moderate, w weak, vw very weak.

Some error in the numerical values of McKechnie et al. is possible as these were obtained from a small diagram in their paper.

determined structure. Dr Gatehouse[22] and his colleagues hope to repeat Skarstad and Geller's work.

Skarstad and Geller say that their structure relates to the 'high temperature' form. They suggest that the transition between the two forms occurs somewhere between 360 and 530 K. Unfortunately they provide no further information. They also suggest that the form of silver tungstate which precipitates from a solution of $AgNO_3$ and Na_2WO_4 depends on the temperature and pH conditions of the reaction.

McKechnie et al.[23] have taken up this point. They report x-ray powder diffraction results for Ag_2WO_4, $Ag_2W_2O_7$ and $Ag_2W_4O_{13}$[24] precipitated under different conditions of temperature and pH. They suggest that there are two crystallographically distinct forms of silver tungstate which they label α and β. At 85 °C or above the α form was precipitated while at 5 °C or below the β phase formed. Mixtures were formed at intermediate temperatures, and the form produced was also affected by pH. When heated above 523 K, McKechnie et al.[23] state that β-Ag_2WO_4 is converted irreversibly into α-Ag_2WO_4.

In the present work, silver tungstate has been precipitated from solution at temperatures of 273 K, 300 K and 353 K. The x-ray diffraction patterns of the 273 and 353 K forms were identical and correspond closely with McKechnie et al.'s α-Ag_2WO_4.

It has been reported[24] that the ditungstate may be precipitated in a hydrated form. To investigate this possibility with Ag_2WO_4, precipitation was repeated at 273 K and x-ray diffraction photographs obtained for samples of precipitate (1) still damp straight from the filter paper and (2) after drying

overnight at 110 °C. Both photographs were identical with those produced earlier. Particular care had to be taken with the low temperature work as a crystalline hydrate of sodium tungstate often formed on cooling that solution.

No experiments were undertaken during this project with controlled pH.

As mentioned earlier, the x-ray photographs obtained at Leicester are similar to those of α-Ag_2WO_4 (see table 10.1).[23] Close comparison is not possible since I have taken the data of reference 23 from a very small diagram.

Two other sets of x-ray powder data are given in table 10.1. One is from Bottelberghs.[25] Agreement between his data and those obtained here is excellent. The final column in table 10.1 is taken from JCPDS.[26,27] Here, agreement is less good except in the region of strong lines corresponding to lattice spacings between 2.5 and 3 Å. It is interesting to note that, in a much earlier study, Graham and Hepler[28] report considerable variation in the heat of precipitation of Ag_2WO_4 from solutions of Na_2WO_4 and $AgNO_3$. They attribute this variation to the formation of varying quantities of polytungstate ions.

Turkovic et al.[29] indicate that slight decomposition of silver tungstate may occur at temperatures above about 520 K. Evidence for this is not strong but Raman studies of samples heated in air and in oxygen led to the conclusion that slight loss of oxygen takes place around 570 K. No evidence was found for this from thermal studies by Turkovic et al. (t.g.a.), by Bottelberghs (t.g.a.) or in this work (d.t.a., t.g.a.).

Even though Turkovic et al. consider their results to be

inconclusive, it was decided initially not to subject the calorimetric sample to temperatures above 390-400 K. For practical reasons outlined in the next section this decision had to be reversed.

Heat capacity of silver tungstate

The calorimetric sample was prepared by mixing aqueous solutions of $AgNO_3$ and Na_2WO_4 in proportions required by the stoichiometry

$$2AgNO_3 + Na_2WO_4 = 2NaNO_3 + Ag_2WO_4$$

The precipitate was a very fine, off-white powder.

Care was taken to ensure that Na^+ ions were not in excess in the solution. This resulted from the finding that silver tungstate undergoes ready ion exchange with alkali metal ions.

This was discovered by accident during infra-red studies, and is apparently similar to the behaviour of the glasses (see chapter 9). The precipitated tungstate was washed thoroughly with water. No sodium could be detected in the solid. The sample was dried at 383 K for 36 h. The procedure was carried out in a darkened room.

The dried sample was loaded immediately into the calorimeter. Unfortunately the powder was very difficult to pack into the vessel. Despite continued tapping down, only 16.688 g was loaded for the first series of measurements. About 8 Torr helium was introduced. The two series of runs on this sample (80-165 K) were the first of many carried out on silver tungstate extending over a period of more than two months.

In the first measurements, drift periods were long, two

hours or more, and this combined with the small mass of the sample relative to that of the vessel produced a noticeable scatter of points about a smooth curve.

The first sample was removed. The powder was then pressed in a die press (to about 7-8 ton $inch^{-2}$)† and the resulting pellets lightly crushed if necessary. Generally this was not the case since the pellets flew apart as soon as the restraining plungers were removed.

The second sample was of 47.675 g and was sealed with 17 Torr helium.

Drift periods were now even longer (series 3 up to 5-6 h)[43] before linear sections were obtained. Eight heat capacity points were recorded before this series was abandoned.

Two possible problems were considered

(i) a helium leak

(ii) thermal conductivity problems resulting from the small particle size.

A helium leak alone could not be responsible as work on alumina with no exchange gas involved equilibration times of less than an hour. In addition, the vessel, when removed from the system and held on a balance, showed no tendency to increase in weight. On opening, there was an audible hiss as air entered the vessel. It is, of course, possible that a solder crack had opened up at low temperature, allowed the escape of helium, and then closed as the temperature was raised.

The vessel closing cap and groove were thoroughly cleaned and fluxed. At this stage the sealing system was improved with the introduction of the sealing pin.

† $\sim 10^8$ Pa

The sample was removed, melted and coarsely crushed (sample mass, series 4, 49.537 g). Again drift curves were very long, though heat capacity measurements were extended to 265 K with a further eight points.

This time, when the sample was removed, a prolonged series of vacuum tightness tests was carried out. This revealed a very slow leak which was significant only over a period of several hours.

The solder surrounding the cap was removed, and both cap and surrounds cleaned with 50% HCl. The solder was replaced by a lower melting variety (see earlier chapters). This appeared to produce a good seal. A fifth series of heat capacity measurements was thus made on the fused silver tungstate (with 18 Torr helium).

Calorimeter mass (in air)	42.426 g
Sample mass	48.677 g

A small correction was made for the heat capacity of extra solder. The results are listed in chronological order in table 10.2 and plotted in figure 10.3. The presence of the anomaly was confirmed by three further scans through the transition region.

The results for the previous samples (series 1-4) are not illustrated. The points lie on a curve about 2-4% below that illustrated. The earlier experiments did not extend as far as the anomaly. In order to produce the heat capacities of the mixtures in chapters 8 and 9, the experimental data were fitted to a polynomial (see figure 10.3).

$$C_p/\mathrm{J\ K^{-1}\ mol^{-1}} = 20.48 + 0.816(T/\mathrm{K}) - 1.54\times10^{-3}(T/\mathrm{K})^2 + 8.94\times10^{-7}(T/\mathrm{K})^3$$

Table 10.2
Molar heat capacity of silver tungstate Ag_2WO_4

T/K	C_p/J K^{-1} mol^{-1}	T/K	C_p/J K^{-1} mol^{-1}	T/K	C_p/J K^{-1} mol^{-1}
series 5		156.36	113.8	280.70	149.5
80.12	76.9	159.32	114.9	285.41	149.4
82.36	77.3	162.24	116.2	289.46	149.0
85.29	78.7	165.77	117.3	series 7	
88.14	80.2	169.91	118.9	282.46	148.5
90.94	81.6	174.03	120.3	285.89	149.0
93.67	83.7	178.10	121.7	289.25	150.2
96.44	85.3	182.13	123.3	292.60	150.0
99.15	86.4	187.10	124.7	296.56	149.5
101.73	88.1	192.94	126.9	series 8	
series 6		198.67	128.9	276.77	152.1
104.40	89.6	204.32	130.3	277.93	151.8
108.12	91.5	209.94	132.2	279.08	150.1
111.76	93.5	221.21	135.6	280.24	148.5
115.35	95.6	226.64	137.1	283.14	148.4
118.86	97.2	232.01	138.6	287.70	149.2
122.31	98.9	237.35	140.0	292.25	150.0
125.70	100.7	242.66	141.5	296.76	150.2
129.04	102.5	247.90	143.0	301.22	150.7†
132.30	104.1	253.92	145.1	305.75	152.5
135.53	105.3	260.90	147.1	series 9	
144.24	107.1*	266.72	148.2	272.59	151.7
147.27	110.3	271.34	151.0	275.94	152.4
150.33	111.4	276.05	151.3	279.29	150.0
153.36	112.7				

*Electrical fault during heating period.

†A curve fit beyond 298 K is given by I Barin, O Knacke and O Kubaschewski, Thermochemical Properties of Inorganic Substances, Springer-Verlag, 1973, p 10:

C_p(298.15 K)/J K^{-1} mol^{-1} = 148.4 (this work 150.6)

C_p(300.00 K)/J K^{-1} mol^{-1} = 148.6 (this work 150.8).

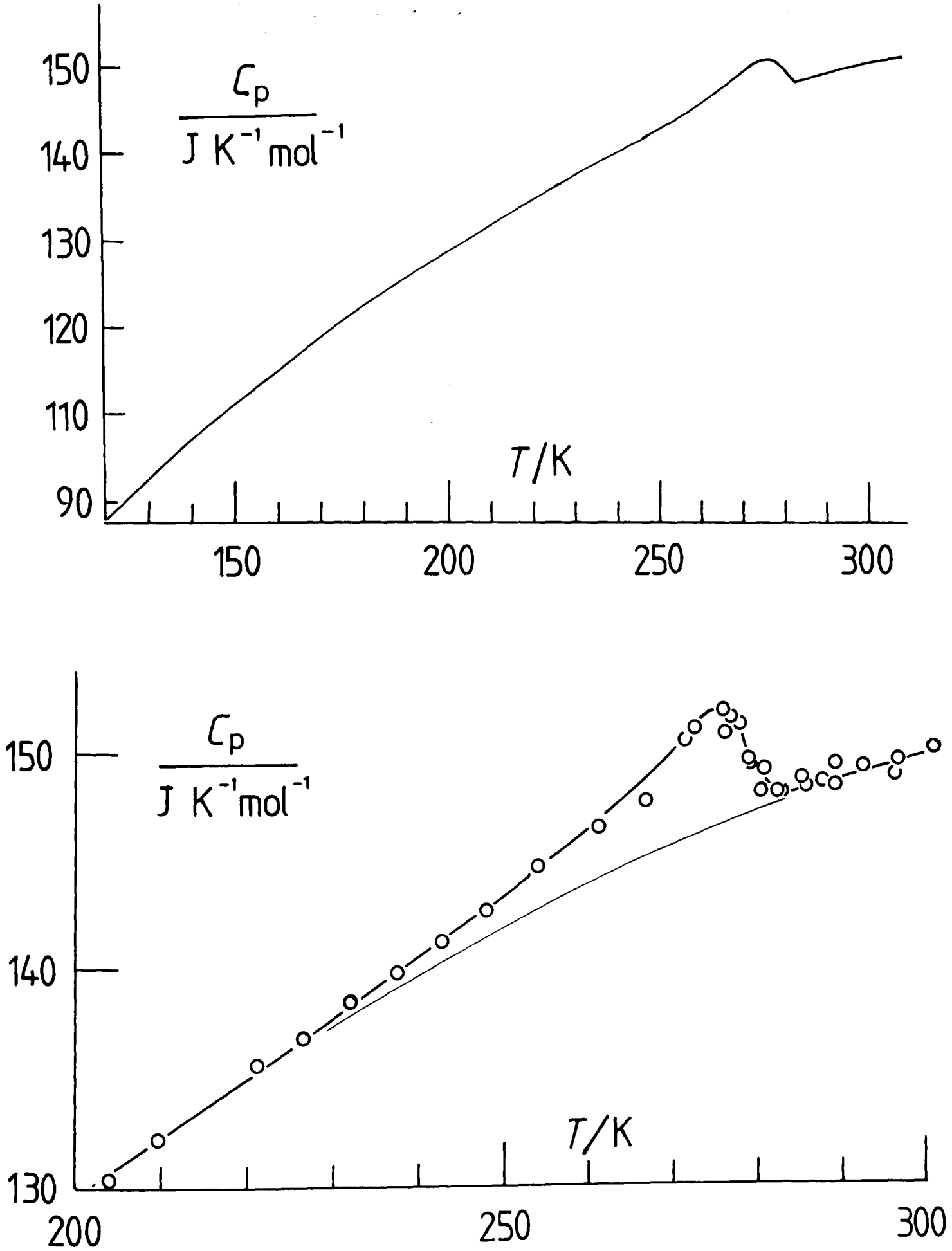

Figure 10.3 Molar heat capacity of silver tungstate (fused sample). The lower, more detailed plot of the anomaly shows the experimental points and the fitted 'base' curve (thinner solid line, see text). The area between the solid curves corresponds to an excess enthalpy of about 115 J mol^{-1}.

The experimental points lying between 237 and 290 K were omitted from the fitting procedure.

Since the anomaly was unexpected, it was decided to reinvestigate the heat capacity of the empty vessel in this region. Early work on the empty calorimeter had not produced a well defined heat capacity curve beyond about 280 K, though the smooth curve for alumina suggested that no anomaly occurs in this range. It was feared, however, that the anomaly could result from some change in the vessel since that time (new solder or sealing pin).

The new results are listed in table 10.3. There is no anomaly. The results lie slightly above the previous empty vessel results, but this can be accounted for almost entirely by the extra solder used.

Table 10.3

Experimental and calculated heat capacity of the empty vessel

experimental		calculated		
T/K	C_p/J K^{-1}	T/K	C_p/J K^{-1}	
			A	B
273.05	11.58			
275.06	11.59	275	11.60	11.56(11.59)
277.04	11.61			
278.99	11.66			
280.92	11.69	280	11.65	11.61(11.64)
282.79	11.67			
284.67	11.70	285	11.71	11.66(11.69)
286.60	11.72			
288.49	11.77			

A, Calculated on the basis of the new experimental points using

$$C_p/\text{J K}^{-1} = 8.404 + 0.011\,6(T/\text{K}).$$

B, Calculated from equation (7.1). The figures in parentheses are obtained by correcting for the slightly increased mass of solder used in this run.

Unfortunately it is possible to say only that the calorimetric silver tungstate contains an anomaly near 277 K. It may be that during the melting of the sample, some non-stoichiometry has been introduced, even though no evidence of this is available (d.t.a.,t.g.a. and i.r. and x-ray of samples before and after melting). In view of the work of Turkovic et al.[29] such a possibility cannot be ruled out.

To eliminate this possibility, towards the end of this project, a further run with freshly prepared silver tungstate was attempted. Again the sample size was small (19.935 g) and equilibration times long (well over an hour) despite the introduction of 35 Torr exchange gas. The run was abandoned.

It is clear that confirmation of the transition in stoichiometric silver tungstate requires data from another source. The transition is too small to be visible by d.t.a. or probably even d.s.c. I have asked Mr PD Hatton (SERC Daresbury) to perform a variable temperature x-ray powder diffraction investigation - though such a small, apparently high order, transition may not be visible by this means. I have also informed Dr BM Gatehouse of the heat capacity results as he intends to perform single crystal work on this system (see earlier).[22]

Small thermal events have been recorded in solids (see, for example reference 30, the heat capacity of the perovskite $SrTiO_3$).

Chihara has described a number of small broad transitions involving slight reorientation of large ions ($[PCl_6]^-$)[31] or molecules (chloranil).[32] An interpretation of these transitions in terms of soft mode theory has been given.[33]

There is certainly scope for such transitions involving the

the large planar $[W_4O_{16}]^{8-}$ ions. There are, however, many other possibilities including Ag^+ redistribution or a

centrosymmetric $\longrightarrow$ non-centrosymmetric $[W_4O_{16}]^{8-}$

transition. An unsuccessful search for a transition of the latter type was made by Turkovic et al. [29] in the temperature range 300-900 K.

Until further low temperature data for this compound are available, speculation as to the nature of this transition is unjustified.

Other thermodynamic properties of silver tungstate

The melting point of silver tungstate has been reported to lie at various temperatures between 857 and 893 K.[34] According to Flor and Sinistri,[35] silver tungstate undergoes a first order transition at 865 K and melts at 877 K. Overlapping of the two peaks could be responsible for some ambiguity in the interpretation of earlier d.t.a. results. To the best of my knowledge, however, the transition has been confirmed by only one other set of authors,[36] and they are from the same university as the authors of reference 35. In view of the exact correspondence of the transition and melting temperatures it may be that both sets of authors are using the same experimental data. The authors of reference 36 do not refer to Flor and Sinistri's work so it is impossible to tell.

Takahashi et al., who quote a melting point of 893 K do not observe the transition,[27] and nor does Faurie in his study of the Ag_2WO_4-WO_3 phase diagram.[37] It is interesting to note that Faurie quotes a melting point for the composition Ag_2WO_4 of 883 K.

Samples containing excess WO_3, however, melt incongruently with peaks at 863 and 883 K.

Unfortunately the d.t.a. heater for the instrument built during this work is not powerful enough for operation much beyond 700 K.

Various thermodynamic quantities have been obtained for silver tungstate at room temperature. By means of solution calorimetry, Graham and Hepler[28] derive a value for the enthalpy of formation of the crystalline solid at 298.15 K (-965 kJ mol^{-1}). Pan,[38] from electrochemical measurements using a silver-silver tungstate electrode, quotes values for the formation enthalpy (-954 kJ mol^{-1}), Gibbs energy (-831 kJ mol^{-1}) and entropy (-414 JK^{-1} mol^{-1}). As with other data for this compound, there is an uncertainty in the results because of the possibility of formation of poly-anions.[28]

The $AgI-Ag_2WO_4$ phase diagram

According to Takahashi et al.,[27] there are three compounds in the composition range between AgI and Ag_2WO_4. One is $Ag_6I_4WO_4$ (see chapter 8). The others are given as $Ag_4I_2WO_4$($2AgI : 1Ag_2WO_4$) and $Ag_5IW_2O_8$($1AgI : 2Ag_2WO_4$).

It seemed reasonable, to complete this project, to study the heat capacity of these two compounds. The latter, $Ag_5IW_2O_8$, is mentioned by Skarstad and Geller,[20] though it is not clear whether they have actually prepared the compound. The compound has been prepared by an electrochemical method by Suthanthiraray et al.[39] They identify their product solely on the basis of approximate correspondence of their x-ray diffraction pattern with that of Takahashi et al.[27]

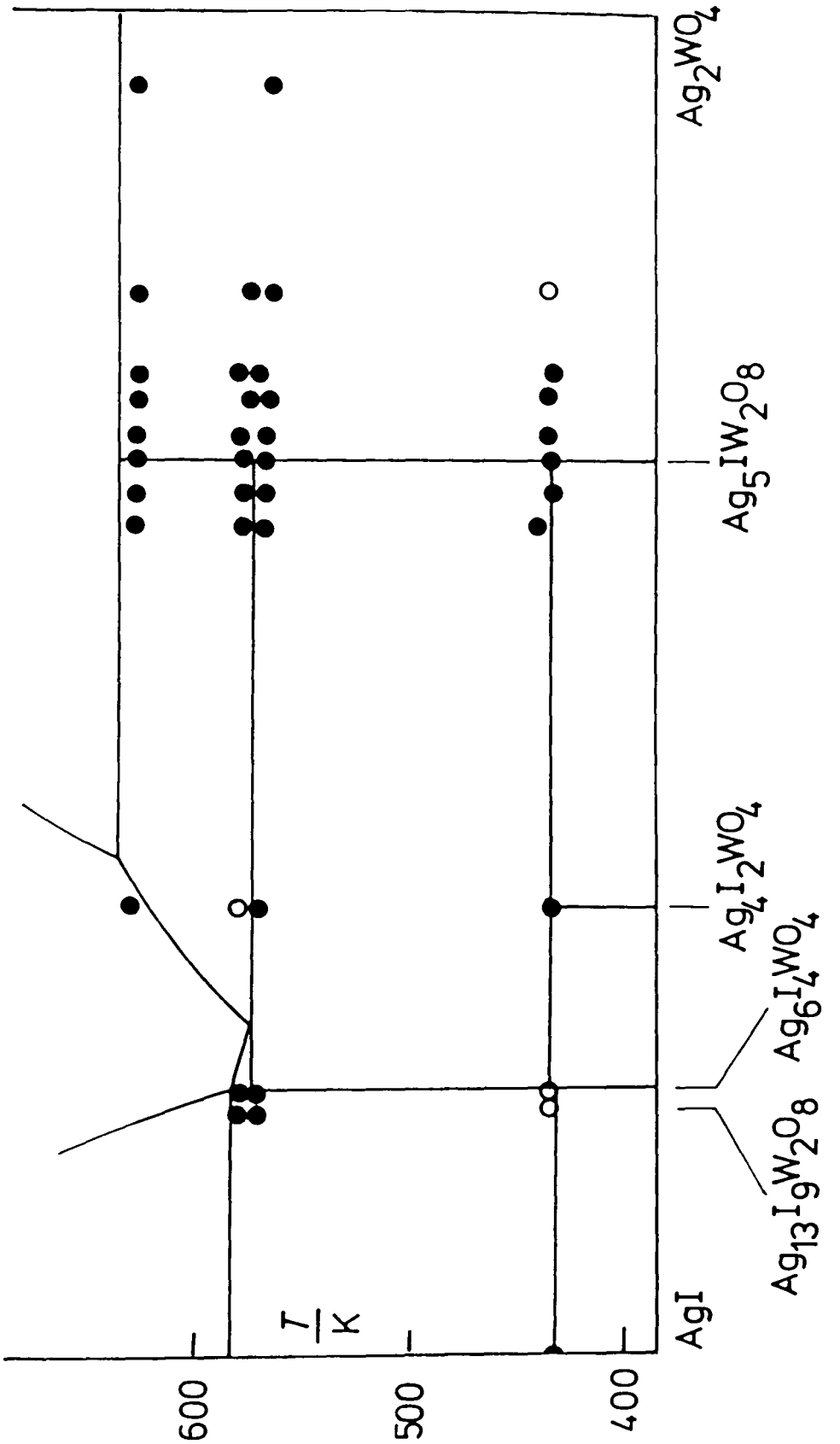

Figure 10.4 The $AgI-Ag_2WO_4$ phase diagram: solid lines according to Takahashi et al.[27]; circles are d.t.a. results obtained during this work (open symbols, small or irreproducible features). D.t.a. sample size 2 mg (Takahashi et al. 0.8 g). These d.t.a. points could result from phase separation during cooling of the melt followed by extremely slow solid state reaction. Facilities were not available for continuing the solid state reaction beyond a few days.

A number of attempts were made to prepare the compound $Ag_5IW_2O_8$ by solid state reaction and by fusion of the components, either ground together or co-precipitated from solution. Preparation was carried out in porcelain, or occasionally nickel, crucibles. At a later date preparations were repeated by a project student[40] with the components sealed in evacuated glass ampoules. In all cases but one, the x-ray diffraction photographs of the products are almost identical to that of silver tungstate. The exception was produced by prolonged solid state reaction of a pressed pellet of $Ag_6I_4WO_4$ and Ag_2WO_4. This photograph differred only in the relative line intensities (A348). In no case was a diffraction pattern similar to that of Takahashi obtained.

Ag_2WO_4 appeared to be the dominant phase at all compositions studied down to 50 mol% Ag_2WO_4.

Despite the study of numerous compositions by thermal and x-ray analysis, no clear picture of this system has emerged.

The phase diagram as reported by Takahashi et al.[27] is shown in figure 10.4. They give no indication of the 'width' of the single phases. On the diagram are marked the results of thermal analysis carried out during this work. The two sets of data are not consistent. Prolonged annealing at temperatures below the solidification point suggest that the points do not result from phase separation as the melt cools, though this cannot be ruled out. Where possible, results were obtained for samples formed by slow cooling of the melt and for samples prepared by annealing quenched glasses. It should be noted that glasses containing more than 50 mol% Ag_2WO_4 showed strong Ag_2WO_4 lines in their x-ray photographs. In these cases the thermal behaviour of the samples was identical, though there were often slight differences in the x-ray powder diffraction photographs.

I make no further comments concerning the differences between the two sets of results; any conclusions must await the completion of further studies.[40]

One final feature worthy of note is the ubiquitous endotherm near 150 °C. It occurs in silver iodide rich samples, it reappears beyond the electrolyte phase and again in glassy samples, even those showing no x-ray evidence of silver iodide.

$Ag_4I_2WO_4$

A new x-ray pattern, showing no Ag_2WO_4, AgI or $Ag_6I_4WO_4/Ag_{13}I_9W_2O_8$, was obtained for the composition 2AgI : $1Ag_2WO_4$. Takahashi et al.[27] also prepared a compound of that composition, though the two x-ray patterns do not correspond particularly closely (table 10.4). Magistris et al.[36] found no evidence for this compound in their study of the AgI-Ag_2WO_4 system.

Many of the lines in the photographs for this composition are broad and there is a significant diffuse background. These features are characteristic of Ag^+ electrolytes, but time did not permit conductivity studies to be made. Takahashi et al.[27] suggest that this compound is not an electrolyte.

Table 10.4

X-ray powder diffraction data for the composition $Ag_4I_2WO_4$

$d/\mathring{A}$	
this work (A382)*	ref. 27
11.01(10)	
6.64(5)	
4.18(10)	4.31(w)
3.74(15)	3.79(s)
3.58(1)	
3.45(10)	3.48(w)
3.12(8)	3.02(m)
2.98(1)	2.94(m)
2.91(100)	2.87(mw)
2.84(5)	
2.71(40)	2.71(m)
2.67(30)	
2.48(5)	
2.43(5)	
2.29(5)	2.31(m)
2.23(1)	2.25(vw)
2.18(1)	
2.02(1)	
1.96(1)	1.97(mw)
1.91(5)	1.92(w)
1.84(1)	
1.79(5)	
1.64(8)	
1.60(2)	
1.55(4)	

Figures and letters in parentheses represent relative intensities: s strong, m moderate, mw moderate to weak, w weak, vw very weak.

*Prepared by annealing the glass for 24 h at 420 K. Slight differences were apparent for samples prepared by different routes.

Silver tungstate - an additional note

In a very recent study, Jensen and Lou[41] have investigated the precipitation reactions occurring in solutions of $AgNO_3$-$NaNO_3$-Na_2WO_4. The product is complex and time dependent. To explain their results they require at least four other Ag-WO_x species to be precipitated. The presence of varying proportions of these in 'silver tungstate' could well influence its thermal behaviour - the heat capacity anomaly reported here, the high temperature d.t.a. endotherm[35] and the temperature dependent Raman data of Turkovic et al.[29]

They show x-ray powder diffraction results for three compositions. The results reported here correspond closely with those given for stoichiometric Ag_2WO_4, though the line at 5.31 Å (table 10.1) is significantly stronger. Their non-stoichiometric samples contain very strong lines at 3.7 and 5.2 Å and other strong features not present in the patterns obtained during this work.

On this basis, the calorimetric sample is predominantly stoichiometric Ag_2WO_4. It is not possible to predict, however, the effects of very small amounts of other 'compounds' on the properties of silver tungstate or, for that matter, of electrolytes made from silver tungstate.

Jensen and Lou found no evidence of sodium in any of their precipitates.

References to chapter 10

1 H G Leduc and L B Coleman, *Solid State Ionics*, 1981, 5, 469.

2 K S Pitzer, *J Amer Chem Soc*, 1941, 63, 516.

3 H Schmalzried, *Progr Solid State Chem*, 1981, 13, 119.

4 S Geller, *Science*, 1978, 11, 87.

5 K Funke, *Progr Solid State Chem*, 1976, 11, 345.

6 J C Phillips, *Rev Modern Phys*, 1970, 42, 317.

7 T A Fjeldly and R C Hanson, *Phys Rev B*, 1974, 10, 3569; R C Hanson, T A Fjeldly and H D Hochheimer, *Phys Stat Solid(b)*, 1975, 70, 567.

8 C M Perrott and N H Fletcher, *J Chem Phys*, 1968, 48, 2143; 1968, 48, 2681; 1969, 50, 2770; 1970, 52, 3372; 1970, 52, 3373.

9 J Nölting and D Rein, *Z Phys Chem NF*, 1969, 66, 150.

10 W Jost, *J Chem Phys*, 1971, 55, 4680; N H Fletcher, *J Chem Phys*, 1971, 55, 4681.

11 K H Leiser, *Z Phys Chem(Frankfurt)*, 1954, 2, 238; S Hoshino, *J Phys Soc Japan*, 1957, 12, 315.

12 M B O'Reilly, *Phys Stat Solid(a)*, 1978, 48, 489.

13 Yu Ya Gurevich and A K Ivanov-shits, *Elektrokhimiya*, 1977, 13, 1593.

14 A Fontana, G Mariotto and M P Fontana, *Phys Rev B*, 1980, 21, 1102; E Cazzanelli, A Fontana, G Mariotto, F Rocca, V Mazzacurati, G Ruocco and G Signorelli, *Solid State Ionics*, 1981, 5, 473; V Mazzacurati, G Ruocco, G Signorelli, E Cazzanelli, A Fontana and G Mariotto, *Phys Rev B*, 1982, 26, 2216; E Cazzanelli, A Fontana and G Mariotto, *J Phys Colloq(France)*, 1981, 42(C6), 196.

15 C M Perrott and N H Fletcher, *J Chem Phys*, 1969, 50, 2344; W Jost and G Kubaschewski, *Z Phys Chem NF*, 1968, 60, 69.

16 S Hoshino, T Sakuma, H Fujishita and K Shibata, *J Phys Soc Japan*, 1983, 52, 1261; H U Beyeler and S Strässler, *Phys Rev B*, 1979, 20, 1980; H U Beyeler, P Brüesch, T Hibma and W Bührer, *Phys Rev B*, 1978, 18, 4570.

17 J B Boyce, T M Hayes, W Stutius and J C Mickelsen, *Phys Rev Letters*, 1977, 38, 23; A F Wright and B E F Fender, *J Phys C*, 1977, 10, 2261.

18 B R Lawn, *Acta Cryst*, 1964, 17, 1341.

19 K F Gebhardt, P D Soper, J Merski, J J Balle and W G Flygare, *J Chem Phys*, 1982, 72, 272; H Roemer and G Luther, *Ferroelectrics*, 1981, 38, 919; K Funke and A Jost, *Ber Bunsenges Phys Chem*, 1971, 75, 436.

20 P M Scarstad and S Geller, *Mater Res Bull*, 1975, 10, 791.

21 R D Armstrong, R S Bulmer and T Dickinson, *J Solid State Chem*, 1973, 8, 219.

22 B M Gatehouse, Monash University, personal communication, 1983.

23 J S McKechnie, L D S Turner, C A Vincent, F Bonino, M Lazzari and B Rivolta, *J Inorg Nucl Chem*, 1979, 41, 177.

24 B M Gatehouse and P Leverett, *J Chem Soc Dalton*, 1976, 1316.

25 P H Bottelberghs, Thesis, University of Utrecht, 1976.

26 Powder Diffraction File Inorganic Phases, Joint Committee on Powder Diffraction Standards (JCPDS), 1980.

27 T Takahashi, S Ikeda and O Yamamoto, *J Electrochem Soc*, 1973, 120, 647.

28 R L Graham and L G Hepler, *J Amer Chem Soc*, 1958, 80, 3538.

29 A Turkovic, D L Fox, J F Scott, S Geller and G F Ruse, *Mater Res Bull*, 1977, 12, 189.

30 V Franke and E Hegenbarth, *Phys Stat Solid(a)*, 1974, 25, K17.

31 H Chihara, M Nakamura and K Masukane, *Bull Chem Soc Japan*, 1973, 46, 97.

32 H Chihara and K Masukane, *J Chem Phys*, 1973, 59, 5397.

33 H Chihara, N Nakamura and M Tachiki, *J Chem Phys*, 1973, 59, 5387.

34 Gmelin Handbuch der Anorganischen Chemie, Silver Volume 4, Springer-Verlag, 1974, p 347.

35 G Flor and C Sinistri, *Z Naturforsch a*, 1970, 25, 1484.

36 A Magistris, G Chiodelli and G V Campari, *Z Naturforsch a*, 1976, 31, 974.

37 J-P Faurie, *Bull Soc Chim France*, 1971, 1170.

38 K Pan, *J Chinese Chem Soc (Taiwan)*, 1954, 1, 26.

39 S A Suthanthiraraj, B V R Chowdari and S Radhakrishna, *Thin Solid Films*, 1983, 101, 131.

40 E Speers, B Sc project, Leicester Polytechnic, 1983-4

41 J B Jensen and J Lou, *Acta Chem Scand A*, 1983, 37, 617.

42 It appears that discrepancies among microwave data result from different sample preparation methods: K Funke, A Gacs, H-J Schneider, S M Ansari, N Martinkat, H Roemer and H-G Unruh, *Solid State Ionics*, 1983, 11, 247.

43 Similar behaviour has been reported for powdered and pelletized zinc bromide: M A White, C Chieh, A Anderson and L A K Staveley, *J Chem Phys*, 1984, 80, 1254.

11

Electrolytes formed by Combination of Silver Iodide and Organic Iodides

Preliminary work undertaken in this project confirmed that combinations of alkylammonium, sulphonium or carbonium iodides with silver iodide can produce solid electrolytes. It appears that these combinations produce well defined compounds. The electrolytes are not two phase mixtures, nor is an extension of the stability range of α-AgI involved.

There are a number of ways by which the stoichiometry of these compounds can be determined. Since they were made because of their electrical properties, conductivity measurements were obviously the first means used to determine optimum electrolyte composition. Plots of conductivity against mole fraction AgI show maxima, the exact position of which depends on the organic iodide used.[1]

The fairly broad maxima make only an approximate estimate of composition possible. Compounds made up on this basis show little or no evidence of silver iodide in their x-ray powder diffraction patterns (see table 11.1).

The absence of γ or β-AgI can be shown in another way. The low temperature forms of AgI undergo a first order transition at 419 K. This involves a large latent heat and is easily visible by means of d.s.c. or d.t.a. techniques. D.s.c. traces show the disappearance of the transition peak as progressively larger proportions of tetra-alkylammonium salt are added to

silver iodide.[4]

Tetraethylammonium iodide itself has a first order transformation near 460 K.[2,5] This appears as a broad d.s.c. peak (the transformation is probably 'sluggish').[3] This too disappears in the electrolyte, though this does not in fact provide evidence for compound formation. D.s.c. of mixtures containing potassium iodide and tetraethylammonium iodide show irreproducible transition behaviour.[4]

Electrolytes were also prepared with tetraethylammonium bromide. The crystal structure of NEt_4Br is identical to that of NEt_4I.[2]

It was expected that NEt_4Br alone would have a transition corresponding to that in NEt_4I. This is the case, though data concerning the transition in NEt_4Br do not appear to have been published. In table 11.2, literature data[5] and results obtained in this work are compared. For d.s.c. work, indium was used as the enthalpy standard. The uncertainties in the latent heats are large as the organic compounds have broad shallow peaks. This also makes the transition temperatures difficult to establish with any certainty. The temperatures reported were obtained by d.t.a. using very small samples (less than 2 mg). Temperature calibration of the instrument was checked using the standards listed.

Electrolyte stoichiometry, estimated both from disappearance of the AgI peak and peak area changes, is about 6AgI : $1NEt_4X$. This compares favourably with the conductivity data of Owens.[6]

Table 11.1

X-ray powder diffraction data for two tetra-alkylammonium iodide-silver iodide electrolytes prepared during this work. Data for AgI and NMe_4I are given for comparison

		$d/\text{Å}$	
$(AgI)_5NEt_4I$	$(AgI)_{6.5}NMe_4I$	NMe_4I	AgI
A361	A366	A357	A365*
14.56(100)	10.14(100)	5.63(30)	3.97(15)
11.86(50)	8.69(100)	4.65(30)	3.74(100)
10.34(30)	6.34(10)	4.01(100)	2.30(70)
8.55(5)	4.75(5)	3.27(10)	1.96(30)
7.19(20)	4.40(5)	3.02(35)	1.63(1)
5.60(3)	4.11(5)	2.82(5)	1.49(3)
4.99(5)	3.97(5)	2.70(25)	1.33(5)
3.98(30)	3.64(100)	2.52(25)	1.25(5)
3.78(10)	3.53(1)	2.41(1)	1.15(1)
3.58(10)	3.39(5)	2.31(20)	1.10(5)
3.50(10)	3.17(1)	2.24(20)	
3.35(5)	2.99(30)	2.06(5)	
3.20(3)	2.65(1)	1.99(2)	
2.84(1)	2.58(25)	1.95(15)	
2.63(1)	2.38(1)	1.88(8)	
2.39(3)	2.32(3)	1.86(8)	
2.31(15)	2.28(5)	1.83(10)	
2.21(1)	2.24(1)	1.78(10)	
2.16(3)	2.20(5)	1.75(12)	
2.05(1)	2.16(5)	1.72(1)	
1.97(8)	2.12(100)	1.70(10)	
	2.09(5)	1.69(10)	
	2.06(5)	1.60(5)	
	1.96(1)	1.58(1)	
	1.90(1)	1.56(3)	
	1.84(1)	1.53(3)	
	1.64(1)	1.50(5)	
	1.53(1)	1.45(3)	
	1.49(1)	1.43(1)	
	1.39(5)	1.39(12)	

*Predominantly γ-AgI containing ~ 10-15% β.

Table 11.2

Transition temperatures and enthalpies for tetraethylammonium bromide and iodide

	T/K		ΔH/kJ mol^{-1}		temperature standards
	d.t.a.*	ref. 5	d.s.c.	ref. 5	
NEt_4I	459	458-465	17±2†	21	saccharin m.p. 501 K
NEt_4Br	430		14±2		benzanilide m.p. 436 K
					AgI 419 K

*Heating rate 0.1 K s^{-1}; on cooling both transitions occur at about 6 K lower (difference for AgI less than 1 K).

†The large estimated uncertainties result from the broad, shallow peak shape.

One of the reasons for the ease of preparation of these electrolytes is the existence of the AgI transition at 419 K. It is known that solids are more highly reactive at transition temperatures and this is certainly true of AgI.[7] This has an interesting effect on the d.s.c. traces of AgI-organic iodide mixtures. Such traces are shown in reference 4 for mixtures containing ammonium and sulphonium salts.

Accurate determination of electrolyte stoichiometry relies on single crystal structure determination. There are many of these studies.[8]

The choice of calorimetric sample

An electrolyte was chosen from among those identified by crystallography. An additional requirement was that the compound should have been used as an electrolyte, and the two materials

(single crystal and electrolyte) shown to be identical in structure. This is important since some doubt has been cast on how similar single crystals and electrolytes, of apparently the same composition, really are.[9]

Tetramethylammonium iodide-silver iodide

A detailed study of alkylammonium iodide-silver iodide systems has been made by Owens and his colleagues.[6,10] On the basis of conductivity studies a composition of 6.7AgI : $1NMe_4I$ was established. Smyth, Tompkins and Ross[11] obtained an optimum conductivity at 6AgI : $1NMe_4I$. The exact stoichiometry and single crystal structure have been reported by Geller and Lind.[12] They also report the preparation of a powdered electrolyte for conductivity studies, whose x-ray pattern is identical to that obtained from single crystals. Owens comments that his powder patterns are the same as those of Geller and Lind. Unfortunately I have been unable to obtain powder data either from Geller or Owens. The powder results obtained in this work are given in table 11.1.

From the single crystal data,[12] it is possible to calculate the various lattice spacings.[13] It is not possible to obtain line intensities without considerable extra data. All the high d spacing lines given in table 11.1 can be assigned, on the basis of the calculation, to reflections from particular crystal planes. This is not possible for the more closely spaced planes since the calculated lines are too numerous.

Preparation of $[NMe_4]_2Ag_{13}I_{15}$

The preparation method was based on those of Owens and Geller and Lind.[6,12]

The x-ray powder diffraction photograph of the product showed no evidence of AgI or the organic component. D.t.a. scans of the compound revealed a very small event near 420 K, equivalent in area to less than three or four percent of the original AgI. Samples prepared with a slight excess of NMe_4I behaved similarly. Repeated cycling did not remove the peak - if anything, after a number of runs, it became more pronounced. It was assumed therefore that the peak results from slight breakdown of the compound as the temperature is raised.

High temperature properties of the electrolyte

In view of the report by Owens[6] that there is a second highly conducting compound in the AgI-NMe_4I system (4:1), further thermal and x-ray studies were made.

$[NMe_4]_2Ag_{13}I_{15}$ melts at about 545 K, apparently without significant decomposition since the sample can be melted several times without any visible change in behaviour. Decomposition becomes noticeable beyond 600 K. Melting is probably incongruent. The x-ray pattern of the cooled melt shows the presence of the original compound, γ-AgI and other lines.

Owens reported that the 4:1 compound was present in samples prepared at temperatures above 440 K. In this work, no evidence for this compound has been found. No d.t.a. event is visible between room temperature and melting, and x-ray studies of the quenched melt show no significant unidentified phase.

Andrews et al.[14] report that $[NMe_4]_2Ag_{13}I_{15}$ decomposes at 457 K. No d.t.a. evidence for this was obtained during this work. The x-ray studies suggest that if decomposition occurs, it is reversible. Since some of the decomposition data in reference 14 are certainly in error (NEt_4I-AgI electrolyte, for example), it may be that this is also the case for $[NMe_4]_2Ag_{13}I_{15}$.

Heat capacity of $[NMe_4]_2Ag_{13}I_{15}$

The calorimetric sample was a buff-coloured powder. Heat capacity measurements were carried out on a sample of 34.863 g (0.020 2 mol).

The measurements were performed in three stages. In the first, measurements were made between 78 and 165 K. About 10 Torr exchange gas was included and no solder correction was necessary. Drift periods were longer than with alumina but not inconvenient (maximum 35 min).

At 165 K measurements were interupted for about a week (for a conference). Pumping was continued for that time. The second stage consisted of measurements between 165 and 220 K. Drift periods were very much longer, an hour or more, and there was more scatter of the points about a smooth curve.

It was assumed that a very small leak in the calorimeter vessel had allowed the helium exchange gas to be pumped away. The sample container was removed and helium readmitted; this time 30 Torr. Since the most likely point of leakage was considered to be the cap, extra solder was used in resealing.

In addition, some alterations were made to the shield heater circuit to allow for more precise measurement of small

sample heater voltages. Slight recalibration of the voltmeter proved to be necessary. In view of this, it was thought that there might be a slight disagreement between different runs. This proved to be the case. Using the same data for the heat capacity of the empty vessel, stage three results were about one percent higher than those from stage one. About half of this could be accounted for by increasing the heat capacity of the vessel to allow for the extra solder. To bring the two sets of data into line, the heat capacity of the vessel was increased such that the heat capacity results from stage one and stage three overlapped in the temperature interval 160-170 K. This amount (0.12 J) was added to the heat capacity of the vessel for all stage three points, in place of the solder correction. The close coincidence of stage two and stage three results between 170 and 220 K suggests that this was a reasonable procedure. It does mean, however, that if voltage calibration during stages one and two was in error, then all reported molar heat capacity values should be increased by 4-5 J mol^{-1} (about 0.5%).

The results are given in table 11.3 and figure 11.1. A small deviation from the smooth curve, slightly more than can be accounted for by experimental scatter, is apparent for the one point between 270 and 275 K. It is assumed that this is a result of moisture in the sample. A similar observation was made by Coulter et al.[15] for tetramethylammonium iodide alone. All the tetramethylammonium halides are hygroscopic to some extent, the fluoride most strongly and the iodide least. This property has been commented on for the chloride and may be the cause of disagreements about transition positions in that compound.[16,17]

Table 11.3

Molar heat capacity of the electrolyte $[NMe_4]_2Ag_{13}I_{15}$

T/K	C_p/J K^{-1} mol^{-1}	T/K	C_p/J K^{-1} mol^{-1}	T/K	C_p/J K^{-1} mol^{-1}
stage 1		stage 2*		stage 3	
79.10	708	174.41	944	158.22	912
83.89	720	180.26	952	160.71	918
86.43	728	183.47	952	163.15	918
89.05	736	187.35	966	166.16	926
91.60	744	191.24	958	169.73	934
94.11	750	195.67	964	173.87	936
96.54	760	200.24	974	177.38	944
98.93	766	204.81	978	181.54	952
101.28	774	209.35	978	186.31	956
104.32	784	213.87	992	191.05	964
107.34	790	218.37	994	195.76	970
110.30	798			201.50	982
113.23	806			208.41	988
116.14	814			215.16	994
119.00	820			221.86	1008
121.80	826			228.65	1010
124.56	836			235.29	1024
127.29	842			242.81	1030
129.99	856			251.28	1042
132.66	864			257.12	1046
135.31	872			268.14	1054
138.41	888			272.36	1072†
141.94	906			278.61	1064
145.41	932			282.93	1076
148.27	956				
150.72	962				
152.57	916				
153.83	910				
155.08	908				
156.33	910				
158.18	912				
160.63	916				

*Some additional uncertainty resulting from long equilibration times.

†See text.

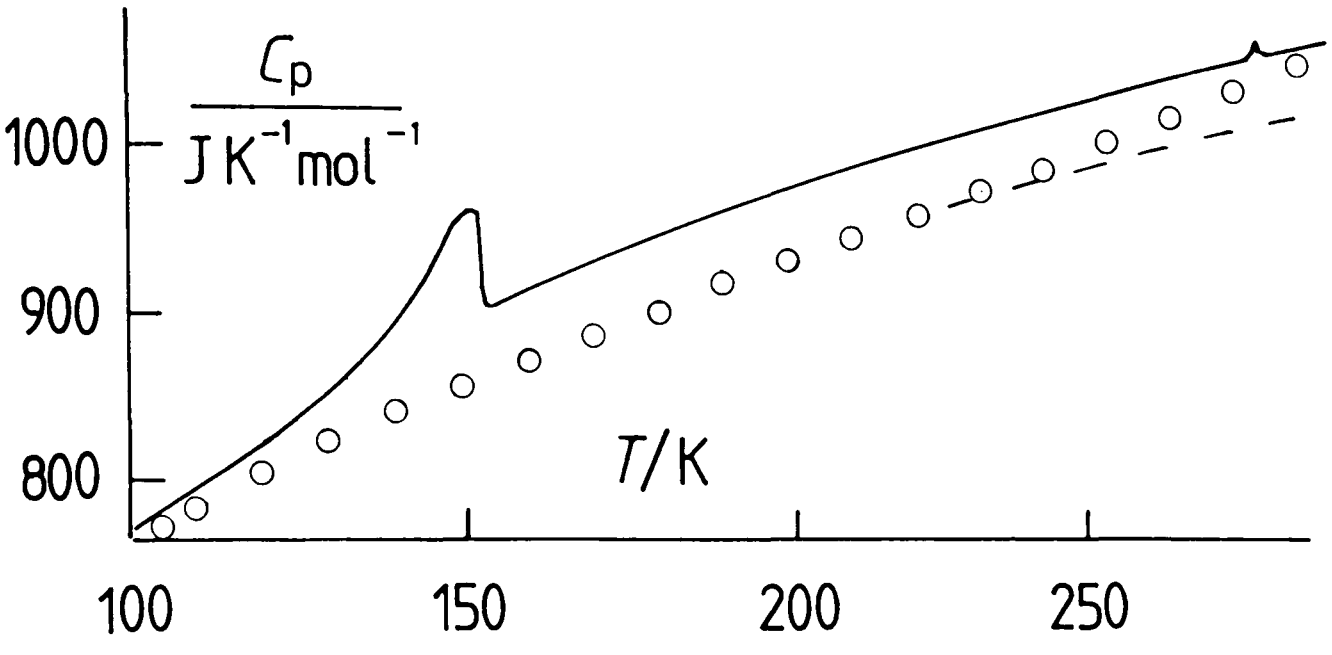

Figure 11.1 Molar heat capacity of $[NMe_4]_2Ag_{13}I_{15}$ (solid line): o heat capacity of a mixture 13 AgI + 2 NMe_4I. Between 100 and 79 K the circles fall on the solid line. The broken line represents the mixture heat capacity extrapolated as described in the text.

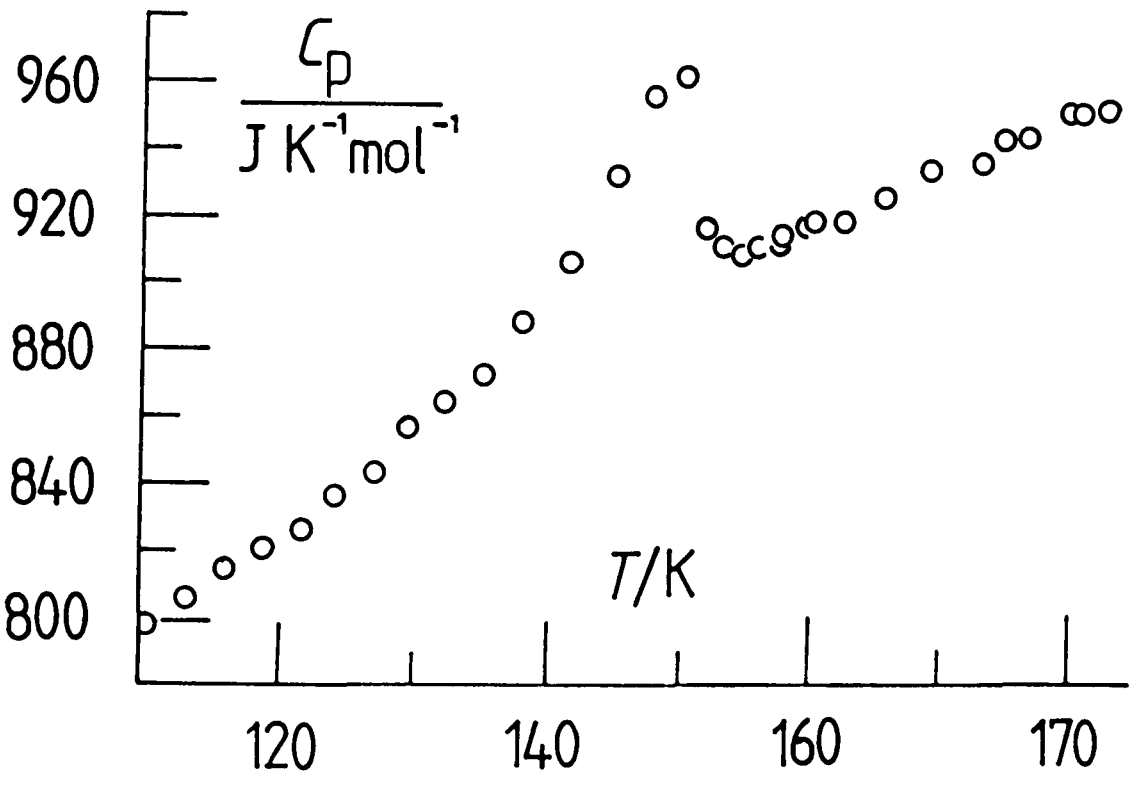

Figure 11.2 Detailed heat capacity of $[NMe_4]_2Ag_{13}I_{15}$ in the transition region.

The 'peak' on figure 11.1 would require only 1-2 mg of free water.

The transition region near 150 K is shown in more detail in figure 11.2. It appears to be slightly rounded. It was thought that this may result from the average nature of each heat capacity point. Two further runs were therefore carried out; one in the region 147-157 K with temperature increments of 0.9 K. These points are not on the figure but the curve had exactly the same shape as that shown. The final series of points was recorded between 149.5 and 151 K with increments of 0.15 K. Ten heat pulses, each of 2.76-2.77 J, produced temperature increments of 0.15 K. Unfortunately the accuracy with these small values is poor so that all one can say is that between 149.5 and 151.0 K, the heat capacity does not vary by more than 5%. The limiting factor is the temperature resolution.

Single crystal measurements, by the a.c. method for example, are necessary to decide whether this shape is characteristic of the compound or is the result of slight inhomogeneity within this sample.

The heat capacity of the mixture $13AgI+2NMe_4I$ is also illustrated in figure 11.1. Below about 100 K this coincides with the experimental curve. The convergence of the two curves in the high temperature region is a result of the sharply rising heat capacity of silver iodide in that region (see chapter 10). If Pitzer's last three points are deleted and a graphical extrapolation is made beyond 230 K, the broken curve is obtained. This will still include disordering of AgI itself but it does not seem reasonable to approximate the heat capacity

of AgI by the classical limit $3NR$. The heat capacity of AgI already exceeds that value below 140 K.

The transition may not, of course, be related to the onset of conductivity. Both the transition and the 'excess' heat capacity may be explicable in terms of some structural change, and change in the vibrational spectrum of the compound relative to that of the components. At this temperature, such a change would necessarily involve vibration (or vibration-rotation) within the NMe_4 group. It can be seen from figure 1.1 that reduction in frequency of a vibrational mode produces an increase in the heat capacity of that mode (if we assume that each mode can be represented as an Einstein oscillator). This is true provided that the mode has not reached its high temperature limiting value. Many such modes are available in NMe_4I but it is difficult to see what could cause the required changes.

In NMe_4I rotation about the N-C bond and rotation of the NMe_4 unit is unhindered.[15,16] Note that this contrasts with the situation in NMe_4Cl.[17] Since the heat capacity curves of the compound and mixture coincide at low temperature, it is likely that free rotation also occurs in the electrolyte. Loss of rotational freedom (i.e. rotation $\longrightarrow$ vibration) could lead the'excess' heat capacity but this would be most unusual.

In the crystal structure determination, the individual carbon and nitrogen atoms could not be located.

Silver ion disordering thus appears to be the most likely cause of the transition and excess heat capacity.

No other studies of the low temperature properties of this electrolyte have been made since the original work of Owens.[6] He measured the conductivity between 220 and 370 K. There was

no evidence of a transition to the non-conducting state. Some of the other compounds studied did, however, show a change in slope of the conductivity plot.

The room temperature crystal structure [12] shows that the unit cell is rhombohedral, space group *R*32, and contains one formula per unit cell: a = 11.5 Å; α = 67.35°.

In common with other Ag^+ electrolytes, the structure is built up of iodide tetrahedra. Silver ion sites are within these tetrahedra and channels between sites, through faces of the tetrahedra, allow movement of the Ag^+ ions.

There are 41 Ag^+ sites per unit cell for the 13 ions.[12] The situation is complicated by the fact that there are eight non-equivalent sites and Ag^+ distribution among the sites is not random. One pair of sites is not significantly occupied so it is perhaps more correct to say that there are 39 sites available to Ag^+ ions.

The environment of each site, Ag-I distances, nature of adjacent sites and site-site distances are detailed by Geller and Lind.[12] It seems reasonable to assume that since there are site energy differences, the site occupancies will vary with temperature.

It is therefore likely that the transition marks a sharp change in site occupancy distribution between 120 and 150 K. Following the transition, the excess heat capacity represents continuing randomization of the Ag^+ distribution which is still incomplete at room temperature. Whether the Ag^+ ions are completely ordered below 120 K, only detailed structural studies will tell.

Configurational disorder in $[NMe_4]_2\ Ag_{13}I_{15}$

The heat capacity, neglecting points between 122 and 157 K, was fitted to a polynomial function and the excess enthalpy represented by the peak calculated to be

$$\Delta_{tr}H = 760\ J\ mol^{-1}.$$

In order to estimate the excess entropy, a plot was drawn of C_p/T against T for

(i) the experimental results

(ii) the curve fit to the experimental results

(iii) the constituents $2NMe_4I + 13AgI$.

The transition entropy was calculated to be

$$\Delta_{tr}S = 5.34\ J\ K^{-1}\ mol^{-1}. \qquad (11.1)$$

This, however, represents only part of the excess entropy of the compound relative to that of the constituents. At 300 K, the total excess entropy (again obtained from the C_p/T plot) is

$$\Delta S(\text{excess}) \simeq 45\ J\ K^{-1}\ mol^{-1} \qquad (11.2)$$

If the heat capacity of AgI were represented by

$$C_p = 3NR$$

then

$$\Delta S(\text{excess}) \simeq 68\ J\ K^{-1}\ mol^{-1} \qquad (11.3)$$

The excess entropy is assumed to result from Ag^+ disordering, and may thus be described as Ag^+ configurational entropy.

The total configurational entropy available to 13 silver ions distributed randomly among 39 sites can be evaluated

$$\Delta S(\text{config}) = R\ln W$$

where W is the number of possible configurations.

In this case

$$\Delta S(\text{config}) = 186 \text{ J K}^{-1} \text{ mol}^{-1} \qquad (11.4)$$

well above the values of equations (11.2) or (11.3).

We can thus agree with Geller and Lind[12] that Ag^+ distribution at 300 K is not random.

It is possible to calculate the configurational entropy on the basis of fixed distributions among site-types, as has been done for the simpler system $RbAg_4I_5$ by Topol and Owens,[18] but this requires a knowledge of site-type occupancies. Even this may not be a particularly profitable procedure because the statistical calculations make no allowance for entropy reduction caused by short range ordering[18] (non-occupancy of adjacent sites for example).

More complete calculations can be carried out, involving fitted values for site energy differences and Ag^+-Ag^+ repulsion, as shown by Wiedersich and Johnson for $RbAg_4I_5$.[19] In their calculation the vibrational heat capacity of the lattice is approximated as a Debye function.

There is clearly uncertainty in the calorimetric configurational entropy since its value depends on the choice of 'base line' vibrational heat capacity. For example, for $[NMe_4]_2Ag_{13}I_{15}$, equation (11.2) probably represents a minimum estimate and equation (11.3) a maximum (see also Hibma's work discussed later).

Such calculations are therefore useful only in providing a qualitative picture of behaviour at the atomic level.

The system pyridinium iodide - silver iodide

Heat capacity studies have been reported for one of the compounds in the pyridinium iodide -silver iodide system, (pyridinium)Ag_5I_6. One covers only the range 1.8-20 K,[20] revealing no unusual behaviour. The other study is by differential scanning calorimetry between 150 and 400 K.[21]

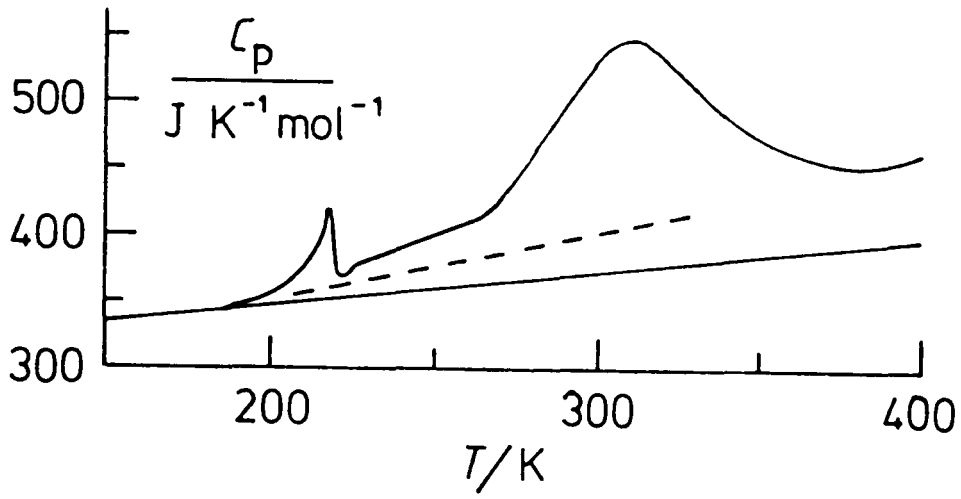

Figure 11.3 Heat capacity of(pyridinium)Ag_5I_6 (adapted from reference 21): lower solid curve, base line heat capacity drawn by Hibma using $C_p(AgI) = 6R$; broken line, heat capacity of the components using Pitzer's heat capacity of AgI (see chapter 10).

Hibma's data (reproduced in figure 11.3) suggest that the d.s.c. heat effect between 280 and 350 K is large. Geller and Owens,[22] however, state that the heat effect (from their own d.s.c. study) is small.

A crystallographic study of the low temperature phases of (pyridinium)Ag_5I_6 also appears to cast some doubt on Hibma's original results.[23] On the basis of the crystallographic work,

it was suggested that the low temperature transition found by d.s.c. was second order. A further transition, this time first order, was found at 180 K, and this is not seen in Hibma's plot.[21]

Both the low temperature transitions are said to be associated with orientational disordering of the pyridinium ions (pyridinium iodide itself undergoes a disordering transition at 250 K). The nature of the transition at 300-330 K is not known but it has been suggested that it involves a gradual transition from a disordered state, in which few Ag^+ are mobile, to a disordered state in which all Ag^+ are mobile.[22,23] Conductivity results are consistent with this.[21,22]

A more detailed heat capacity study of this compound in the range 100-400 K would clearly be worthwhile.

References to chapter 11

1 C F Randall, Ph D Thesis, Leicester Polytechnic, 1978; S Hackwood, Ph D Thesis, Leicester Polytechnic, 1979.

2 E Wait and H M Powell, *J Chem Soc*, 1958, 1872.

3 D A Johnson and J F Martin, *J Chem Soc Dalton*, 1973, 1585.

4 P G Hall, Transfer Report, Leicester Polytechnic, 1982.

5 J Levkov, W Kohr and R A Mackay, *J Phys Chem*, 1971, 75, 2066.

6 B B Owens, *J Electrochem Soc*, 1970, 117, 1536.

7 C N R Rao and K J Rao, Phase Transitions in Solids, McGraw Hill, 1978.

8 See for example S Geller, P M Skarstad and S A Wilber, *J Electrochem Soc*, 1975, 122, 332; M M Thackeray and J Coetzer, *Electrochim Acta*, 1979, 24, 495.

9 S Hackwood and R G Linford, *Chem and Ind*, 1980, 523.

10 B B Owens, J H Christie and G T Tiedeman, *J Electrochem Soc*, 1971, 118, 1144.

11 D M Smyth, C H Tompkins and S D Ross, Paper presented at the 24th Annual Power Sources Symposium, Atlantic City, 1970.

12 S Geller and M D Lind, *J Chem Phys*, 1970, 52, 5854.

13 International Tables for X-ray Crystallography, The International Union of Crystallography-The Kynoch Press, 1968; see volumes 1 and 2.

14 K C Andrews, S Hackwood and R G Linford, *J Power Sources*, 1979, 4, 165.

15 L V Coulter, K S Pitzer and W M Latimer, *J Amer Chem Soc*, 1940, 62, 2845.

16 M Stammler, *J Inorg Nucl Chem*, 1967, 29, 2203; L W F T Pistorius and A A V Gibson, *J Solid State Chem*, 1973, 8, 126; S Albert, H S Gutowski and J A Ripmeester, *J Chem Phys*, 1972, 56, 3672.

17 S-S Chang and E F Westrum, *J Chem Phys*, 1962, 36, 2420.

18 L E Topol and B B Owens, *J Phys Chem*, 1968, 72, 2106.

19 H Wiedersich and W V Johnston, *J Phys Chem Solids*, 1969, 30, 475,

20 H G Leduc and L B Coleman, *Solid State Ionics*, 1981, 5, 469.

21 T Hibma, *Phys Rev B*, 1977, 15, 5797.

22 S Geller and B B Owens, *J Phys Chem Solids*, 1972, 33, 1241; see also S Geller, *Science*, 1972, 176, 1016.

23 T Hibma and S Geller, *J Solid State Chem*, 1977, 21, 225.

12

Copper Ion Conductors

At least three room temperature polymorphs of copper (I) iodide exist.[1] The thermodynamically stable form, γ-CuI, is not a good ionic conductor at room temperature, though it has been speculated that at least one of the other polymorphs may be better.

Beyond about 500 K, there is a large excess heat capacity[2] that is associated with Cu^+ disordering and ionic conductivity.[3] Completion of this disordering at a continuous phase transition does not occur because the process is interrupted by a first order structural phase transition at 642 K.[2,4] At 680 K a further first order transition takes place. The high temperature α-phase has the same structure as the γ-phase except that now Cu^+ disordering is complete. The high temperature phases exhibit the characteristics of solid electrolytes.[3,5]

A number of room temperature Cu^+ electrolytes have been obtained. Some of these are apparently similar to $RbAg_4I_5$[6] while others are related to the alkylammonium iodide - silver iodide systems.[7-9] The inorganic systems have limited stability ranges and are destroyed by atmospheric moisture. The organic systems, while difficult to prepare free of the parent copper halide,[10] have poor electrical stability. Decomposition voltages are given by Faucheu et al.[9] as 0.56 V and 0.78 V for the iodide and bromide electrolytes, respectively. This precludes

the use of these electrolytes in Cu| |I_2 (0.83V) and Cu| |Br_2 (1.05 V) cells, as has been demonstrated by Takahashi and his co-workers.[7] They obtained the thermodynamically expected voltages with sulphur, selenium or tellurium cathodes but not with iodine or bromine.

The electrolytes studied in battery systems at Leicester Polytechnic are based on CuI and sulphonium iodides.[11,12] These mixtures do not, in general, form well defined chemical compounds. The x-ray powder diffraction photographs are all dominated by γ-CuI though other lines are present.

A systematic survey of x-ray results of previous workers in this department revealed no Cu^+ electrolyte that was a single phase. Thus no CuI-sulphonium iodide electrolyte was considered suitable for a heat capacity study. In the course of this survey, and during preliminary work for other studies, two new copper(I) compounds were isolated. These have been characterized only tentatively as they were obtained during the last two months of this project.

The first evidence for one of these compounds appeared in the d.s.c. trace of the electrolyte formed from copper(I) iodide and 4-methyl-1,4-oxathianium iodide (molar ratio 5.5:1). The trace exhibits an endothermic feature not seen for CuI or the organic iodide alone. This occurs near 420 K and is accompanied by darkening of the sample. In view of the demands of the adiabatic calorimeter, this observation was not pursued for some time.

The x-ray powder diffraction photograph of the electrolyte sample is not easy to interpret. γ-CuI is clearly present.

Table 12.1

X-ray diffraction data for some compounds described in this chapter

	$d/\mathring{A}$	
McCrone milled Cumoti	2CuI:1  I	1CuI:1 
A396	A395	A397
10.09(40)	10.05(100)	13.4(90)
7.63(20)	7.60(30)	9.63(100)
5.84(1)	5.89(1)	8.28(50)
4.71(1)	4.70(1)	7.25(50)
4.44(18)	4.41(25)	5.38(15)
4.30(5)	4.26(5)	4.82(15)
3.95(30)	3.92(60)	4.10(90)
3.81(5)	3.80(10)	3.96(25)
3.49(100)*	3.53(5)*	3.63(15)
3.41(15)	3.41(40)	3.52(80)
3.30(15)	3.30(25)	3.20(25)
3.10(5)	3.10(10)	3.05(25)
3.04(10)*		2.97(5)
2.97(10)	2.96(20)	2.84(25)
2.69(5)	2.68(10)	2.78(5)
2.65(1)	2.64(3)	2.67(1)
2.52(5)	2.52(15)	2.52(20)
2.39(5)	2.39(8)	2.49(20)
2.28(10)	2.28(15)	2.41(20)
2.19(5)	2.19(10)	2.30(15)
2.14(70)*	2.14(1)*	2.18(10)
2.08(1)	2.09(1)	2.05(20br)
2.05(8)	2.05(15)	2.02(1)
2.02(8)	2.01(15)	1.98(15)
1.96(5)	+ 20-30	1.96(15)
1.91(1)	faint	1.82(5)
1.87(1)	lines	1.73(1)
1.83(30)*		1.69(1)
1.79(1)		1.65(1)
1.76(1)*		1.58(1)
1.73(1)		1.55(1)
1.69(1)		1.52(1)
1.51(10)*		1.50(1)
1.39(15)*		
1.35(5)*		
1.23(15)*		
1.16(10)*		

* γ-CuI.

There are many other, broad, faint lines which do not correspond to those of either starting material. To increase the extent of reaction - if one occurs- between the constituents, the electrolyte was ground, as a n-hexane slurry, in a McCrone mill for 20 minutes. Neither compound is soluble in n-hexane. I thank Mr G Eaton of Leicester University for showing me how to use the mill.

The x-ray photograph now showed the presence of γ-CuI and another component that is certainly not the organic starting material (table 12.1).

A sample of CuI and 4-methyl-1,4-oxathianium iodide (about 5:1) were added to boiling acetonitrile (in which CuI is slightly soluble). The clear liquid was decanted off, some CuI remaining undissolved. The clear liquid was cooled to about -10 °C whereupon clear, needle shaped crystals formed. The x-ray powder photograph was identical to that of the second component in the McCrone mill ground electrolyte. The original d.s.c. feature at 420 K corresponds to melting and decomposition of the new compound.

Chemical analysis (C,H,N by Mr G Mistry and spectrophometric determination of copper as Cu^{II} by myself) suggests that the new compound has a composition

$$2CuI:1\ O\langle\ \rangle SMe\ I$$

The x-ray lines are all sharp suggesting that this compound is not an electrolyte. Conductivity studies have not been performed.

Another compound was prepared from CuI and the parent heterocycle thioxane. This forms from acetonitrile as powdery

white crystals, and is probably similar in structure to the morpholine complex described by Schramm and Fischer.[13] Many related complexes are known.[14] Chemical analysis (C,H,Cu) suggests a CuI:ligand ratio of 1:1. The powder diffraction pattern is given in table 12.1.

While the cells studied at Leicester exhibit approximately the same voltages as cells studied elsewhere, they differ in one other important respect. They are characterized by induction periods of a hundred hours or more before a plateau voltage is obtained. During this period, the cell voltage rises slowly from zero.[15] Initiation of the induction period requires the presence of the electrodes. No electrolyte preparation or pretreatment method has been discovered which allows cell voltages to be observed immediately.

Extended x-ray absorbtion fine structure

To investigate the copper systems more closely, an extended x-ray absorp tion fine structure (EXAFS) study of the electrolyte and battery systems was undertaken. This work was performed with the synchrotron radiation source at the SERC Daresbury Laboratory. An exploratory grant from the SERC allowed us, in principle, 24 h of EXAFS time. The experimental section of this work was performed in cooperation with Mr C Johnson of this department who had made electrochemical studies of these battery systems,[15] and the data analysis was in cooperation with Dr S S Hasnain of the Daresbury Laboratory. Some of the results have been submitted for publication.[16]

The Daresbury synchrotron ring houses a number of radiation

exit ports. At the time of our work, the EXAFS port offered x-rays of energy from about 4 keV to 25 keV. The x-ray intensity is not uniform over the whole range and this has consequences that will be mentioned later.

All elements are characterized by edges in their x-ray absorption spectra. Each edge corresponds to the ejection of an electron from the atom. Above the edge, the x-ray absorption falls steadily until another edge is reached for ejection of the next most tightly bound electron.

Above and close to the edge, the absorption curve is not smooth but shows oscillations which may extend for several hundred electron volts. The phenomenon has been known for some time but its use has been limited because of the extraordinarily difficult data analysis.[17] Most EXAFS work is still restricted to a small number of institutions which can offer both the data analysis facilities and a high energy x-ray source.

The oscillations above the edge are said to result from interference between the outgoing electron wave and portions of that wave reflected back by neighbouring atoms.[18]

The true EXAFS region extends from about 50 eV above the edge. The area closer to the edge is considered separately as it includes contributions from other complicating factors such as multiple scattering of the outgoing wave. Analysis of this region (XANES, x-ray absorption near edge structure) is still in its infancy.

EXAFS is very sensitive to the immediate environment of the emitting atom. It can thus provide structural information

for systems that cannot readily be studied by x-ray diffraction, such as glasses, or whose x-ray patterns are very complicated, such as enzymes. See for example the papers in reference 19.

In view of the above comments, EXAFS appeared to offer the possibility of examining the local structure around the mobile ions in solid electrolytes. By studying the Cu^+ electrolytes as made and after use in a cell, it was hoped to obtain information concerning the processes taking place during the induction period.

Sample preparation

Electrolyte was diluted with boron nitride powder, which is transparent to x-rays, ground and passed through a sieve to obtain a particle size less than 38 μm. The proportion BN: electrolyte was determined following a method intended to maximize signal noise ratio:[18,20]

$$\mu z = 2.55$$

where z is the sample thickness and μ is the total absorption coefficient

$$\mu = \Sigma_\alpha \, n_\alpha \sigma_\alpha$$

Here σ_α is the absorption cross section for element α, and n_α is the density of that element within the sample. Values of x-ray cross sections were obtained from reference 21.

We were told at Daresbury that this criterion is not important with their instrumentation. Since, in almost all cases, this method did produce a satisfactory spectrum, the calculation still provides a good basis for selecting a sample thickness.

The samples were mounted in slits (15 mm x 4 mm) in brass or aluminium holders 0.4 mm thick. The powders were held within the slits by means of Kapton windows. Kapton is a plastic material which contains no high atomic number atoms. It thus has a negligible x-ray absorption coefficient. Sellotape, a very much simpler window material to use, was less satisfactory because it discoloured, apparently due to reaction of the electrolyte with the adhesive over a period of days. For samples prepared at Daresbury for immediate use, Sellotape was preferred.

An alternative preparation method was used for some materials. This involved collecting the milled sample, from a suspension in n-hexane, on a Millipore filter. The sample was then protected by depositing rubber on to it from solution in n-hexane.[22] Good uniform samples were obtained but time did not permit their EXAFS examination.

The EXAFS spectra

The copper *K* absorption edge is at 8.98 keV. This is a particularly convenient region for EXAFS study since it lies close to the intensity maximum available from the x-ray source. Scanning through the energy region of interest (8.6-9.5 keV) is performed by means of a double crystal monochromator (we used the silicon 220 plane). A double crystal is used to remove unwanted energy harmonics. The two crystal surfaces are slightly out of parallel alignment. This reduces the intensity of the required x-ray energy, but reduces the harmonics to a much greater extent.[23]

Correct positioning of the sample in the x-ray beam was

accomplished using a laser beam coincident with the x-ray path. Obviously during sample positioning the x-ray source was closed off. A further check of alignment was occasionally made by replacing the sample with a covered Polaroid film, and exposing this to the x-ray beam.

The x-ray intensity was measured before and after the sample by means of gas ionization counters (optimum gas and pressure conditions were selected for us by Dr P H Quinn). The plots produced initially are presented as $\ln(I_t/I_o)$ against crystal monochromator angle (in millidegrees).

Computer programs available at Daresbury correct for the variation in x-ray intensity with energy and convert the monochromator angle scale to energy. Examples of the resulting plots for some of the copper systems studied are illustrated in figure 12.1. A further program then allows the background x-ray absorption to be subtracted.

Other programs enable calculated spectra to be produced for various structural models, and radial distribution functions to be obtained both for the experimental spectra and the models. This final stage of the data analysis was performed by Dr S S Hasnain (Daresbury) on the basis of structural models prepared by us (at Leicester).

The EXAFS spectrum for CuI is shown in figure 12.2 (*a*). The data fit the known structure of γ-CuI,[24] and agreement between the experimental and calculated fourier transforms is good (figure 12.2 (*b*)). Iodine is an extremely strong scatterer, and the nearest neighbour iodine atoms dominate the spectrum. This can be seen in figure 12.2 (*c*) where the calculated

spectrum is based on a single shell model only. The fit is not significantly worse than that of figure 12.2 (*a*) which is based on four shells.[16]

The EXAFS spectrum of Cumoti is shown in figure 12.3. The calculated spectrum is based on a four shell model.

The spectrum for Cumoti taken from a working cell is shown in figure 12.4 (*a*). It is clear, even without data analysis, that the electrolyte from the working cell is different from the unused electrolyte. The data for the unused electrolyte are very similar to those for CuI and can be fitted well by a model based on the known structure of γ-CuI.[16] The used electrolyte cannot be fitted in the same way, but the data can be interpreted if we assume that copper now has a new close neighbour at 2.25-2.30 Å. The only atom available that can approach this closely and that is a sufficiently strong scatterer is sulphur. The data can be fitted reasonably well if it is assumed that one iodine first neighbour in four is replaced by sulphur (see figure 12.4 (*b*)). More detailed fitting parameters are given in reference 16. Unfortunately, the spectrum is so dominated by contributions from the first anion shell that conclusions concerning changes in long range order are not possible.

The XANES spectra (figure 12.5) also show that changes have occurred in the electrolyte Cumoti.

It is also not possible to comment on how charge balancing is achieved; both incorporation of excess Cu^{+} or oxidation of some Cu^{+} to Cu^{2+} could occur in the working cell.

Close approach of sulphur to the copper would require partial, or complete, breakdown of the sulphonium cation. This, together

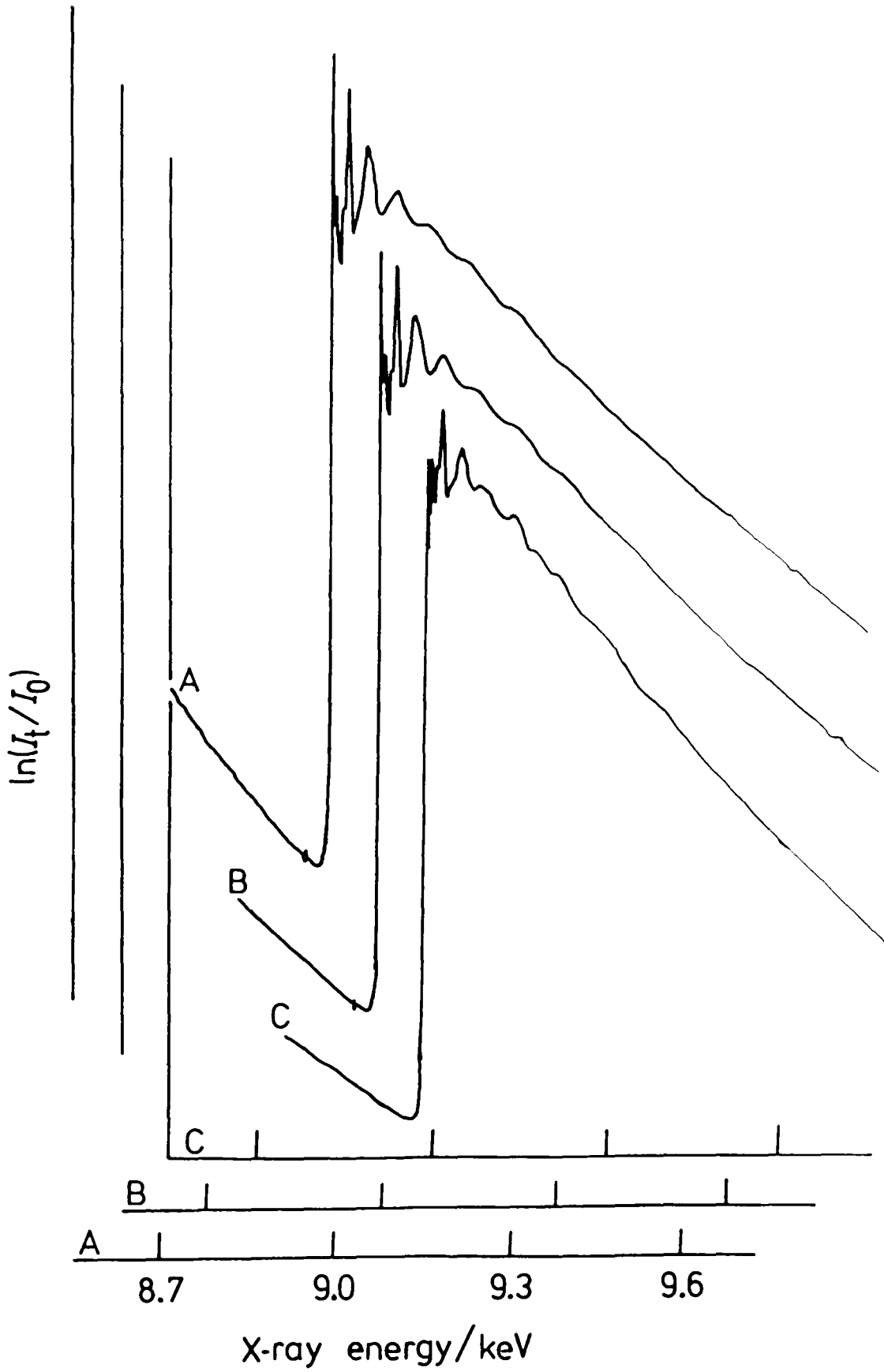

Figure 12.1 EXAFS spectra for a number of Cu^{+} electrolytes: A Cumoti (5.5 CuI:1  I); B Cumuti (5.5 CuI:1  I); C Cumoti from a discharged cell, 0.36 V and 10 μA cm^{-2} for 2000 h. I_o intensity of incident beam; I_t intensity of transmitted beam.

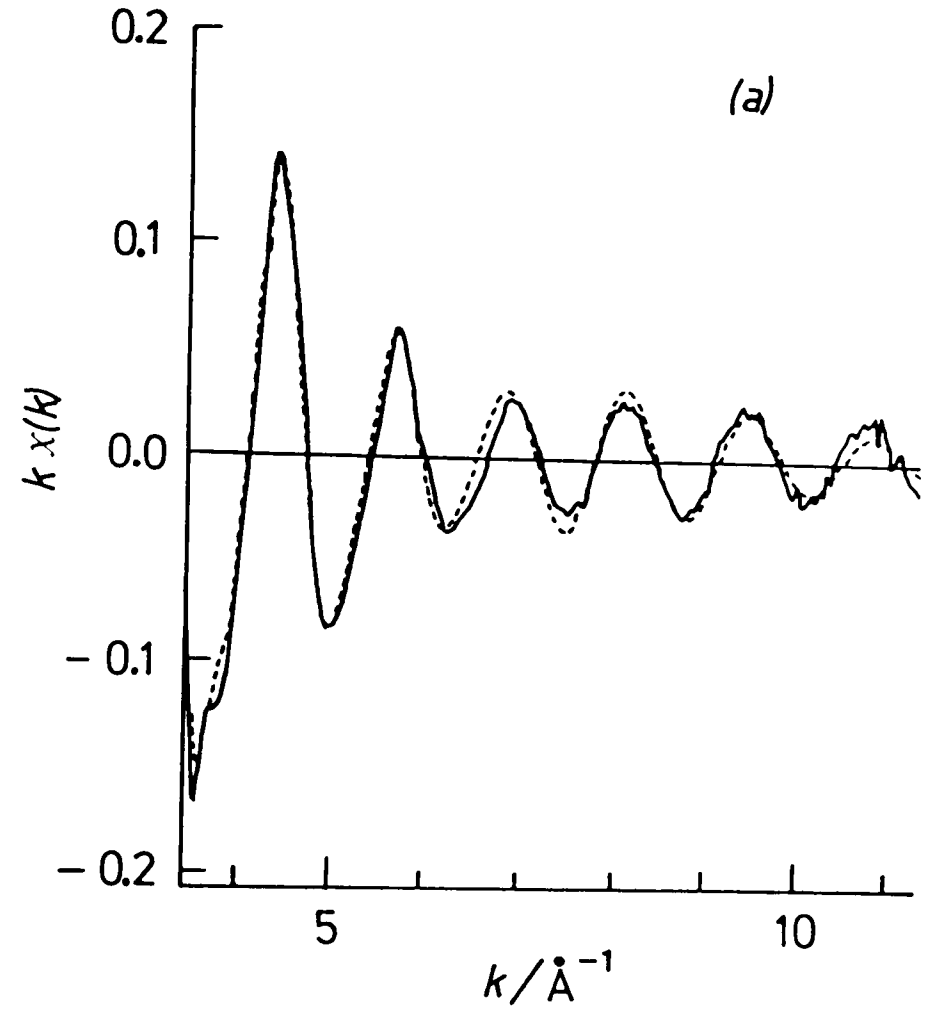

Figure 12.2 For caption see following page.

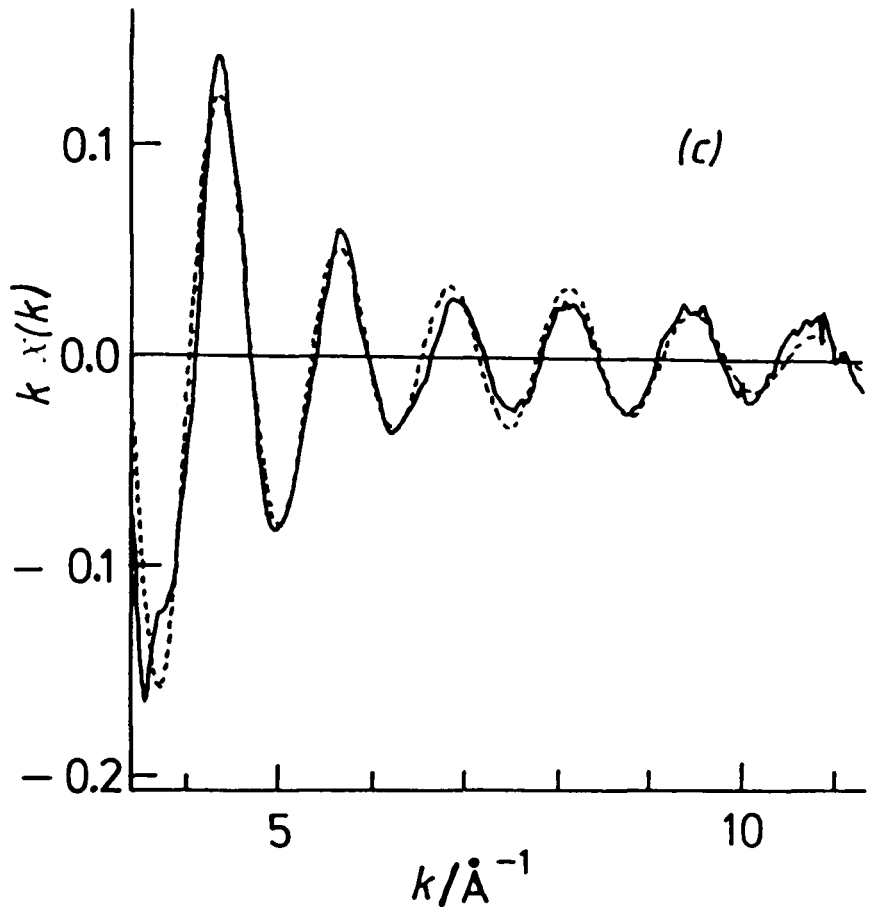

Figure 12.2 Experimental (——) and theoretical (- - -) EXAFS spectra for CuI (*a*). The theoretical spectrum is based on a four shell model, the fitting parameters for which are given in reference 16. (*b*) Fourier transforms of the spectra in (*a*). (*c*) EXAFS spectra for CuI; in this case the theoretical curve is based on a single shell model with four iodine neighbours at 2.54 A. $\chi(k)$ is a relative intensity function. The fourier transform is a form of radial distribution.

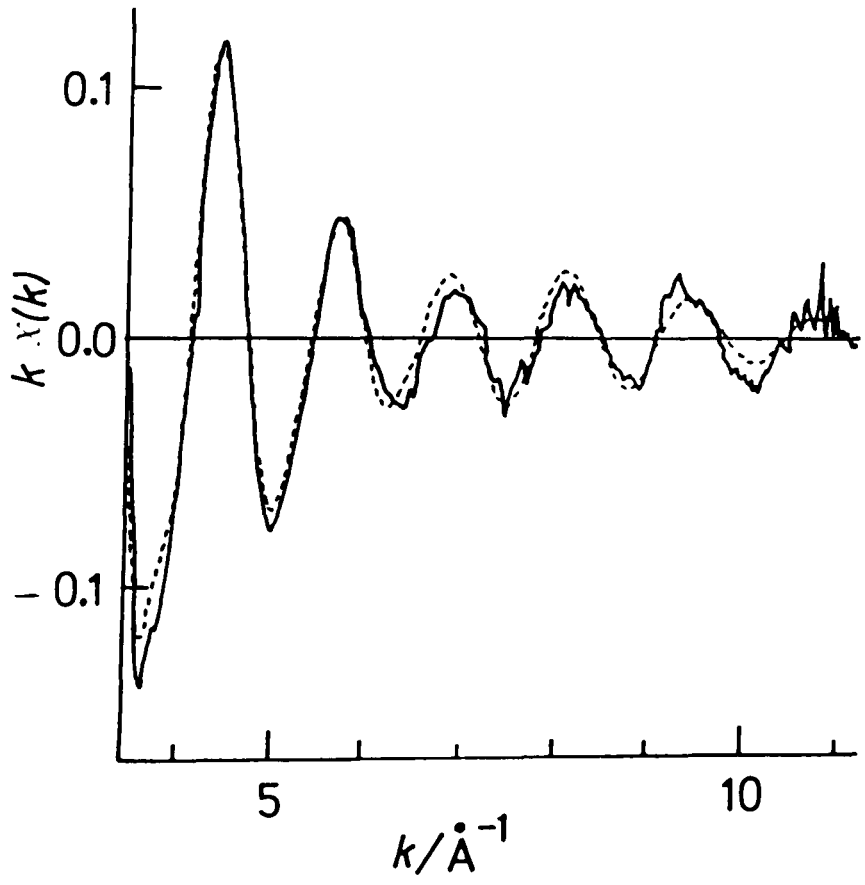

Figure 12.3 Experimental (——) and theoretical (- - -) EXAFS spectra for Cumoti. Note the similarity to figure 12.2(*a*) and (*c*).

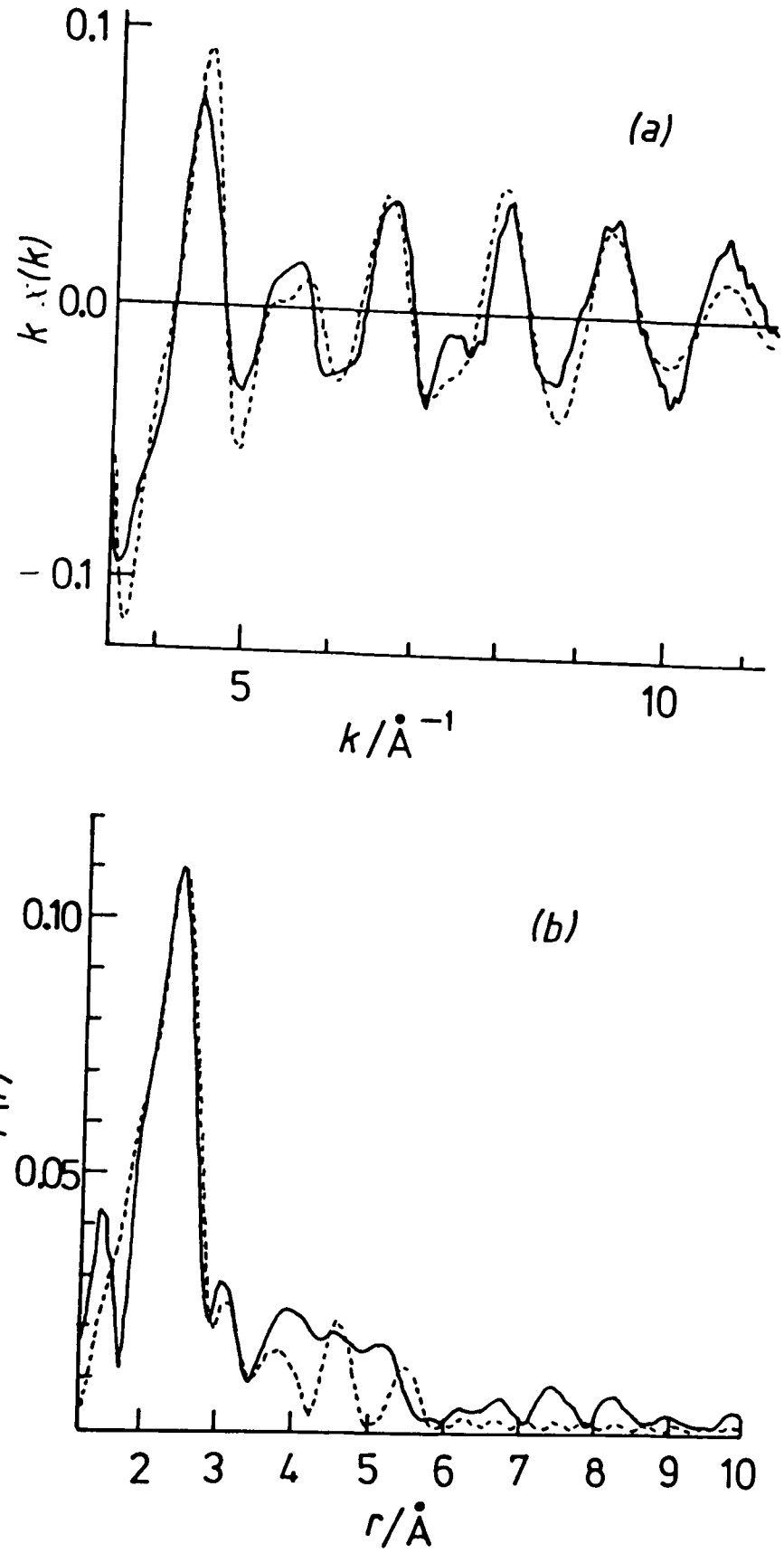

Figure 12.4 Experimental (——) and theoretical (- - -) EXAFS spectra (*a*) and fourier transforms (*b*) for Cumoti taken from a discharged cell. The model on which the theoretical curves are based provides the copper atom with three iodine neighbours at 2.58 Å and one sulphur at 2.29 Å. The distance in Cu_2S is 2.26 Å. Further details are given in reference 16.

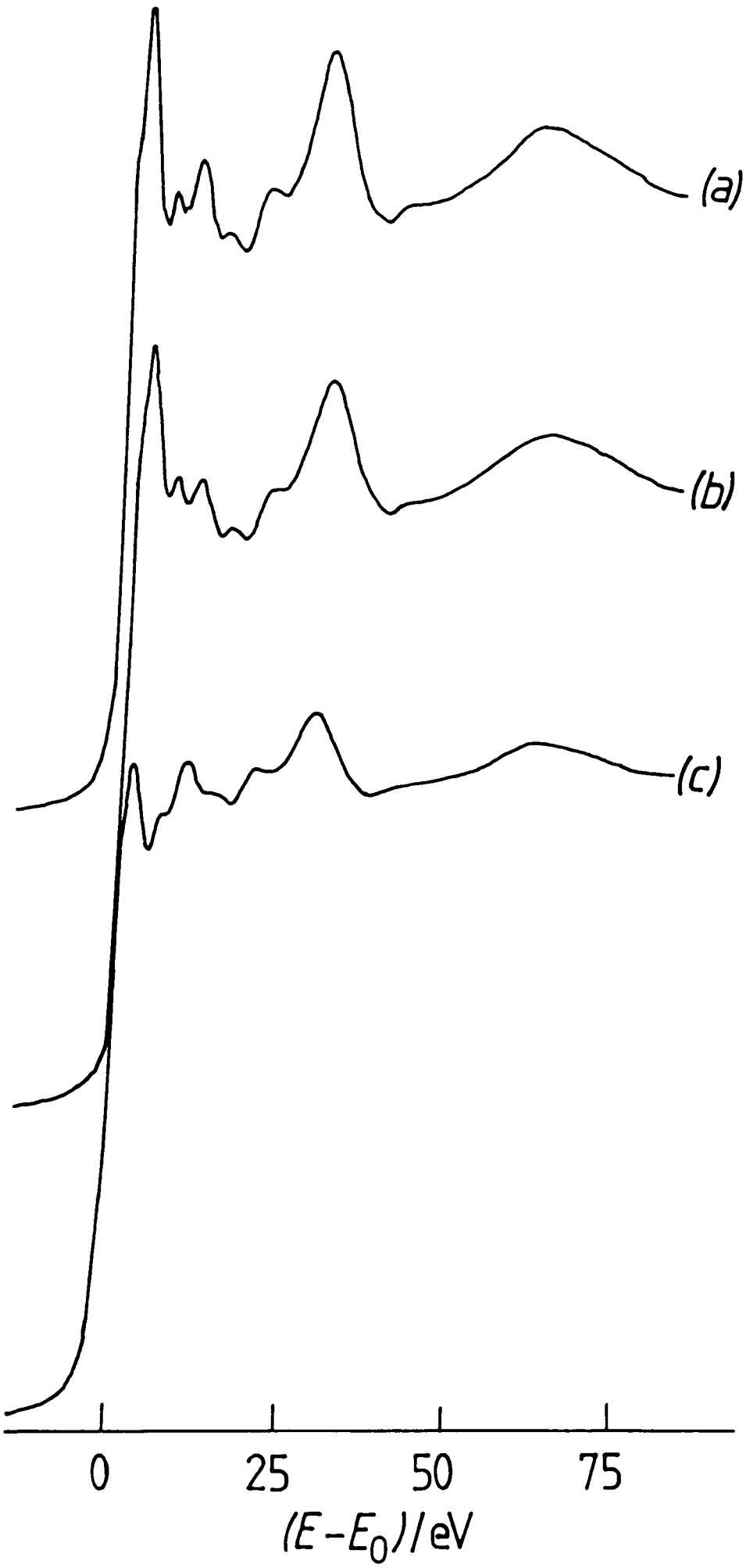

Figure 12.5 The XANES region of the x-ray absorption spectra for (*a*) CuI, (*b*) Cumoti, (*c*) used Cumoti. E_0 is the energy of the copper absorption edge.

with the ensuing sulphur diffusion, could be responsible for the cell induction period.

An examination of these possibilities is the subject of current work in this department.

In order to obtain more model compounds for comparative work, it is hoped that a phase diagram study of the CuI-Cu_2S system will be possible.

Two other copper systems were investigated. The spectrum of the electrolyte 5.5CuI:1 ⟨⎺⟩SMe I is identical to that of Cumoti.

Results for samples taken from a cell with a magnesium anode indicate that the copper has been almost wholly displaced from the electrolyte. The copper edge signal indicated a reduction in copper content to 20% or less relative to that of the original electrolyte. Absorption was too weak to allow the EXAFS spectrum to be resolved. This result substantiates inferrences drawn from electrochemical studies.[25]

Iodine

Since the EXAFS work was exploratory, some studies were carried out on other edges. A study of iodine was considered valuable since all the electrolytes used at Leicester contain iodine. These investigations were made with $RbAg_4I_5$ and CuI. Unfortunately, in the former, background absorption by Rb and Ag was so great that the fine structure could not be resolved.

The iodine *L* edges occur at 4.557, 4.852 and 5.188 keV.[21] The fine structure above two of these in CuI is shown in figure 12.6. The spectra look extremely promising but time did not permit analysis.

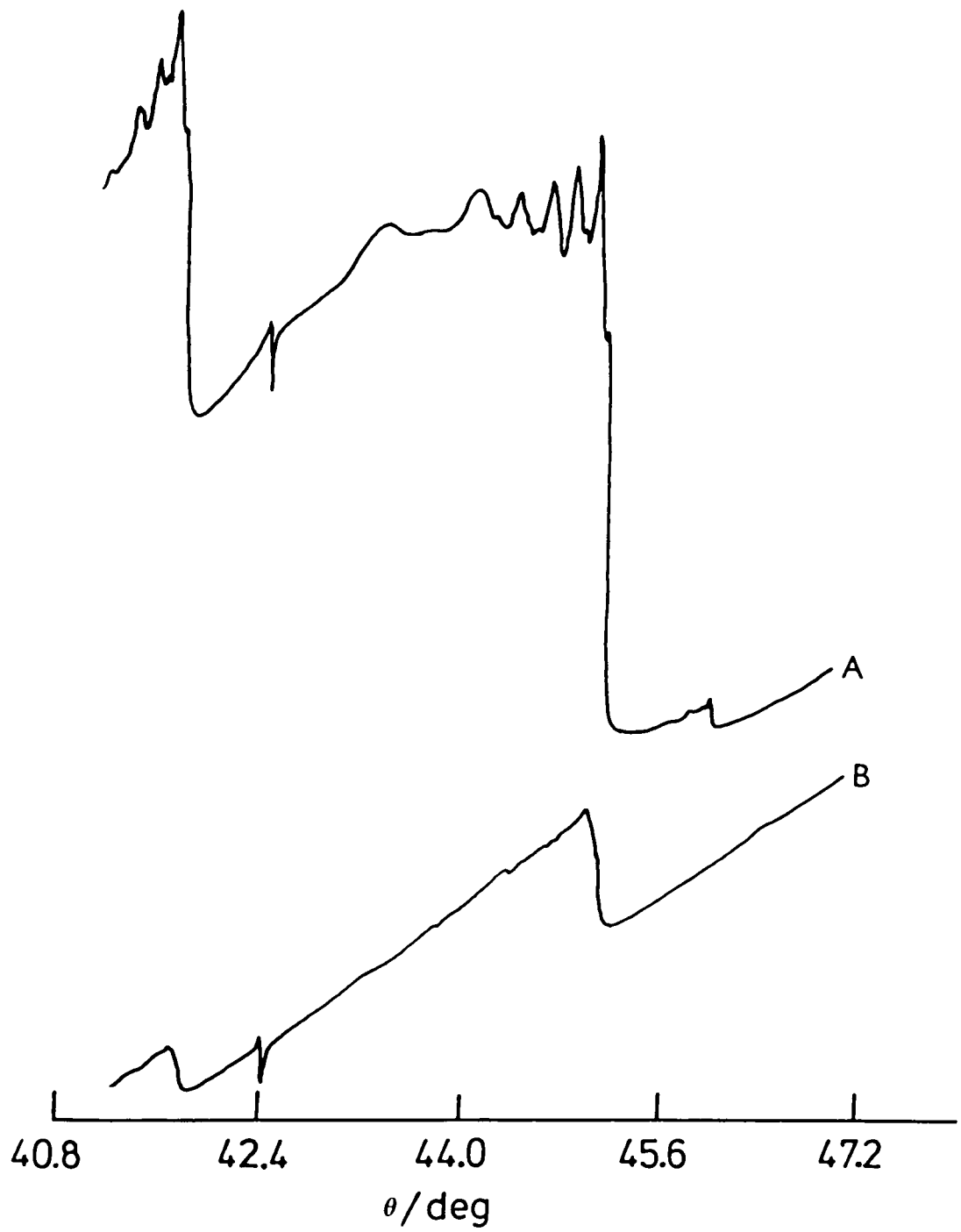

Figure 12.6 The *L*II and *L*III iodine x-ray absorption edges in CuI (A) and $RbAg_4I_5$ (B). The vertical scale is $\ln(I_t/I_o)$ and θ is the monochromator angle. Note the silicon crystal glitch visible on both spectra and the copper overtone edge on spectrum A.

Two features are worthy of note, and concern errors in the collected data. These errors occur in all spectra but are more significant in the low energy region where x-ray intensity is relatively low.

Harmonics

A small feature is visible below the lowest iodine edge. The energy of this weak edge (4.48 keV) is just half that of the copper edge (8.98 keV). The x-ray monochromator has passed a significant quantity of radiation with twice the energy of that required, and it is absorption of this harmonic that is visible on the EXAFS spectrum. It is important here because the x-ray source 9 keV region is much more intense than the 4.5 keV region.

Glitches

Before the *L*II edge a sudden discontinuity appears in the absorption spectrum, a 'glitch'. This represents a spurious reflection from monochromator crystal planes other than (220). Programs at Daresbury allow the positions of these to be predicted. They can be removed from the spectrum if required.

Rubidium

An EXAFS spectrum was obtained for rubidium in $RbAg_4I_5$. The source x-ray intensity at this energy (15.2 keV) is relatively low so resolution is not as good as for copper. The intensity of the harmonics, however, is negligible so the two Si(220) planes can be set parallel to make the most of the radiation available.

The rubidium spectrum was not particularly extensive so is not shown. The data were not analysed.

Future work

A detailed application has been submitted to the SERC for further EXAFS time at Daresbury. It is hoped that this will allow the studies of Cu^+ electrolytes to be extended, and will also allow studies to be undertaken of Ag^+ glasses.

References to chapter 12

1 R Batchelor and T Birchall, *Acta Cryst B*, 1982, 38, 1260.

2 S Miyake, S Hoshino and T Takenaka, *J Phys Soc Japan*, 1952, 7, 19.

3 B K Verma, V Pratup and H B Lal, *Japan J Appl Phys*, 1981, 20, 1665.

4 H-U Schrader and J Nölting, *High Temperatures-High Pressures*, 1980, 12, 561.

5 J B Boyce and B A Huberman, *Solid State Comm*, 1977, 21, 31.

6 T Takahashi, R Kanno, Y Takeda and O Yamamoto, *Solid State Ionics*, 1981, 3/4, 283; K Nag and S Geller, *J Electrochem Soc*, 1981, 128, 2670; S Geller, K Nag and A K Ray, *J Electrochem Soc*, 1981, 128, 2675.

7 T Takahashi, O Yamamoto and S Ikeda, *J Electrochem Soc*, 1973, 120, 1431; T Takahashi and O Yamamoto, *J Electrochem Soc*, 1977, 124, 37.

8 M Lazzari, R C Pace and B Scrossatti, *Electrochim Acta*, 1975, 20, 31.

9 J Faucheu, G Nguyen Minh, J Rosenberg and G Robert, *J Chim Physique (France)*, 1979, 76, 166.

10 J M Shemilt, B C H Steele and J E Weston, *Solid State Ionics*, 1981, 2, 1.

11 R H Dahm, S Hackwood, R G Linford and J M Pollock, *Nature*, 1978, 272, 522.

12 S Hackwood and R G Linford, *Chem and Ind*, 1980, 523.

13 V Schramm and K F Fischer, *Z Naturwiss*, 1974, 61, 500.

14 F A Cotton and G Wilkinson, Advanced Inorganic Chemistry, Wiley, 4th edn, 1980, p 805-807.

15 C Johnson, Ph D Thesis, Leicester Polytechnic, 1983.

16 R G Linford, P G Hall, C Johnson and S S Hasnain, Daresbury Laboratory Preprint DL/SCI/P410E, SERC Daresbury Laboratory, January 1984; *Solid State Ionics*, submitted for publication.

17 For a review of early EXAFS work see L V Azaroff, *Rev Modern Phys*, 1963, 35, 1012.

18 P A Lee, P H Citrin, P Eisenberger and B M Kincaid, *Rev Modern Phys*, 1981, 53, 769.

19 F W Lytle in Physics of Non-crystalline Solids, North Holland, 1965, p 12 (glasses); S Doniach, P Eisenberger and K O Hodgson in Synchrotron Radiation Research, Plenum Press, 1980, chapter 13 (biological materials).

20 T M Hayes, Leicester University (visiting professor), personal communication, 1982.

21 W H McMaster, N K Del Grande, J H Mallett and J H Hubbel, Compilation of X-ray Cross Sections, California University Livermore Lawrence Radiation Laboratories, UCRL 50174, 1970.

22 E D Eanes, J L Costa, A MacKenzie and W K Warburton, *Rev Sci Instrum*, 1980, 51, 1579.

23 C Kunz in Synchrotron Radiation (Topics in Current Physics 10), ed C Kunz, Springer-Verlag, 1979, p 55.

24 J B Boyce and T M Hayes in Physics of Superionic Conductors (Topics in Current Physics 15), ed M B Salamon, Springer-Verlag, 1979, p 5; *Phys Rev B*, 1981, 23, 2876.

25 C Johnson, R J Latham and R G Linford, *Solid State Ionics*, 1982, 7, 331.